A feasibility study looking into the design and manufacture of a composite chassis for Formula Student

Anton Kasjanics, Joe Edwards, Thomas Gough & Thomas Rickard

This report is submitted in partial fulfilment of the requirements for the Degree of Master of Engineering, Faculty of Engineering and the Environment, University of Southampton.

Acknowledgements

We would like to thank Scott Walker and Owen Tutty for their guidance during the course of this project and Formula Student for their financial support.
Special thanks goes to Andy Robinson, for help over numerous tasks including health and safety forms, test machine training, composite manufacturing and general answering of questions during work in the Testing and Structures Research Laboratory. Thank you also to Jeanne Blanchard for a training exercise in composite layup.
We would also like to thank EDMC for providing assistance in manufacturing, as well as supplying offcuts.

GDP Academic Integrity Statement

I the undersigned confirm that the material presented in this project report is all my own work. References to, quotations from, and the discussion of work of any other person have been correctly acknowledged/cited within the report in accordance with University of Southampton guidelines on academic integrity.

Signed: . . . . . .
Name (Print in Full): . . . . . .
Date: . . . . . .

Signed: . . . . . .
Name (Print in Full): . . . . . .
Date: . . . . . .

Signed: . . . . . .
Name (Print in Full): . . . . . .
Date: . . . . . .

Signed: . . . . . .
Name (Print in Full): . . . . . .
Date: . . . . . .

Nomenclature

(AG_{eg})	Equivalent shear rigidity N
(EI_{eq})	Equivalent flexural rigidity Nm^2
δ	Displacement m
σ_c	Core strength MPa
σ_f	Facesheet strength MPa
$\sigma_{t,ult}$	Ultimate tensile strength of facesheet MPa
σ_u	Yield strength MPa
σ_y	Yield strength MPa
τ_{all}	Allowable shear strength of core material
τ_c	Shear strength MPa
b	Panel width m
b_i	Insert diameter m
b_p	Typical potting radius m
c	Core thickness m
D	Diameter of potting m
d	Distance between facesheet centres m
e	Edge distance m
E_s	Young's modulus of facesheet GPa
E_c	Core Young's modulus MPa
E_f	Facesheet Young's Modulus GPa
F	Load N
G_c	Core shear modulus MPa
h	Core height m
h	Panel height m
I	Area moment of inertia m^4
$K_e^{'}$	Stress concentration factor
L	Panel span length m
r_i	Insert radius m
r_p	Potting radius m
S_c	Core height m
t_s	Facesheet thickness m
t_f	Facesheet thickness m
u	Indentation depth m
v_s	Poisson's ratio of facesheet
W	Panel width m
CFRP	Carbon Fibre Reinforced Plastic

CLT	Classical Laminate Theory
GRP	Glass Reinforced Plastic
IMechE	Institute of Mechanical Engineering
SES	Structural Equivalency Spreadsheet
SUFST	Southampton University Formula Student Team

Contents

List of Figures

Nomenclature

(AG_{eg})	Equivalent shear rigidity N
(EI_{eq})	Equivalent flexural rigidity Nm^2
δ	Displacement m
σ_c	Core strength MPa
σ_f	Facesheet strength MPa
$\sigma_{t,ult}$	Ultimate tensile strength of facesheet MPa
σ_u	Yield strength MPa
σ_y	Yield strength MPa
τ_{all}	Allowable shear strength of core material
τ_c	Shear strength MPa
b	Panel width m
b_i	Insert diameter m
b_p	Typical potting radius m
c	Core thickness m
D	Diameter of potting m
d	Distance between facesheet centres m
e	Edge distance m
E_s	Young's modulus of facesheet GPa
E_c	Core Young's modulus MPa
E_f	Facesheet Young's Modulus GPa
F	Load N
G_c	Core shear modulus MPa
h	Core height m
h	Panel height m
I	Area moment of inertia m^4
$K_e^{'}$	Stress concentration factor
L	Panel span length m
r_i	Insert radius m
r_p	Potting radius m
S_c	Core height m

t_s	Facesheet thickness m
t_f	Facesheet thickness m
u	Indentation depth m
v_s	Poisson's ratio of facesheet
W	Panel width m
CFRP	Carbon Fibre Reinforced Plastic
CLT	Classical Laminate Theory
GRP	Glass Reinforced Plastic
IMechE	Institute of Mechanical Engineering
SES	Structural Equivalency Spreadsheet
SUFST	Southampton University Formula Student Team

1 Introduction

By Thomas Rickard

1.1 Formula Student

Formula student UK is an annual motorsport competition organised by IMechE for university students. Teams are required to design, test and build a single seater race car that satisfies the regulations. The competition is made up of static and dynamics events. The static events consist of:

- Business Presentation (75 points)
- Engineering Design (150 points)
- Cost and Sustainability (100 points)

The dynamic events consist of:

- Acceleration (75 points): This is a straight line 75m acceleration test. A car with good power to weight ratio will perform well here.
- Skidpan (50 points): This event involves driving a figure of 8 and tests the mechanic grip
- Sprint (150 points):
- Endurance (300 points): A 22km event which tests the cars reliability and economy.
- Fuel economy (100 points): This is measured during the endurance event.

The competition is held at Silverstone during July over the course of five days. Cars must pass scrutineering in order to compete in the dynamics event. Scrutineering involves a technical inspection of all systems to ensure the cars satisfy the rules and meet safety requirements.

1.2 SUFST

Every year SUFST [1], the Southampton University Formula Student Team designs and manufactures a single seater race car for participation in the UK Formula Student Competition. This year marks the third successive year a car will be build for the competition. All cars have so far been entered into class 1. The GDP team aims to work with SUFST helping to develop their future ideas and concepts.

Figure 1: The SUFST 2012/13 car.

During the second year several improvements were made; the addition of a shear plate at the rear allowed removal of the transmission box and the alignment of load paths. The chassis could then be made shorter and lighter, reducing the mass to 282kg.

1.2.1 Current Problems

The car is currently too heavy as a result of the chassis and over-engineered unsprung masses (Uprights, brakes and wheels). The chassis stiffness could also be improved.

1.2.2 Future Developments

For severals years SUFST have used a steel tube space frame chassis due to the ease of construction and the flexibility it provides for design changes. They are however looking to construct a composite chassis to increase their competitiveness. A composite chassis could theoretically be lighter while offering increased strength and stiffness over a space frame, which is of great benefit to a race car. Designing a composite chassis however is difficult and requires fairly advanced modelling, testing and manufacturing skills, as well as a strict design regime.

Considering this, SUFST have asked the GDP team to carry out relevant research into composite chassis. This will be followed by the construction of a prototype which aims to de-risk future implementations. A notable limitation is that a majority of the construction must take place in house and this will restrict the use of some advanced manufacturing techniques.

1.3 Tasks, aims and objectives

The main aim of this project is to determine the feasibility of designing and manufacturing a composite chassis for a Formula Student car. It should be able to be manufactured at the University and not rely substantially on outsourced equipment or work.

The objectives for this project include:

- Design a composite chassis which conforms to Formula Student Regulations (i.e. suspension pickup points, engine mounting points, driver positioning).
- Simulate the structural mechanics using FEA.
- Validate the FEA by testing material specimens as required by Formula Student rules.
- Construct a scale model to evaluate the manufacturing techniques.

1.4 Available resources

The resources available to the team influence the design and manufacturing techniques used. Notable equipment and facilities available to the team include:

- EDMC, specialists in manufacturing metal items
- Woodworking shop
- Laser cutters
- Resin infusion and vacuum bagging facilities
- Testing machines

Notable equipment and facilities not available to the team includes:

- Autoclave capable of curing a size car
- Large CNCing machine

2 Literature Review

2.1 FS Chassis types

By Joe Edwards

'The automotive chassis provides the strength necessary to support the vehicular components and the payload placed upon it' [2]. With this in mind, the relative advantages and disadvantages of particular chassis designs will be discussed in this section. The discussion will then lead onto how the solution chosen can lead to favourable dynamic behaviour.

The design of the chassis itself is a product of the role it's to be used for. Whilst the content will be aimed at general chassis design, the positive and negative attributes carry over readily to the Formula Student chassis design in which the project will undertake. The two primary chassis design ethos' are a framed or monocoque solution. The prior is where a distinction is made between the structural members and the external bodywork, where as the latter allows the bodywork to be utilised to withstand the structural load. Both types obviously have their own merits, which will be explored further.

Framed or 'Space Frame' solutions as seen in Figure 3 are more simplistic than monocoques in terms of design complexity. They require relatively simple design solutions when looking at mounting various parts of the payload and vehicular components. These solutions can typically be brackets that are either welded or bolted and dowelled onto the frame. In contrast monocoque solutions require any brackets to be integral with the frame, sandwiched between the two skins as seen in figure 2. This allows any load to be transferred directly onto the frame that will be much stronger than a bracket alone. A Monocoque (as seen in figure 4) enables the designer to move vehicular components around easily as the mounting points are wherever there is a free surface. This reduces the need for complex mounting brackets to fit a pre-existing space frame.

Figure 2: Monocoque bulkhead integrated brackets.

The Space Frame solution also offers better versatility when looking at bodywork; this is because a multitude of options can be adapted to fit the space frame at the cost of the bodywork alone. The monocoque solution can change the shape of its bodywork albeit at great cost. As the bodywork is itself structural it requires a far greater manufacturing effort to be created. As a result it's imperative that any design that is finalised has had all theoretical optimisation carried out, to minimise the

likelihood of an up-issued design.

Figure 3: SUFST 2013/14 space frame chassis.

The design effort for the space frame chassis is also greatly reduced, involving only solid body modeling with no complex 3D surfacing required. This can also be the case with the monocoque solution. However in order to fully utilise the advantages of the monocoque chassis, the cross sectional area must be reduced whilst still accommodating the payload. As a compromise 3D geometries can provide a good solution, however the higher the complexity of the surfaces used, the greater the manufacturing cost required. Something similar to the surfaces in figure 4 would be a desirable solution.

Figure 4: Example of a cut and fold monocoque chassis.

A structurally efficient design could be relatively easily achieved with a space frame solution, but at

a weight penalty. This is why the more structurally efficient monocoque chassis was studied further, as it was a far more appropriate design for the Formula Student competition.

When looking at the manufacturing process, the Space Frame solution required only the tubing itself and a welding jig, with any mistakes being relatively inexpensive to correct. A monocoque chassis is very dependent on the manufacturing process and therefore the design created. This is why with intelligent design and using simplistic manufacture as a key design variable an appropriate and versatile chassis concept can be designed for the Formula Student Society.

Whilst the vehicle dynamics of the chassis aren't the primary focus of this project, being sympathetic to practices that improve their characteristics will improve the overall understanding of a racing chassis design and allow a chassis concept that isn't just manufacturable but competitive too.

Using a monocoque chassis allows versatility when it comes to mounting vehicular components, as any part of the skin is effectively a hard point within reason. For example an engine would not be mounted where high stress concentrations were predicted on FEA.

'This flexibility allows for the main masses to be located as close to the COG as possible. This in turn lowers the yaw inertia'. [3]

'The designer must provide a structure that joins together the suitably positioned masses and that is stiff and strong enough to cater to all loads fed into it, whilst having the smallest possible cross section and the lowest possible mass'. [3]

The most prevalent aspect of the monocoque chassis over a space frame would be mass reduction. This would this increase the acceleration as well as improve the rate of turning achievable. Both qualities of which are incredibly important in the Formula Student competition.

Figure 5: Sandwich panel with carbon fibre skins and Nomex core.

Using FEA the carbon fiber layup procedure can also be optimised to ensure the material qualities suit that specific part of the car, this is done by optimising the carbon fiber layup orientation. For example 'High-modulus carbon fiber can be used where stiffness is critical, and high strength fibers used where impact loads and load concentrations, such as suspension loads, must be fed into the structure' [3]. The incredible stiffness of a sandwich panel layups in monocoque chassis' can also increase the predictability of a vehicles dynamic performance, as it eradicates joint movement as well

as ensuring weight distribution won't vary greatly in corners.

2.1.1 History of composite construction in racing cars

The first example of a composite chassis in racing occurred in the 1920s, however the main purpose of the wood and steel composite was to reduce costs as opposed to improve performance. Whilst not making it to the track, the first 'modern' composite chassis was created by Cooper in the 1960s, where an outer aluminium skin was combined with an aluminium honeycomb core and GRP inner skin. This became the basis for Formula 1 chassis design during the 70s, where the cut and fold method was used to combine an aluminium skin and honeycomb core [4].

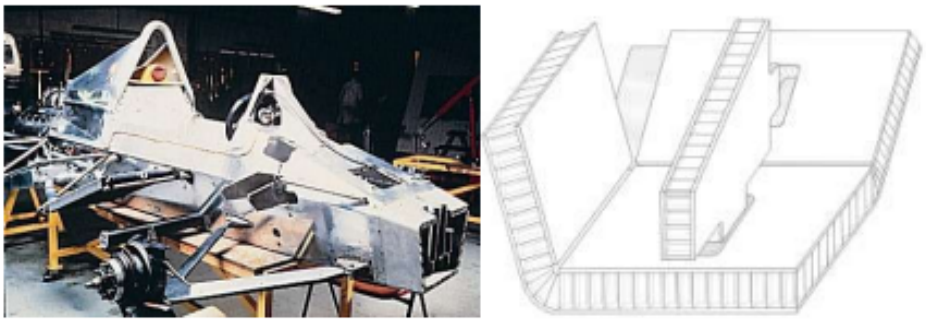

Figure 6: Cut and Fold Aluminium honeycomb chassis from the late 1970s.

The first carbon fibre composite chassis to participate was from McLaren in 1980, using a male mould with a composite inner and outer skin, epoxy film adhesive and honeycomb core. Whilst racing with this, Lotus was also developing a cut and fold chassis with a carbon and Kevlar reinforced epoxy [4].

In the 1980s, two paths were taken. Lotus took a cut and fold approach to develop a low tech chassis, whilst McLaren used the US aerospace partner Hercules [3] to lay piles around a male mould inside out. This led to the outer skin being laid against the honeycomb core, leading to a poor outer finish. It was the moulded McLaren approach with was adopted by other teams, whilst the 1983 ATS D4 incorporated a female moulded chassis, improving the external surface. Some teams developed full carbon chassis like the Ferrari 126C3 whilst others kept separate bodywork. For the most part moulds were formed of upper and lower halves, however this changed in the late 1990s due to the changing shape of the chassis and stress placed along the car centre line. This led to splitting the chassis into a main tub moulding with a smaller floor moulding. Metallic bulkheads were also discarded and replaced with either carbon or honeycomb bulkheads, or removed completely, replaced with thicker piles of carbon fibre through the adoption of FEA [5]. Finally in the 2000s, even greater complexity led to breaking the tub into several sections. The BAR004 chassis was composed of top front section, fuel tank/roll over section, full length lower section, seat back and rear bulkhead.

2.1.2 Benefit and disadvantage of construction techniques - moulded vs. cut and fold (drives design type)

The cut and fold method of chassis construction offers many advantages over the typical moulded procedure. One of these is the lack of equipment available to create a moulded chassis, such as an autoclave large enough to build even a scale model. Without these tools, it is not feasible within

the budget to rent or pay an outside company for the facilities. Unlike a moulded chassis, cut and fold can be manufactured using prefabricated panels with the outer and inner skins already bonded to a honeycomb core [6]. This means an autoclave isnt required to combine the layers. Another cost saving is that a mould isnt required to shape the chassis. Instead it is shaped by cutting into the inner surface to allow the material to bend in place [6], and held there through a jig. This can be constructed in wood, reducing the cost further.

The process of developing a moulded chassis is far more time consuming that a cut and fold one. Firstly, a plug has to be made from foam, onto which the mould can be constructed around using, for example, fibreglass and resin. This must then be treated with wax to stop the fibreglass sticking to the first, outer layer, comprising multiple layers of carbon fibre. The honeycomb core can then be attached, followed by the inner layer. Afterwards, this must be vacuum bagged to minimise voids [7] before curing in an autoclave. Then the composite can finally be removed from the mould, before being attached to the other half [8].

A negative of a cut and fold chassis is that the complexity of the structure is limited due to bending the sheets into place. A mould on the other hand can be constructed with small intricacies on the surface, allowing greater aerodynamic detailing. However, this shouldnt be of major concern as the main aim is to gain structural performance as opposed to small improvements in shaping the surface.

2.2 Formula Student Rules and regulations

By Thomas Gough

Rules for the chassis are defined in section T of the FSAE rule [9] in the following sections:

- Monocoque main hoop (T3.35)
- Monocoque front hoop (T3.36)
- Cockpit Opening size (T4.1)
- Cockpit internal cross section (T4.2)
- Drivers seat positioning (T4.3)
- Floor close-out (T4.4)
- The firewall (T4.5)

2.2.1 Monocoque General Requirements

The main aim of the general requirements for a monocoque chassis is to prove equivalency to steel grade SAE/AISI 1010. To help with calculations, a spreadsheet entitled the Structural Equivalency Spreadsheet (SES). This must demonstrate the design is equivalent to a welded frame in terms of:

- Energy dissipation
- Yield and ultimate strength in
  - Bending
  - Buckling

- Tension

Furthermore, information must include:

- Material types
- Cloth weights
- Resin type
- Fibre orientation
- Number of layers
- Core material
- Layer-up technique

2.2.2 Inspections

Whilst not all aspects can be inspected at the event, the following should be possible to be confirmed by the technical inspector:

- Verification of main hoop outer diameter and thickness where it protrudes above the monocoque.
- Visual verification the main hoop goes to the lowest part of the tub locally. It can be integrated into the laminate.
- Mechanical attachment of main hoop to tub exists and matches SES at all points shown on SES.
- Visual or feel that front roll hoop is installed, and verify mechanical attachment against SES.

Items such as size and composition of front roll hoop, when integrally bonded to the monocoque, must be proven with documentation showing dimensions and inclusion in the layup.

2.2.3 Testing Requirements

The flexural rigidity of the monocoque must be calculated as the flexural rigidity of a flat plate with the same composition about the neutral axis of the laminate. Curvature of the panel and geometric cross section of the monocoque must be ignored in these calculations. Calculations not referencing T3.30 may take account of actual geometry of the monocoque.

A test panel measuring 275mm x 500mm, with the same design, laminate and fabrication as the monocoque side impact zone must undergo a 3 point bending test. It must have at least the same properties as two baseline steel impact tubes with the following properties:

Outside dimension x wall thickness for side impact structure:

- Round 1.0 inch (25.4mm) x 0.065 inch (1.65mm)
- or Round 25.0mm x 1.75mm metric

- or Round 25.4mm x 1.60mm metric
- or Square 1.00 inch x 1.00 inch x 0.047 inch

Bending and buckling strength calculations:

- Youngs Modulus: $(E) = 200GPa(29,000ksi)$
- Yield Strength: $(\sigma_y) = 305MPa(44.2ksi)$
- Ultimate Strength: $(\sigma_u) = 365MPa(52.9ksi)$

This must be reached for:

- Buckling Modulus
- Yield Strength
- Ultimate Strength
- Absorbed Energy

where the buckling modulus (flexural rigidity) is the product of the Young's Modulus E and area moment of inertia I. The absorbed energy is referred to as

Absorbed Energy: Teams are required to make an equivalent test with two side impact baseline steel tubes (SAE/AISI 1010) such that any compliance in the test rig can be accounted for and to establish an absorbed energy value of the baseline tubes. Baseline tubes must be tested to a minimum displacement of 12.7mm (0.5 inch). The calculation of absorbed energy will use the integral of force times displacement from the initiation of load to 12.7mm (0.5 inch). In addition, test panels for each ply schedule used in regulated regions of the monocoque, measuring 275mm x 500mm must have a 3 point bending test.[9]

2.2.4 Testing Equipment

The 3 point bending load applicator must be metallic with a radius of 50mm. It must overhang the test piece to prevent edge loading, and no material is allowed between the load applicator and items on test.

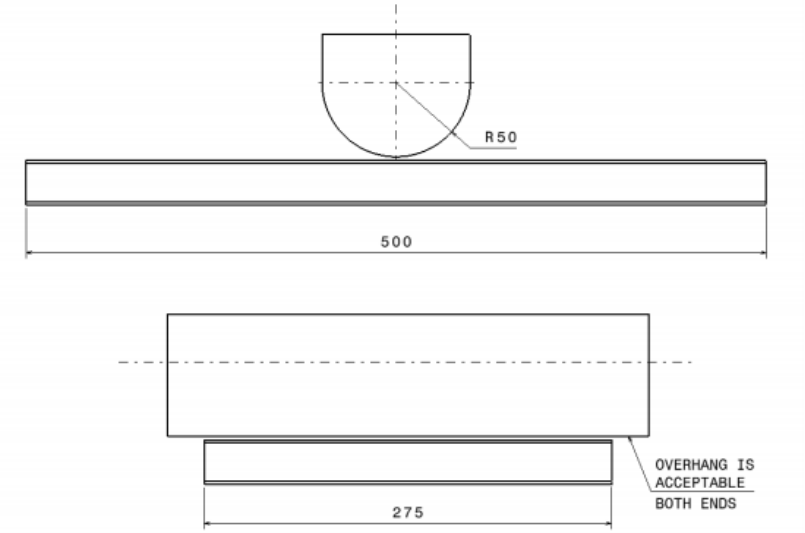

Figure 7: Visualisation of three point bending test with dimensions of load applicator.

The shear test load applicator must be completed by measuring the force required to push or pull a 25mm diameter flat punch through a flat laminate sample measuring at least 100mm x 100mm. This must have identical core and skin thickness to the monocoque and manufactured using the same materials and processes. The fixture must support the entire sample, except for a 32mm hole aligned co-axially with the punch. The sample cannot be clamped to the fixture.

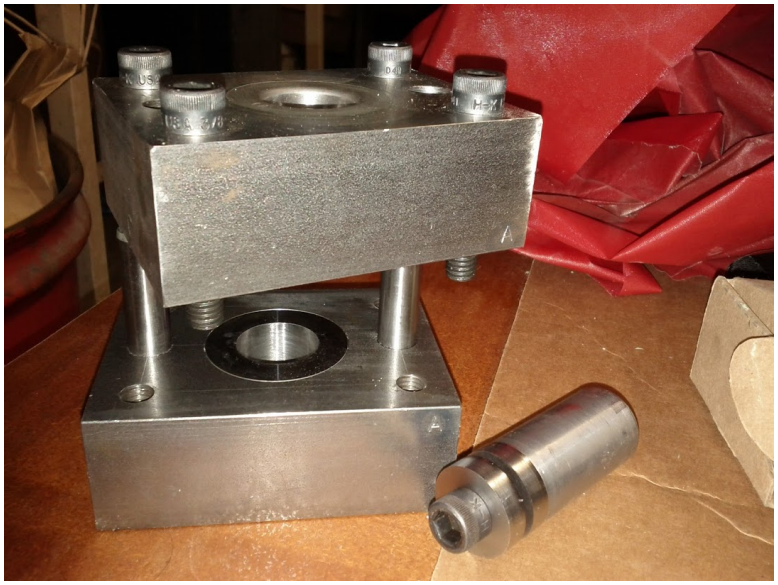

Figure 8: Example of a perimeter shear test applicator in open configuration.

The first peak in the load-deflection curve must be used to determine the skin shear strength this may be less than the minimum force required by T3.33.3/T3.34.4. The maximum force recorded must meet those requirements. (The edge of the punch and hole in the fixture may include an optional fillet up to a maximum of 1mm.)

2.2.5 Roll Hoop and Attachments

The main roll hoop must be constructed of a single piece of uncut, continuous, closed section steel tubing and extend to the bottom of the monocoque. There must be attachment points at the top and bottom and at intermediate locations, whilst mounting plates welded to the hoop must be a minimum of 2.0mm thick steel.

The front roll hoop is prohibited from being constructed of composite material. The attachment must comply with T3.40, although fully laminating it within the monocoque is acceptable. This must be equivalent to at least 4 mounts compliant to T3.40. Adhesive must not be the sole method of attachment.

In any direction, each attachment point between the monocoque and the other primary structure must be able to carry a load of 30kN. The laminate, mounting plates, backing plates and inserts must have sufficient shear area, weld area and strength to carry this in any direction. Each attachment point requires a minimum of 2 8mm Metric Grade 8.8 bolts.

Although there are also regulations for the strength of the attachment points, this will not be a major factor of the monocoque structure. It must be tested through a required load being applied to a representative attachment point with the proposed layup and attachment bracket.

2.3 Designing a chassis for a Formula Student car

By Thomas Rickard

Designing a race car starts with the tyres. Once the tyres are chosen and all relevant data is known the suspension is designed to make best use of them depending on what the team wants from the car in terms of vehicle dynamics. The chassis is then designed around these suspension points, powertrain unit and the drivers cell. It is used to interlink all the component that make up a race car and transfer the loads effectively.

2.3.1 Primary aims of chassis design

A typical track at a formula student event is tight and twisty with cars often averaging around 35 mph. This type of track used lends itself to specific suspension geometry. Short-long arm suspension is almost always used as it offers good performance. [10, p.627] Parameters such as caster, camber and king-pin angle are optimised for the desired handling characteristics and this helps resolve the location of the chassis connections.
One of the most import characteristics of a chassis is its torsional stiffness. Torsional stiffness is a measure of the resistance provided by the chassis to twisting. A stiff chassis is key to be able to design and predict the handling characteristics through the suspension and steering systems. When a chassis is relatively flexible its ability to control lateral load transfers is unpredictable and so difficult to set up and control. Lateral load transfer is the transfer of load from the inside wheels to the outside wheels. [10, p.678]
Formula student cars often use the engine as a stressed member to improve torsional stiffness while reducing weight. As a general idea of stiffness, a normal road car will range from 5000 to 13000

Nm/deg where as a Formula one car will typically be 15000Nm/deg and above. Space frame chassis can be stiffened by the use of triangulation to minimise tubes being placed in bending. Composite stressed skin chassis potentially offer the stiffest solution for a given weight. [2:679]

2.3.2 SUFST chassis design

The current design uses steel tubes arranged to produce a space frame. The chassis was designed to be simple to build as it was the first time it was produced in house. As such a flat floor was used along with relatively simple triangulated geometry. FEA showed a stiffness of 800Nm/deg was achieved. This has not be validated by any experimental data.

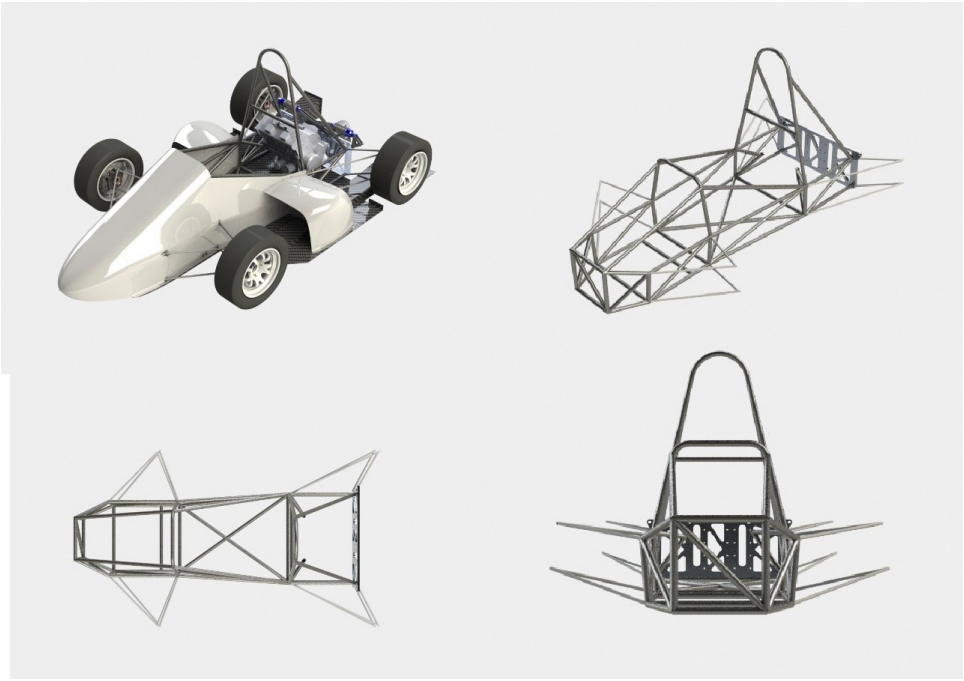

Figure 9: The SUFST 2013/14 car.

A shear plate has been used to create a shorter chassis giving a more responsive and centralised mass distribution [11]. It also forms mounting points for several systems including frame, suspension and the differential eliminating the need for extra brackets. This reduces the overall weight and cost. The structure also enables easy access to the engine. The notable areas of possible improvement are weight and stiffness.
Some possible design implications of a monocoque are:

- A composite chassis made using the cut and fold method places some restriction on suspension mounting points as panels are flat.
- When considering a monocoque design it must be remembered that bodywork panels are no longer needed, this naturally reduces weight.

2.4 Suspension and steering considerations

By Thomas Rickard

When designing a Formula Student chassis, suspension and steering hardpoints play a major role in the shape and strength required in certain areas. Although the suspension and steering geometry will not be considered in huge detail and optimised it must be thoroughly accounted for in order to create a realistic design with appropriate load paths. Limitations a cut and fold composite chassis has on suspension design will be the primary focus of the research.

Chief judge of FSAE Australasia and Germany, Pat Clarke has written many technical articles detailing FS car design. In one he describes beneficial suspension and steering characteristics and parameters for a FS car [12]. It describes the following as beneficial:

- Camber control when the chassis rolls is critical.
- Camber gain at the suspension is desirable but the effects of King Pin Inclination (KPI) and Caster should be taken into account.
- Good design have lots of caster but not much KPI.
- Bump steer should be avoided and tested for after any design changes.
- A large amount of positive ackerman is good.
- Camber should never go positive on a loaded wheel while cornering.
- Roll steer is not wanted.
- Stiff suspension rates, aggressive anti dive and anti squat geometry are not needed (unless making use of aerodynamics) and compliant suspension rate may provide more mechanical grip if wheel angles are controlled.
- Design should ensure good control of the roll centres.

2.4.1 Suspension Design

The 3 dimensional geometry can be broken down into two 2 dimensional problems, referred to as the front and side views. These two views can be designed separately and brought together at the end with minimal modifications to give a good basic design. Only Short-Long-Arm (SLA) suspension will be looked at as this is almost exclusively used for all FS cars and provides the best performance. Only double wishbone suspension is considered in this case rather than multi-link due to its relative simplicity and ease of modelling. General parameters to be considered in suspension design are:

- Camber
- Caster
- King Pin inclination
- Offset
- Scrub radius and motion
- Instantaneous centres
- Roll centres and axis

- Anti dive and anti squat
- Dynamics movement of all of the above

2.4.2 Wheel side geometry

Reference [10] was consulted for wheel side geometry packaging. When designing suspension the tyres and wheel are considered first. Track width and wheelbase is usually decided based on the rules. For the SUFST cars these are normally a 1300mm track and 2800mm wheelbase. The wheel offset is determined by the brake size and usually kept as low and far outboard as possible. Next comes the kingpin angle and upper ball joint location. These can be decided either by requiring a certain scrub radius or kingpin angle. The kingpin angle and scrub radius will affect the cars steering. Caster can then be added to modify the effect of the kingpin angle. Generally caster causes favourable negative camber gain on the outside wheel during cornering. Figure 10 below shows the geometry referred to.

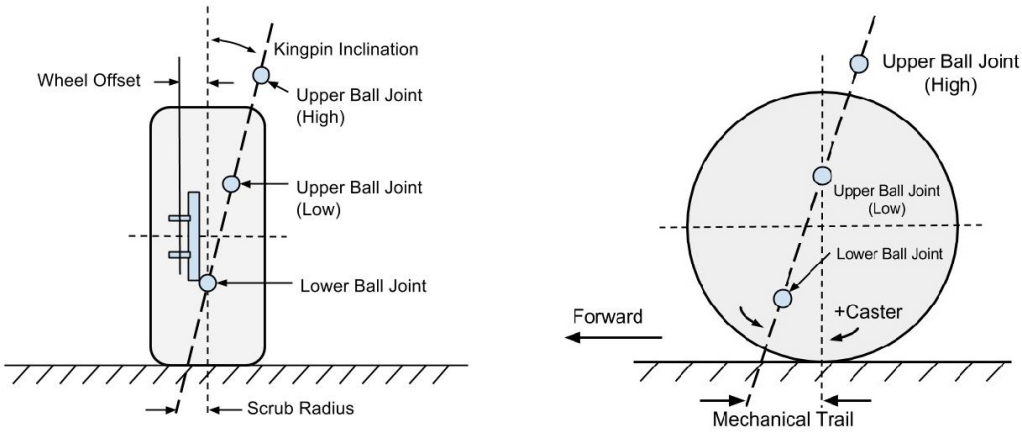

Figure 10: Front and side view of upright geometry.

2.4.3 Front View

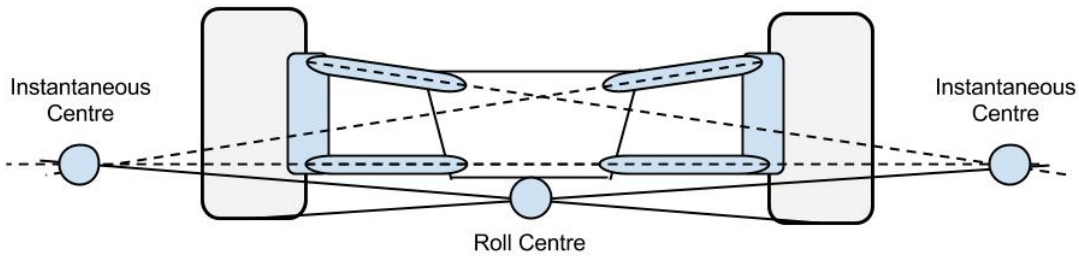

Figure 11: Front view of geometry.

Geometry in the front view determines the camber rate change, scrub motion, steering characteristics and the roll centre. The instant centres (ICs) are points found by projecting lines from the linkages. Projecting another line from the IC to the centre of the contact patch defines the roll centre.

Camber changes affect the amount of traction a tyre can produce. It is import to keep the tyre as upright as possible in order to maximise the traction available. This means the camber should resist change when the sprung mass is displaced vertically or the wheel is displacement by a bump. Realistically the camber will change under these conditions and it should be noted that negative camber is far more acceptable than positive camber which greatly reduces the performance of the tyre [13]. With SLA suspension camber rates can be changed by varying the upper control arm length. Longer control arms also reduce the amount of camber induced.

The roll centre is important because it acts as the force coupling point between the unsprung and sprung masses. The larger the distance between the Centre of Gravity (CG) and the roll centre the greater the force on the spring and damper system. The location also determines the vertical displacement of the sprung mass; if above ground the rolling moment causes the sprung mass to be lifted (jacked up), when below ground the sprung mass is pushed down [10][Chapter 17]. Rather than view the front and rear roll centres separate and compared them to the CG it can be beneficial to view the roll axis. This is created by joining the front and rear roll centres by a line. Another more appropriate and realistic way of view the CG in relation to the roll axis is to draw the mass centroid axis. The figure below shows these axes.

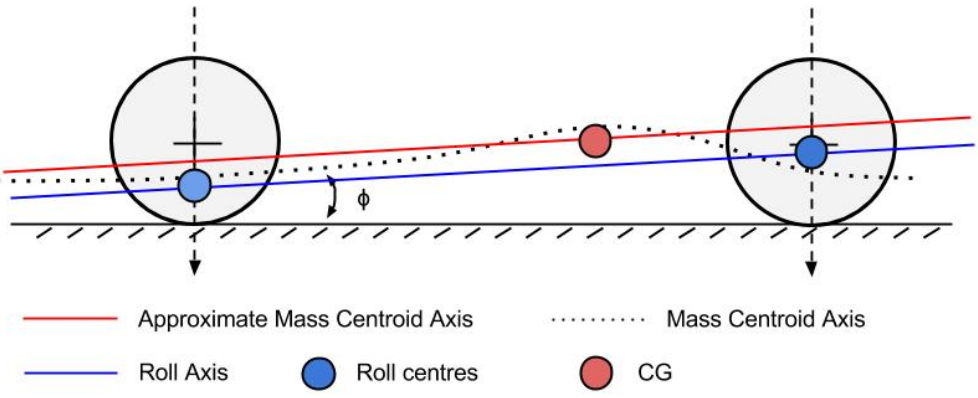

Figure 12: Roll axis.

According to [13][chapter 3] the roll axis should be located parallel to the mass centroid axis so the front and rear roll couples are roughly equal. This helps create linear front and rear roll generation as well as similar lateral load transfer rates making the vehicle neutral and predictable. These roll couples can later be tuned by the use of anti-roll bars.

Scrub motion is the horizontal movement of the contact patch that results from vertical movement of the wheel. It effectively changes the front and rear track widths (at the contact patch) and disturbs the tyre adhesion reducing traction. Ensuring the camber goes negative during vertical displacement greatly reduces scrub.

2.4.4 Side view

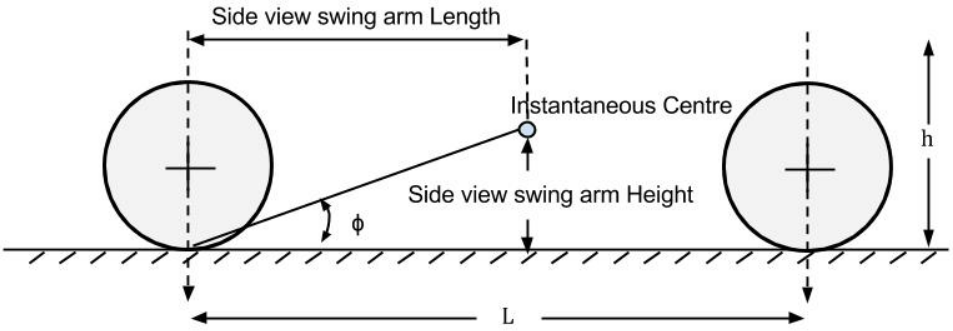

Figure 13: Side view geometry.

Geometry in the side view deals with the forward and rearward forces and motion. It is typically used to provide anti dive and anti squat characteristics reducing the pitching effects under braking and acceleration. The reduced pitching prevents camber changes and scrub motion, preventing traction loss. It should be noted that the use of anti features does not affect the longitudinal load transfer. The percentage anti dive/squat can be calculated

$$antidive/squat = (\%front/rearbraking)(tanF/R)(\frac{L}{h})$$

According to [13] although seemingly beneficial anti features have the effect of stiffening the suspension momentarily under braking/acceleration making it less able absorb bumps. This results in reduced tyre contact with the ground (compliance) and less traction. [13] Suggests that a maximum of 30% anti dive 20% anti squat should be used to avoid tyre compliance issues.

2.4.5 Formula Student suspension requirements

The Formula Student competition imposes certain operational conditions on the cars and these help determine some of the suspension parameter that will work well. The cars generally have a high power to weight ratio. Little aerodynamic force is generated and the cars are restricted to low speed, tight and twisty runs. The competition is held on the main Silverstone track which has a relatively smooth surface. The important performance characteristic are therefore good agility/balance and acceleration out of corners. Good agility/balance can be created by ensuring the roll axis is parallel to the mass centroid axis and moves very little. The front and rear roll centres should move together and remain predictable. To enable good acceleration out of corners the camber must not vary much under squat. The squat could also be limited by using anti squat geometry.

2.5 Structural analysis and FEA

By Antons Kasjanics

To verify whether the chassis structure will be able to withstand the required loads, two approaches

were be used: numerical analysis and testing. Firstly, numerical analysis was carried out to verify whether the structure fails or not under the prescribed loads, which then will be confirmed by testing. The numerical analysis will be carried out by a Finite Element Analysis (further referred as FEA) software package MSC Patran/Nastran.

Finite Element Analysis (FEA) was developed in 1943 by Hrennikoff and Courant. The initial work towards developing numerical analysis can be traced to Rayleigh, Ritz and Galerkin. FEA had its limitations due to the limited computer power, but with the current supercomputer power accurate results can be obtained for a variety of problems.

FEA consists of a computer model, which is separated into small sectors called elements. Each has a finite number of nodes, through which it is connected to other elements. All elements together are called a mesh. Verb to mesh is also used to show the process of dividing a whole model into smaller elements. To simplify the calculation process, the stress distribution across each element is assumed according to the necessity linear, quadratic, etc. Material properties are also defined within the application. The displacements at each node of each of the element and the applied loads are then transferred into a matrix equation, which can then be easily solved by the computer to give the displacements at each node. Stresses in an element can be then calculated through the stress-strain relationship. Provided that the elements are small enough to represent the problem, results acquired will be accurate. The mesh should be denser around regions of predicted high stress and may be coarsened where the stress levels are lower.

For this project the analysis software used, as mentioned before, will be MSC Patran for pre- and post-processing with the MSC Nastran solver. Three software packages were considered before before a conclusion was made: ANSYS Mechanical, DS Solidworks Simulation package and MSC Patran/Nastran.

The following three criteria were used to make decision: User-friendliness, accuracy of methods used and possibility to model composite materials. MSC Patran and DS Solidworks have a user friendly graphical interface, whereas ANSYS Mechanical is heavily command based. Both ANSYS Mechanical and MSC Nastran are widely used in industry, whereas DS Solidworks simulation package is yet to get recognition, if ever. In both DS Solidworks and ANSYS Mechanical composite laminate modelling, if possible, is tedious and not well understood, which is straight-forward in MSC Patran. Also, the Nastran solver was developed in the 1960s to be used by NASA (NASA STRucture ANalysis) and is still very widely used in the aerospace industry. Therefore the choice.

2.6 Project organisation and costing

Initially every group member was tasked to do some research into an area of composite chassis and Formula Student. Training was to be given to half the group for testing and half the group for manufacturing. Two of the group members were trained in both manufacturing and testing so there was some overlap. The project was split up into 3 design stages. This was done due to the iterative nature of the design and testing work. Figure 14 shows an top level flow diagram of the project. Initial designs and tests were carried out in stage 1 and refined in stage 2. Later sections of stage 2 and stage 3 tackled more the more tricky work on inserts and joints after experience had been gained manufacturing and testing bending and shear panels.

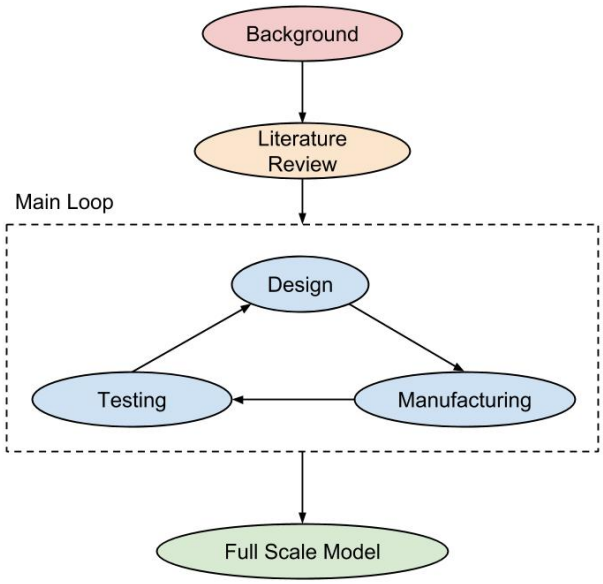

Figure 14: Project flow diagram

A broken down table of expenditures is given in Appendix C.

3 Design: Stage 1

This section looks at the initial design calculations for sandwich panels, using basic theory and later correlating FEA results to the first round of specimen tests. Initial chassis design concepts are also discussed.

Deals with initial design and testing of sandwich panels for 3 point bending and punch test

3.1 Initial steel tube calculations

By Thomas Gough

As stated in Article T3.5.3, if alternative materials are used, calculations for the chosen material must be provided which demonstrate equivalence to the minimum requirements found in Article T3.4.1, as can be seen in Section 2.3.3.

For the side impact structure, the flat sandwich panel must exceed the performance of two baseline steel tubes (SAE/AISI 1010). The following properties are known for a single tube (it should be noted the tubes available had an wall thickness of 1.63mm as opposed to 1.60mm or 1.65mm):

Property	**Value**
Young's Modulus E	200GPa
Yield Strength	305MPa
Ultimate Strength	365MPa
Outer Diameter Do	25.4mm
Wall Thickness t	1.63mm
Inner Diameter Di	22.14mm
Outer Radius y	12.7mm
Pipe Length L	0.5m
Support Length l	0.4m

Table 1: Properties of AISI/SAE 1010 Steel Tube used in side impact zone equivalency calculations.

The flexural rigidity, (known as the buckling modulus in the regulations) is defined as EI, where E is the Young's modulus of the material and I the area moment of inertia. For a hollow cylinder this is given by

$$I = (\frac{\pi}{64})(D_o^4 - D_i^4) \tag{1}$$

Using the known diameters and the Young's modulus given in Table 1 this gives a flexural rigidity of 3455Nm^2 for two steel tubes.

As carbon fibre is a brittle material, the material is not expected to yield before component failure. Because of this only the ultimate tensile stress is considered in calculations. The force at this stress can be calculated through simple bending theory, with the bending moment given from a particular stress as

$$M = \frac{\sigma I}{y} \tag{2}$$

giving an ultimate bending moment 496.5Nm for two tubes. The bending force is then derived with

$$F = \frac{2M}{l}. \tag{3}$$

Knowing the force in the three point bend test is in the middle of the 0.4m support, this gives an ultimate bending force of 4965N for two tubes.

3.2 Effect of core thickness

By Thomas Gough

To investigate the effect of increasing the core thickness, the calculations required to deduce the sandwich panel performance was undertaken with a simplified composite facesheet, assuming a single lamina and isotropic properties. The flexural rigidity of a sandwich beam is the sum of the rigidities of faces and cores measured about the neutral axis [14], giving

$$(EI)_{eq} = \frac{E_f t b^3}{6} + \frac{E_f t b d^2}{2} + \frac{E_c b c^3}{12} \tag{4}$$

Due to the facesheet thickness and the Young's Modulus of the core being much smaller than the core thickness and the Young's Modulus of the facesheet, this can be simplified to

$$(EI)_{eq} = \frac{E_f t b d^2}{2}. \tag{5}$$

To compare the effect of varying both thicknesses, a simple analysis of the effect of changing the skin thickness was undertaken with a single type of carbon fibre, in this case Toray T700S with a Young's modulus of 135GPa [15]. Below shows the required skin and core thicknesses to meet the flexural rigidity of 3455Nm^2 under the side impact zone requirement, assuming an isotropic skin material made of one lamina with no matrix material:

Core Thickness (mm)	**Skin Thickness (mm)**
19	0.5
10	1.5
5	3

Table 2: Example of variation in core and skin thickness required to meet necessary flexural rigidity.

As carbon fibre is much more expensive than the material used in the core, increasing the core thickness will therefore decrease the number of lamina needed, reducing costs. For the initial designs an aluminium honeycomb core was used. Of the thicknesses on offer the thickest was chosen, in this case 20mm.

"The usual objective of a sandwich design is to save weight, increase stiffness or use less of an expensive skin material, or all three. [16]

As the above supports, with a limited budget, reducing the amount of carbon fibre that needed to be purchased, whilst still meeting the structural requirements was key. An effective way of raising the flexural rigidity without using additional carbon fibre layers is to increase the distance of the two

facesheets from the neutral axis d. In doing so, a larger area moment of inertia and therefore flexural rigidity can be achieved, which as shown in equation 5 is proportional to the square of d. The effect of increasing the core thickness and the corresponding change in cost and relative increases in mass, stiffness and bending force in comparison to no core is shown in Table 3.

Core Thickness (mm)	**Relative Mass**	**Relative Stiffness**	**Relative Bending Force**	**Cost of Core Thickness**
0	1	1	1	0
1	1.009	9	3	0.484
5	1.046	121	11	2.42
10	1.093	441	21	4.84
20	1.185	1681	41	9.68

Table 3: Relative performance of a sandwich panel with varying core thickness compared to no core. Cost is based on honeycomb core material used.

3.3 Failure modes

By Thomas Gough

Whilst calculating the deflection at the midpoint of a three point bending panel, the contribution created by shear of the core material has to be considered as well as the bending deflection if a low density core is used [17]. This creates a deflection

$$\delta = \frac{FL^3}{48(EI)_{eq}} + \frac{FL}{4(AG)_{eq}} \tag{6}$$

where $(EI)_{eq}$ is the same as in equation 5. $(AG)_{eq}$ is the equivalent shear rigidity and is equated to

$$(AG)_{eq} = \frac{bd^2G_c}{c} \approx bdG_c \tag{7}$$

if the facesheet thickness is small compared to the core thickness. The corresponding values of deflection with and without the shear deflection could be calculated once the core and skin materials were deduced.

Four main failure modes have been identified in three point bending. These are usually classified between skin failure, which includes the failure mechanisms face yield (microbuckling) and skin wrinkling, and core failure which includes core shear and local indentation [18].

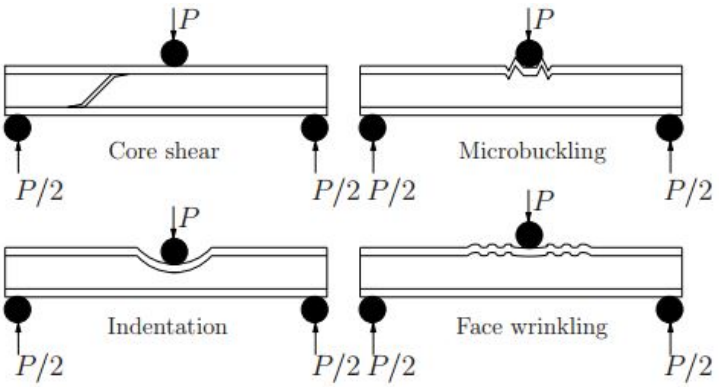

Figure 15: Failure modes of a sandwich panel in three point loading.

The required loads to meet the failure modes were calculated once tests were completed, with all modes required to give a load greater than the 4965N ultimate bending force of the two steel bars.

These four modes are highlighted in Figure 15. Other failure modes exist when using honeycomb cores which are based on the unsupported regions of the skins due to the cell size, which would be considered if a honeycomb core was used. The equations used below are approximate but can be used for minimum weight design studies and failure mechanism maps.

3.3.1 Face yield

Face yielding occurs on the top facesheet due to the axial stress reaching the in-plane strength. For a symmetric panel the stress will be the same in both tension and compression faces, with the compressive face usually the critical one [17]. Ignoring the contribution of the core gives the maximum force of

$$F = \frac{4bdt_f\sigma_f}{L}. \tag{8}$$

Including the shear deflection of the core and this load becomes

$$F = \frac{4t_f\sigma_f\zeta}{L} \tag{9}$$

where ζ is dependent on the facesheet thickness [17]

$$\zeta = \frac{\theta(\frac{t_f^5}{9} + \frac{t_f^3d^2}{3})}{\frac{ht_f^3(\theta-1)}{3} + \frac{t_f^4}{3} + t_f^2d^2} \tag{10}$$

and θ is reliant on the out-of-plane shear modulus of the core and stiffness of the facesheets in in-plane loading [17]

$$\theta = \frac{L}{c}\sqrt{\frac{G_cc}{2E_ft_f}(1 + \frac{3d^2}{t_f^2})}. \tag{11}$$

In realirt the fibre microbuckling strength is degraded by the multi-axial stress state created underneath the load applicator [18]. σ_f should therefore be taken as an approximate value.

3.3.2 Skin Wrinkling

Skin wrinkling is a local elastic instability, and can be seen as the buckling of the beam in axial compression supported on an elastic foundation.

$$F = \frac{2bdt_f}{L}(E_f E_c G_c)^{\frac{1}{3}} \tag{12}$$

A factor of 2 used because of assumed geometrical imperfections in the facesheet to create a conservative estimate [18]. If a honeycomb core is used it is associated with the cell size (known as intra-cell dimpling) [17].

3.3.3 Core shear

Whilst it used to be believed the core collapsed at a uniform shear strength τ_c, giving the equation

$$F = 2bd\tau_c \tag{13}$$

it is now known the facesheets provide additional strenth. As shown below

$$F = 2bd\tau_c + 8E_f b(\frac{t_f}{L})^3\delta \tag{14}$$

additional strength is only attained with weak facesheets which develop 'plastic hinges, giving plastic deformation and increasing the collapse load. With strong facesheets and elastic bending however, little deflection is achieved and the process can be ignored. This will be discovered later [18].

3.3.4 Local indentation

Failure in this case is due to the core crushing under the indenter, with the skin bending stiffness and core stiffness determining how the load is spread at the point of application [17]. An approximate value of the indentation load is used based on Soden (1996), [18] whereby an elastic beam with plastic foundation gives an load which varies with indentation depth u as

$$F = \frac{4}{\sqrt{3}}(\frac{2}{3})^{\frac{1}{4}} b t_f^{\frac{3}{4}} \sigma_c^{\frac{3}{4}} E_f^{\frac{1}{4}} u^{\frac{1}{4}} \tag{15}$$

where u is assumed to be the displacement of the load applicator.

3.4 Classical Lamination Theory Code

By Thomas Rickard/Thomas Gough

A piece of code (Appendix A.1) was written to calculate the Young's Modulus in the in-plane direction during tension. The flexural rigidity could then be calculated using the known geometric properties and equation 5, meaning certain laminate layups could be checked against the required $3455Nm^2$. An example from [19] was used as a starting point. First the properties of the fibre and matrix materials were applied, to which the macromechanical properties could be calculated using the fibre ratio specified. The code could then be compared to tensile test speciments created later to deduce the quality of the manufacturing process, with any voids and defects reducing the Young's Modulus and increasing the error.

From equation 6 the only value unknown at this point is the Youngs modulus of the facesheet E_f and the deflection. The effective stiffness of the laminate facesheet can be determined using Classical Laminate Theory.

Assuming the facesheets are orthotropic, this reduces the necessary number of elastic constants from 81 for a general anisotropic material to four. These are the Youngs moduli E_1 and E_2, the shear modulus G_{12} and the Poisson's ratio ν_{12}. The stiffness matrix in reference to the principal axes for each ply can be written as:

$$\begin{bmatrix} \sigma_1 \\ \sigma_2 \\ \tau_6 \end{bmatrix} = \begin{bmatrix} Q_{11} & Q_{12} & 0 \\ Q_{12} & Q_{22} & 0 \\ 0 & 0 & Q_{66} \end{bmatrix} \times \begin{bmatrix} \epsilon_1 \\ \epsilon_2 \\ \gamma_6 \end{bmatrix} \tag{16}$$

The terms shown above are defined as:

$$Q_{11} = \frac{E_1}{1 - \nu_{12}\nu_{21}} \tag{17}$$

$$Q_{12} = \frac{\nu_{21}E_1}{1 - \nu_{12}\nu_{21}} = \frac{\nu_{12}E_2}{1 - \nu_{12}\nu_{21}} \tag{18}$$

$$Q_{22} = \frac{E_2}{1 - \nu_{12}\nu_{21}} \tag{19}$$

$$Q_{66} = G_{12} \tag{20}$$

Individual stiffness matrix terms are calculated for each layer or ply in the facesheet in their local co-ordinates. This terms are then transferred from the principal fibre directions to the global coordinate system. The global stiffness matrix can then be calculated using the following equations:

$$A_{ij} = Q_{ij}^k(h_k - h_{k-1}) \tag{21}$$

$$B_{ij} = Q_{ij}^{k}(h_k^2 - h_{k-1}^2) \tag{22}$$

$$D_{ij} = Q_{ij}^{k}(h_k^3 - h_{k-1}^3) \tag{23}$$

Where A is the extension stiffness matrix, B is the coupling stiffness matrix, D is the bending stiffness matrix, h_k is the distance between the layers centroid and the laminate centroid and Q_{ij} is the material properties in the global coordinates. This results in:

$$\begin{bmatrix} N_x \\ N_y \\ N_{xy} \\ M_x \\ M_y \\ M_{xy} \end{bmatrix} = \begin{bmatrix} A_{xx} & A_{xy} & A_x s & B_{xx} & B_{xy} & B_{xs} \\ A_{yx} & A_{yy} & A_{ys} & B_{yx} & B_{yy} & B_{ys} \\ A_{sx} & A_{sy} & A_{ss} & B_{sx} & B_{sy} & B_{ss} \\ B_{xx} & B_{xy} & B_x s & D_{xx} & D_{xy} & D_{xs} \\ B_{yx} & B_{yy} & B_{ys} & D_{yx} & D_{yy} & D_{ys} \\ B_{sx} & B_{sy} & B_{ss} & D_{sx} & D_{sy} & D_{ss} \end{bmatrix} \times \begin{bmatrix} \epsilon_{xx} \\ \epsilon_{yy} \\ \epsilon_{xy} \\ k_{xx} \\ k_{yy} \\ k_{xy} \end{bmatrix} \tag{24}$$

The elastic modulus is then found by calculating:

$$E_x = \frac{1}{h}\left[A_{xx} - \frac{A_{xy}^2}{A_{yy}}\right] [20] \tag{25}$$

Whilst the code was used as a simple approximation of the Young's modulus, some effects could not be taken into consideration. One of these is that different layers could not be assigned different properties such as tensile strength or elastic modulus. Another was that woven fabrics could not be applied. If a woven fibre were to be used, it would be treated as a biaxial fibre and split into two layers of the constituent orientations with half the thickness.

Table 4 shows some of the fibres available and their mechanical properties

Product	Details	Fibre	Strength (MPa)	Modulus (GPa)	Thickness (mm)
CF 2/2 Twill	199g	Pyrofil TR30S 3K	4410	235	0.11
CF 2/2 Plain	200g	Pyrofil TR30S 3K	4410	235	0.11
CF 2/2 Twill	450g	Grafil 34-700-12K	4830	234	0.25
CF Spread Tow Plain	160g	Pyrofil TR50S 15K	4900	240	0.08
CF Unidirectional	100g	Pyrofil TR50S 15K	4900	240	0.05
CF Unidirectional	250g	Toray T300	3530	230	0.14
CF Biaxial +/-45	300g	Toray T700	4900	230	0.17
CF Biaxial +/-45	410g	Toray T700	4900	230	0.23

Table 4: Carbon fibre considered to be bought for use in facesheets.

3.4.1 Limitations of Classical Lamination Theory

Whilst some limitations were met in modelling the laminate, Classical Lamination Theory also has limitations. One of these is that it is based on the Kirchhoff-Love hypothesis. This assumes that

- straight lines perpendicular to the mid-surface before deformation are also straight afterwards.
- transverse normals do not experience elongation.
- transverse normals rotate such that they remain perpendicular to the mid-surface after deformation.

This last point in particular means the transverse shear strains are not addressed and are equal to zero. These are required for the prediction of delamination. Whilst this can be estimated by the integration of equilibrium equations this has not been implemented for the code [21].

An additional assumption is that perfect bonding occurs, whereby a bond with no gaps between the lamina is created which is non-shear-deformable and acts as a single lamina [22]. In reality, defects and limitations would reduce the effectiveness of the laminate. This also ignores interlaminar stresses due to assuming no gaps between the lamina.

Classical Lamination Theory is therefore only a good approximation when the plate is thin, with thicknesses roughly ten times smaller than the spans. Due to this, finite element formulations for composite plates are rarely based on Kirchoff-Love plate theory. Instead the Reissener-Mindlin theory for 'thick' plates can be used as found in First-Order Shear Deformation Theory (FSDT) for laminated composite plates, whereby the transverse normals are allowed to rotate, meaning they do not remain perpendicular to the mid-surface after deformation. This means the transverse shear strains γ_{xz} and γ_{yz} are included [23].

Whilst this is the case, the code used based on CLT is only used to determine the Young's Modulus of the facesheet in the x-direction. This value is then used to determine the flexural rigidity, making CLT an adequate tool to gain an approximate value of the stiffness of the facesheets.

3.5 Design and manufacture of test rigs

By Joe Edwards

Three tests were specified in order to validate the sandwich panels structural integrity. This section will detail the; test requirement, design requirement, final designs and analytical validation of the test equipment. There are two specified tests required to satisfy the Formula Student equivalency regulations, these are three point bending and shear tests [9]. Additional testing of the chassis curvature and inserts was to also be undertaken.

3.5.1 Bending test rig

For the three point bending test the sandwich panel must be simply supported at two points 400mm apart, with the center of the supports matching the center of the panel. A 100mm diameter cylinder is then to be pressed evenly under load into the center of the panel, with the cylindrical axis perpendicular to the longest length of the material. According to the '2015 Formula SAE Rules' section T3.31.1 states '*the same properties as two baseline steel side impact tubes for buckling modulus, yield strength, ultimate strength and absorbed energy*' the test rig must therefore be able to test two steel tubes for an equivalency test in addition to the panel.

To satisfy the design criteria the test rig must accurately position the simple pivots, in addition to the central load applicator. Due to the high loads that will be experienced its essential that no component fails and should any part fail, back up mechanisms are in place to ensure safety to all parties and reduce the risk of damaging the other equipment.

Figure 16 shows the rig is hydraulically clamped into place, a housing with four supporting M5 bolts then shrouds the load applicator. The bolts themselves contain the applicator should buckling occur in addition to taking its weight; this removes any pre-load on the panels or bars due to the weight of the applicator itself increasing the simplicity of the analysis. The supporting pivots were positioned using vernier calipers and pencil markings, the position of the supports are therefore accurate to the thickness of the pencil marking, in addition to the machining inaccuracy of the pivot base. This would give minimal inaccuracies relative to the dimensions of the whole rig.

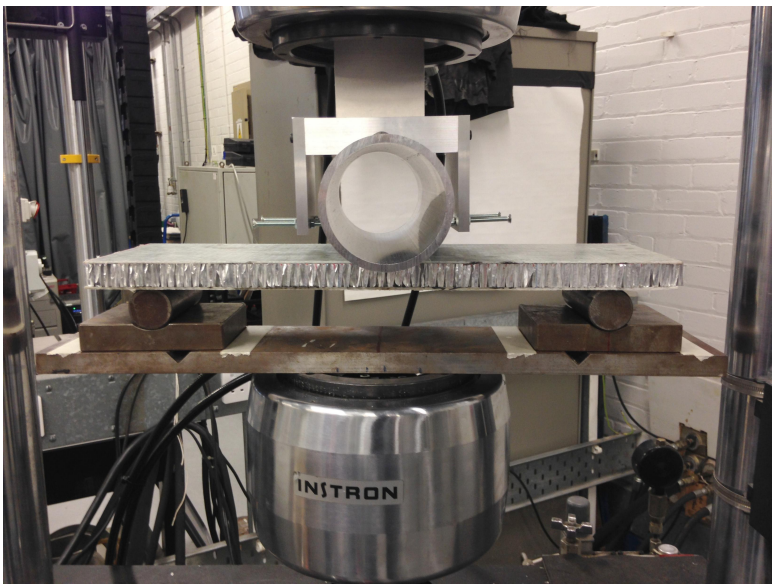

Figure 16: 3 point bending rig with GF-H-3-B panel.

The structural validation of the design was carried out to ensure no component failed, in addition

to the overall deflection of the test rig being minimal relative to the deflection of the test panel, as not to effect the results. The effect of the test rig equipment deflecting would act to decrease the accuracy of the load displacement outputs, as the displacement would be of the rig and panel, as opposed to just the panel itself as the outputs suggest.

Due to the complex geometry of the test rig components, Finite Element Analysis was used to analyse the stress distribution and deflections. This uses the same method and solver as that seen in the Chassis analysis. The simulations involved applying the full load through each component, constrained in such a way to ensure it experienced forces similarly to how it would in the whole assembly. The maximum stress concentration and deflections are seen below. The Tensile Yield Strength is used for the safety factor, as any permanent deformation would render the rig equipment unusable, as such this is the important value. A Tensile Yield strength (TYS) of 414Mpa was used for the Aluminium 2014 [24]. The whole assembly deflection as a result of the 4000N load was 0.025×10^{-3}, which equates to 50.7×10^{-3}% of the 50mm maximum possible deflection as defined by the rig.

Component	**Deflection**	**Maximum Stress concentration (MSC)/MPa**	**Safety Factor (TYS/MSC)**
Gripping Plate	$1.48 \times 10^{-}3$	1.78	233
Notched Panel	$6.67 \times 10^{-}3$	14.00	30
Load Applicator	1.7×10^{-2}	8.64	49
Whole Assembly	0.025×10^{-3}	N/A	N/A

Table 5: Deflection and stress concentration on the bending test rig.

3.5.2 Shear test

For the shear test, the sandwich panel must be fully supported in such a way, as to allow for a 25mm diameter punch to be pushed through the whole panel. According to the '2015 Formula SAE Rules' section T3.31.5 states '*The fixture must support the entire sample, except for a 32mm (1.25) hole aligned co-axially with the punch. The sample must not be clamped to the fixture*'. The test will therefore require a container for the sample with an appropriate cut out, in addition to a punch that can be clamped into the machine.

The shear rig itself is shown in figure 17, the 'box' contains the sample with every face supported to prevent any unwanted movement of the sample except for the 32mm cut out. The lid is fastened using four M5 bolts, this supports the sample in addition to reducing any harmful debris that is produced when the panel fails. This is hydraulically clamped into the machine and remains static. The shear punch is clamped into the actuator and is driven through the sample. A cut out exists on both sides of the rig to ensure the punch doesn't go through the sample and subsequently damage the rig itself.

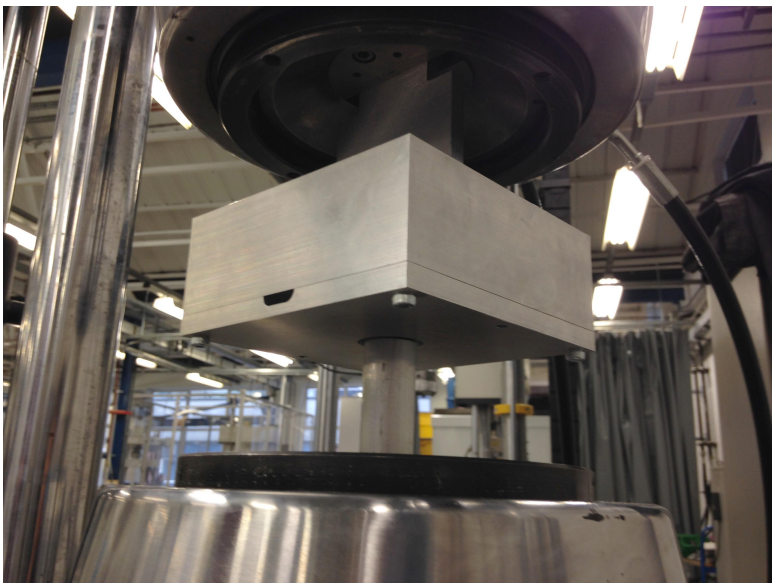

Figure 17: Shear testing rig

Similarly to the Three Point Bending test, the maximum load required by the 2015 Formula SAE Rules, section T3.33.3 [9], of 4000N was applied to each component in the same manner that it will experience during the test. This yielded the following results;

Component	**Deflection**	**Maximum Stress concentration (MSC)/MPa**	**Safety Factor (TYS/MSC)**
Gripping Plate	$1.48x10^{-}3$	1.78	233
Recessed Box	$6.67x10^{-}3$	14.00	30
Top Plate	Nil	Nil	Nil
Shear Punch	9.54×10^{-3}	22.1	18.7
Whole Assembly	$17.69 \times 10^{-}3$	N/A	N/A

Table 6: Deflection and stress concentration on the shear test rig.

The whole assembly deflection as a result of the 4000N load was $17.69x10^{(} - 3)$ mm, which equates to $6.32x10^{(} - 2)\%$ of the 28mm maximum possible deflection as defined by the maximum panel thickness. This is again far too small to have a significant impact on the accuracy of the results.

3.6 Manufacturing Sandwich Panels

By Thomas Rickard

3.6.1 Resin Infusion

There are many different ways of manufacturing fibre reinforced plastics. Some of the most common processes that could be used to manufacture flat panels are:

- Wet layup with/without vacuum bag
- Resin Transfer Moulding (RTM)

- Prepreg - Autoclave Cured
- Out Of Autoclave (OOA) Prepreg - Oven Cured

The best results are often achieved using an autoclave. Although the group did have access to an autoclave which was large enough to cure smaller specimens the decision was taken not to use this method as a full size flat panel could not be manufactured this way. The same argument applied to out of autoclave prepreg. RTM, in particular resin infusion was chosen due the superior quality of laminate achievable over wet lay up. It provide a laminate with very low void content and high fibre volume.

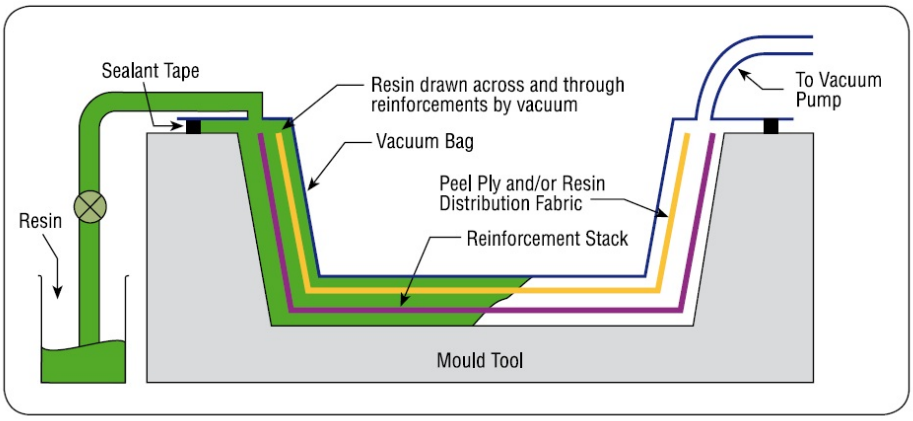

Figure 18: Shows a typical resin infusion stack. Image courtesy of Gurit.

Resin infusion is a type of Resin Transfer Moulding RTM where the upper mould is eliminated and replaced by a vacuum bag.

- Typically the following steps are involved when creating a laminate using resin infusion:
- A release agent is applied to the mould. This could be a chemical release agent or wax and PVA combination.
- The dry fibre layers are then laid into the mould in the desired orientations.
- Peel ply is placed over the fibres to protect them and create a good bonding surface.
- Infusion mesh is placed over the peel ply, this helps the resin diffuse through the laminate.
- The resin inlet and vacuum lines are then placed in the correct positions.
- A vacuum bag is used to cover the stack and is sealed to the moulds flange using sealant tape.
- A vacuum is pulled using a pump and the resin is allowed the flow into the stack infusing the fibres.
- Once full impregnated the resin flow is stopped and the laminated allow to cure under vacuum.

3.6.2 Bonding facesheets to honeycomb

Once the facesheet was removed from the vacuum bag, it could be bonded to the aluminium honeycomb core. In this instance resin was applied to the facesheet to stick to the core. The sandwich panel was then placed in a vacuum bag to bond the parts together.

3.7 Initial tests

by Thomas Gough

A resin infusion was completed using free to use glass fibre to gain experience with the layup proceedure. The sample created was then cut in half before being bonded to the honeycomb core as previously stated, allowing one 500mm x 150mm three point bend panel.

3.7.1 3 point bending test

With the necessary testing rigs dictated by the regulations not ready, a three point test was undertaken on the first glass fibre sandwich panel made using a load applicator not meeting the 50mm radius. The test was carried out to gain familiartity with the testing machinery (in this case an Instron C hydraulic test rig), data aquicition software and testing proceedure.

The results gained from GF-H-3-B1 gave no conclusive proof of the performance of the glass fibre panel. The major issue which occurred during the test was that the top facesheet started sliding along the honeycomb surface, indicating the epoxy had failed under the compressive load, creating a shear between the facesheets and core. This was clear after the test, with half of this facesheet able to be lifted from the honeycomb. This can be seen in Figure 19.

Figure 19: Failure of epoxy used to bond the glass fibre skins and honeycomb core together during GF-H-3-B2 bending test. Failure is shown through the sliding of the top facesheet.

3.7.2 Tensile tests

To gain a correlation to FEA analysis, the unaffected glass fibre facesheet was removed from the panel and cut into sections to perform five tension tests with 100mm x 50mm samples. Values gained from this could then be used to validate FEA analysis, to deduce if it could accurately predict the non-isotropic effects of a composite facesheet.

The results from GF-X-3-T1 can be considered an anomaly. This is because the first attempt was set to a maximum load of 20kN which was met easily by the sample. To readjust the limits the load

was released, meaning the sample had been preloaded before the final run. The performance after yield also shows anomalies, chiefly that the sample didnt snap, but instead kept deforming, with reducing force. This may imply the speciman was slipping in the grips, with the pressure applied by the grip not enough to overcome the tensile force leading to slippage.

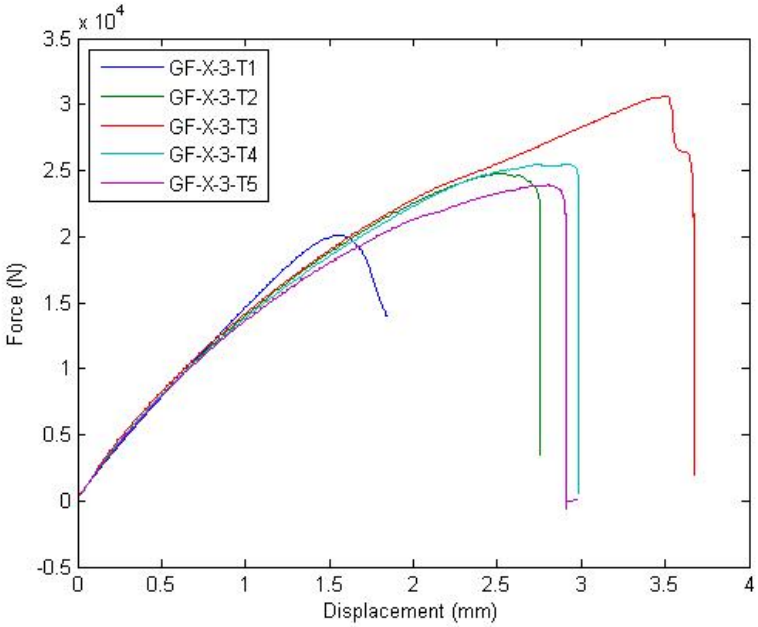

Figure 20: Load displacement graph for five GF-X-3-T tension tests.

Of the four tests considered to have taken place under similar conditions, a reasonable level of precision is shown apart from in GF-X-3-T3, where a much higher load was achieved.

The large inelastic range found in the graph, which should not occur in a composite like this could be due to issues created in the first manufacture. The vacuum bag was found to let in a slight amount of air around part of the seal, which would have compromised performance. Because of this another glass fibre panel was made in order to improve manufacturing techniques before panels were created using carbon fibre bought using the budget.

3.8 Initial FEA

By Antons Kasjanics

Finite element analysis was used for this project to verify, whether the proposed design would perform well before it was manufactured. But one cannot assume the numerical model returns accurate results without validating the model itself against some known values. For this project, results obtained from a finite element code were compared with experimental data.

3.8.1 Validation

To validate the finite element (FE) code, two experiments were conducted to obtain data, which could later be compared with the numerical results composite skin tensile tests and composite sandwich panel three point bending tests. The same experiments were modelled using a FE software MSC

Patran/Nastran. The main assumptions were the following:

- Composite skins are thin enough to be modelled with thin 2D shell elements
- The honeycomb core was modelled using solid 3D hex elements (exact honeycomb geometry has not been modelled
- Small deflections for all of the experiments static linear analysis applicable

3.8.2 FEA on tensile tests

The tensile specimens were modelled as a thin plate 100 x 50 mm shown in figure 21. The plate itself is discretised using 2D QUAD4 shell elements. The final mesh consisted of 52 x 26 elements. A finer mesh with the twice as many elements in each direction has been also tested, but produced the same results; hence the solution for the 52 x 26 is assumed to be converged.

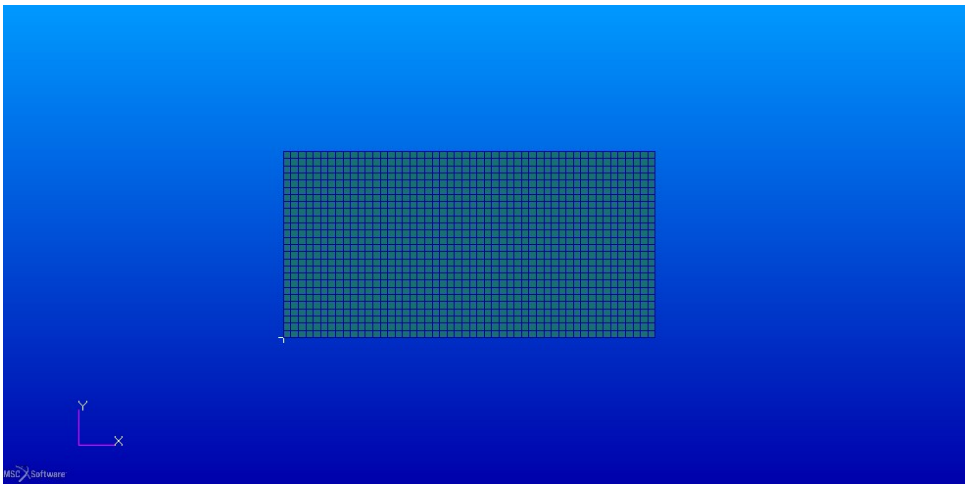

Figure 21: FEA tensile test mesh.

The following loads and boundary conditions were used. The coordinate system has been defined in such a way, that X and Y directions are in-plane and Z is out-of-plane. To comply with the experimental setup, the boundary conditions were defined as follows (left and right in reference to the picture above):

- Translations in all three directions are not allowed on the left side of the plate
- Translations along Y and Z axis are not allowed on the right side of the plate

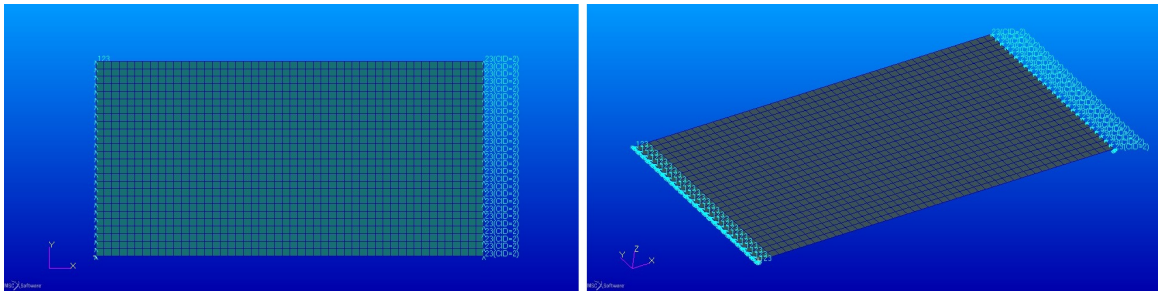

Figure 22: Tensile test boundary conditions.

The loads are to be applied at the left side of the plate. The experimental data gave a resultant force applied on the test specimen, therefore for the FE simulation that force had to be converted into a distributed load:

$$q_x = \frac{Q_x}{w}$$

In the equation above q_x is the distributed load, Q_x is the resultant force applied and w is the width of the plate. The distributed load is applied normal to the element edges on the right side of the panel and is along the X-axis.

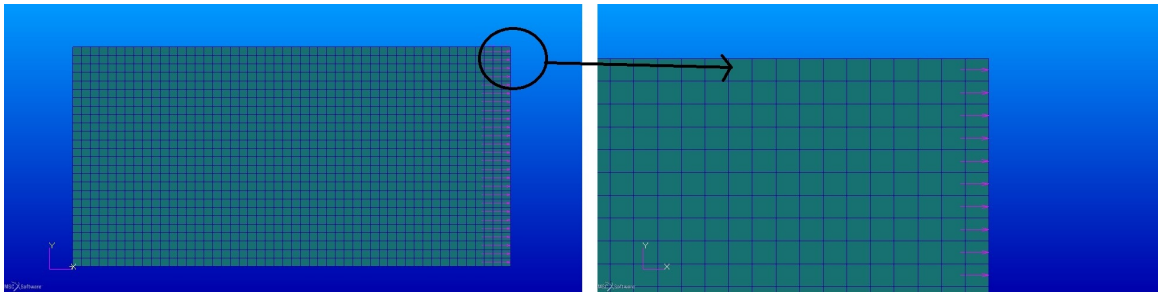

Figure 23: Tensile test load application.

A total of six different loads have been separately applied to the model, plus a zero-load-zero-displacement loading condition.

The material used in the tests was a 450gsm bi-axial Mitsubishi Rayon Grafil 34-700-12K carbon fibre. The values given by the manufacturer for Youngs modulus are ignoring any resin, that was to be used for infusion and not taking into account the fact, that 50% of the material is normal to the loading direction [25].

The lamina material was defined as 2D orthotropic, E11 = E22 for a bi-axial fibre. Using the lamina properties, a three-ply composite material has been defined, with each ply thickness calculated by

$$\text{ply thickness} = \frac{\text{total thickness}}{\text{number of plies}} \times \text{fibre fraction}$$

Total thickness was directly measured after the material has been manufactured. The fibre fraction for these materials is assumed to be 0.66. The lamina stack consisted of three plies, second one being at 45 degrees to the X-axis.

The results show a good agreement of the linear analysis with the experimental data. The analysis is within 5% range of the experiment this value has to be taken into account when calculating the safety factor.

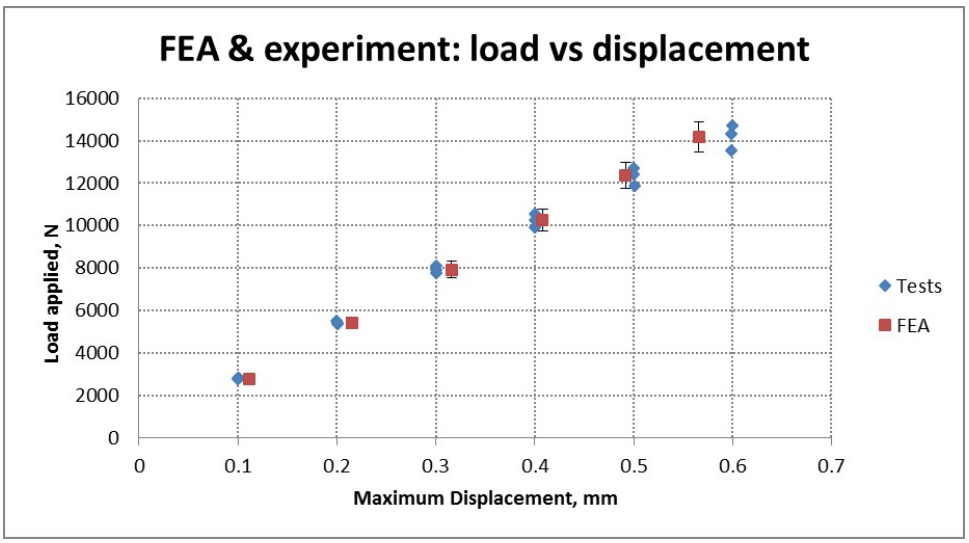

Figure 24: Comparison of tensile test data GF-X-3-T in linear region to FEA simulation.

3.8.3 Fibreglass sandwich panel - 3 point bending test

For the three point bend tests analysis the thickness of the sandwich panels could not be ignored, therefore the core material has been modelled using 3D HEX8 (hexagonal) elements. The skins, as before, were modelled using 2D QUAD4 shell elements. The final mesh can be seen below. Slightly denser mesh in the middle of the panel has been used to make the region of load application slightly more obvious. The panel dimensions were 500x150x25 (skin thickness is ignored during modelling and included during material definition).

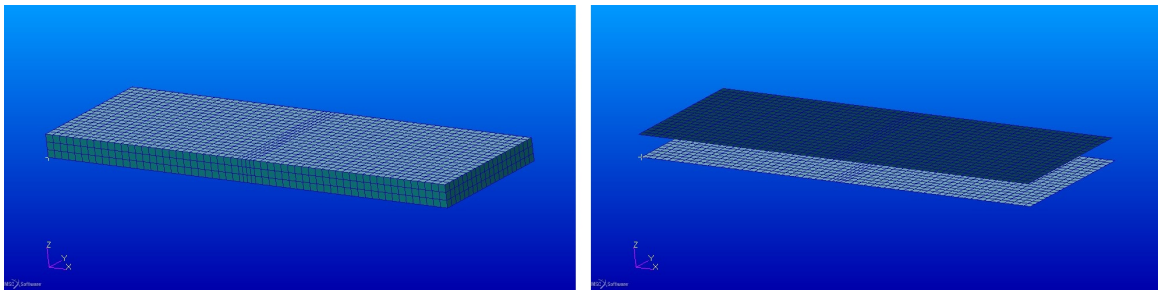

Figure 25: 3 point bending test mesh.

The following loads and boundary conditions were used. The coordinate system has been defined in such a way, that X and Y directions are in-plane and Z is out-of-plane, as seen in previous pictures. The experimental setup suggested that the panel was simply supported; the analysis setup had to be the same. To insure the simple support condition, two lines of nodes, effectively acting as the supports in the experiment, on one of the skins were restricted of any displacements, but the rotations were allowed. The load was applied on the opposite side along the Z axis.

The load has been defined as a distributed load, which has been calculated as before:

$$q_x = \frac{Q_x}{w}$$

In the equation above q_x is the distributed load, Q_x is the resultant force applied and w is the width

of the panel, 150mm in this case. The load has been applied normal to the element edges along the Z axis.

The lamina material was defined as 2D orthotropic, E11 = E22 for a bi-axial fibre. Using the lamina properties, a three-ply composite material has been defined, with each ply thickness calculated by

$$\text{ply thickness} = \frac{\text{total thickness}}{\text{number of plies}} \times \text{fibre fraction}$$

The sandwich panels have been manufactured in one attempt, meaning the core material has been put between the non-impregnated glass fibre sheets before the resin infusion. Due to this fact the exact skin thickness was harder to evaluate and was assumed to be the same as it was for the previously manufactured plates. The lamina stack consisted of three plies, second one being at 45 degrees to the X-axis.

The core material has been defined as isotropic. The material strength and stiffness factors rely only on the core material properties any effect of the resin within the core structure is ignored, because is assumed negligible.

The experimental results showed a linear pattern, but did not go through the zero-load-zero-displacement point, indicating that the test panel has been slightly preloaded. For the finite element model to be validated, the slope of the load-displacement curve should be as close as possible for both tests and FEM. The test results have been adjusted to go through the origin. After this procedure, the analysis results compared very well with the experiment, indicating not only accurate analytical prediction, but also that the quality of manufacture was quite high.

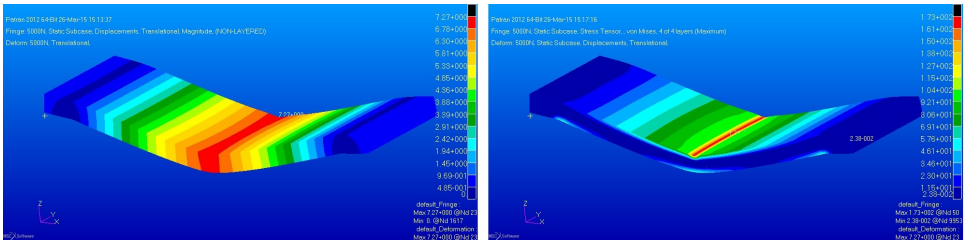

Figure 26: displacement and stress contour fringes for three point bend test with GF-H-3-B panel.

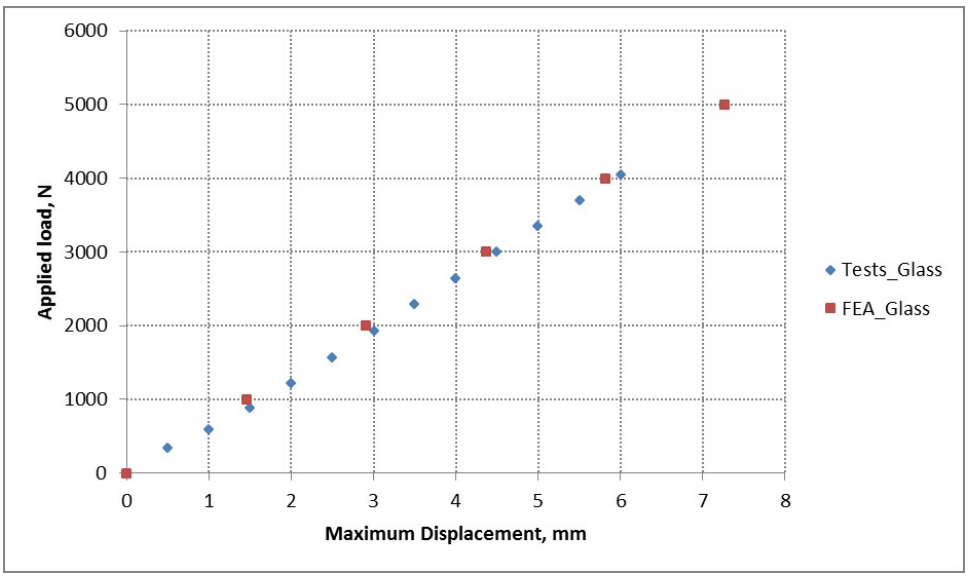

Figure 27: GF-H-3-B 3 point bending test comparison with FEA.

3.9 Initial chassis design concept

By Joe Edwards

3.9.1 Overview

The chassis model has been developed on CAD in conjunction with the practical testing of the various sandwich panel structures. The model itself sets the parameters for the more complex tests, primarily the joint tests. It allows for the geometry of the weakest parts of the car (the largest angled joints) to be computationally analysed and physically manufactured and tested. The results of these practical and computational tests determine the final thickness of the core and face sheets, which in turn determine the thickness of the model panels.

The primary influence on the model geometry was satisfying the 2015 Formula SAE Rules - T.3.10.4, T.4.1.1 and T.4.2.1. These rules stipulate minimum cross sections for the chassis and cockpit area in addition to a 95th percentile male being able to fit within the chassis. Suspension geometry also influenced the final design.

Achieving the aim of the model occurred in three stages. Each stage was modeled in CAD for a visual representation of any manufacturability issues that were of concern at that stage of the project. As a result the model became more complex over time due to the issues that were resolved during development.

The results from each of the model iterations and their subsequent influences on the project will be discussed further in each section.

3.9.2 Initial Chassis Design

The first chassis model was created to get a perspective of the gravity of the design challenge. It allowed the difficulties of manufacture to become apparent, in addition to understanding the practical

testing and subsequent test rigs that were to be designed and manufactured. It also brought into questions things such as suspension design, inserts and the detail to which the design and practical testing should achieve.

The first design iteration of the monocoque chassis was a surface model of the 13/14 SUFST space frame design. This is where the triangulated space frame nodes were carried over to form the corners of the monocoque panels. The front, cockpit, firewall bulkheads and rear of the car were also modeled as can be seen in figure 28.

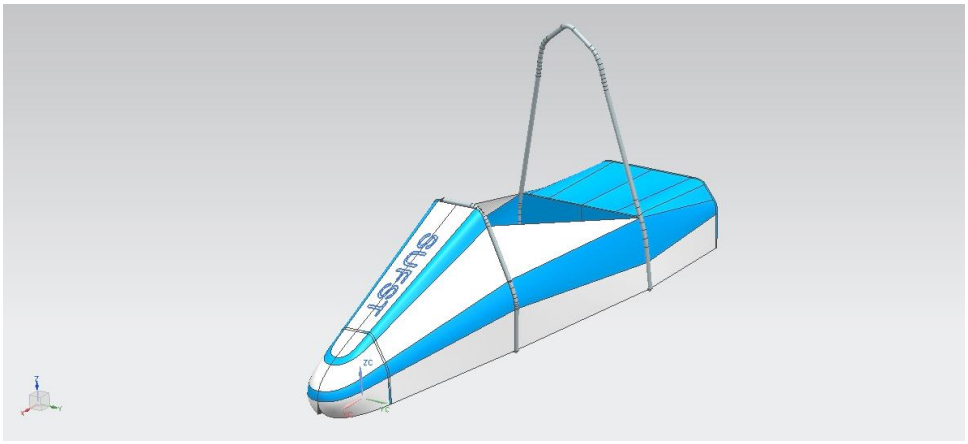

Figure 28: First iteration of chassis design.

The subsequent impact of the model was primarily to ensure the final design had only planar faces with constant radii between every adjacent panel. This improves the; simplicity of the design, ease of manufacture and ease of structural validation.

The simplicity of design is increased due to the chassis primarily being comprised of constant radii blends and planar faces; complex surface modeling is kept to a minimum the foam nose only. Ease of manufacture is achieved due to the flat faces and constant radii blends allowing everything to be made from flat panels using the cut and fold method. As the structural testing on the joints is due to be in tension and compression of radius test panels, constant radii allow for simpler analysis as the stress distribution along the joint. Should the blends have been non uniform this would have added additional complexity when analyzing the failure modes.

3.9.3 Suspension Design and Hard-points

A parametric suspension geometry model designed by SUFST [4] for the 2014/15 car was used to create and evaluate the location of the chassis hardpoints. The model works by creating the front and side 2 Dimensional views as sketches and later linking them together to find the chassis hardpoints. Certain constraints were placed on the chassis hardpoints which corresponded to the manufacturing limitations. The biggest limitation is that the cockpit side geometry must lie on a single plane.

4 Design: Stage 2

This section focuses on the refined 3 point bending and punch tests. Equivalency with Formula Student mandated steel tube is carried out as according to the rules. Also included are improvements made to the panel design through using a different core material. The chassis design is iterated and then tested using FEA. Finally the design of inserts and joints are discussed and manufacturing is carried out.

4.1 Second glass fibre tests

By Thomas Gough

With the first tensile tests showing poor performance with a large inelastic region, another glass fibre facesheet was created in the same manner as before. In this case the vacuum bag worked better, keeping a better seal than the first panel. This was then cut into sections of 100mm x 50mm, giving four tensile tests, three shear tests and a three point bend test of 500mm x 150mm.

4.1.1 Second glass fibre laminate results

Four tensile tensile tests were undertaken, of which GF-X-3-Tb1 and GF-X-3-Tb2 had tape placed over the ends to try and resolve the issue of slipping. This was found to worsen the effect, leading to a reduced ultimate force and longer inelastic section. The GF-X-3-Tb3 and GF-X-3-Tb4 specimens were run without this tape, and lead to much improved performance, as shown in Figure **??**. The first test was ignored from the results due to its poor performance. Tests three and four show a much greater stiffness in the elastic region compared to GF-X-3-Tb2, followed by a sharper drop in load once the maximum load was reached.

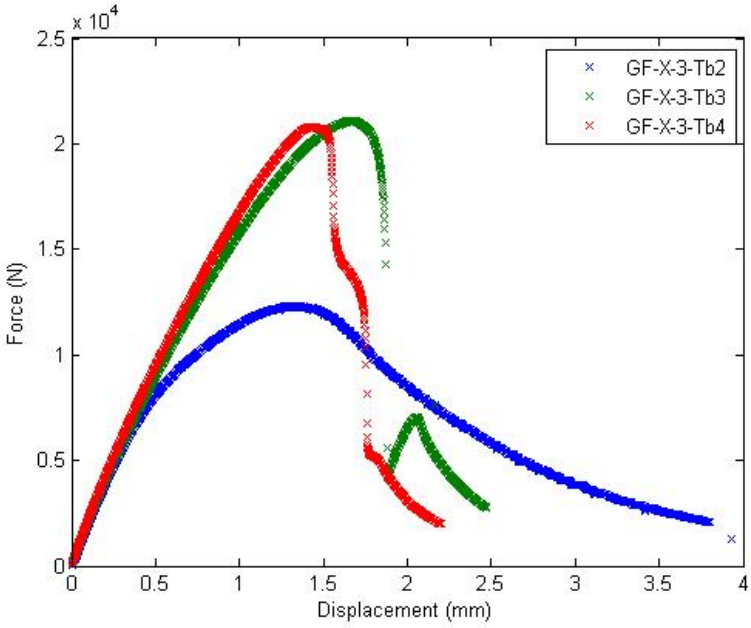

Figure 29: Load displacement graph of second set of glass fibre tensile tests.

To calculate the stiffness of each sample the force at a given displacement in the linear-elastic region

(0.5mm for all the tests) was used to calculate the stress due to the known cross sectional area, whilst the strain could be calculated from the known displacement and original length between the grips of 60mm (20mm was placed in the grip). To deduce the effectiveness of the manufacturing the results were validated against the theoretical value given from the CLT code, in this case being 21.88GPa. The values given are shown in Table 7.

	GF-X-3-Tb2	**GF-X-3-Tb3**	**GF-X-3-Tb4**
Tested maximum Force (kN)	12.34	21.12	20.82
Tested UTS (MPa)	123.4	211.2	208.2
Tested Young's Modulus (GPa)	9.728	10.80	9.509
Calculated Young's Modulus (GPa)	21.88	21.88	21.88
Error (%)	124.9	102.7	91.75

Table 7: Data from the second glass fibre tensile tests.

Whilst removing the tape from the ends of the samples improved the grip, the expected brittle characteristics still didn't occur, with no cracking detected at the peak load. After the test it was deduced that the samples were still slipping due to the pressure of the grips being too low. Grip pressure is usually reduced when testing with composites to avoid compressing the sample too much. However the decision was made to increase the pressure in the next test to try and allow the brittle breakage to occur. Figure 30 shows the damage created by this slipping on a carbon fibre tensile specimen.

Figure 30: Damage created from carbon fibre specimen slipping in grips.

4.2 Carbon fibre tensile tests

By Thomas Gough/Thomas Rickard

With the quality of the manufacturing process deemed to be of a high enough standard despite the tests slipping in the grips, the first carbon fibre facesheets were made in the same fashion as the glass fibre sheets. Five tensile tests of dimensions 100mm x 50mm were made, in this instance consisting for three layers, a biaxial Toray T700SC +/-45 surrounded by Mitsubishi 2/2 Twill 12K 0/90 on either side.

The decision was made to use a combination of woven fabric and biaxial fibres. One reason was the reduction in cost from buying one fabric with strength in two directions as opposed to unidirectional fabric, making biaxial advantageous. The choice of woven fabric however comes with a disadvange.

As a carbon strand is strongest when straight [26], this means that weaving the fibres reduces the theoretical strength. On the other hand, if the fibre is punctured, the surrounding strands behave as if unbroken due to the bends from the weave. In comparison, in a unidirectional fabric, strength is compromised for the entire fibre length. This means woven fabrics have a greater impact strength and toughness than unidirectional layers [26], making them ideal against punctures as is required in the shear perimeter test.

4.2.1 Variations of carbon fibre laminate layup

To gather more data on the effects of different stacking orders and varying the number of plies, a laminate was made combining four different stacking orders. The fibres and their orientations are shown in Figure 31

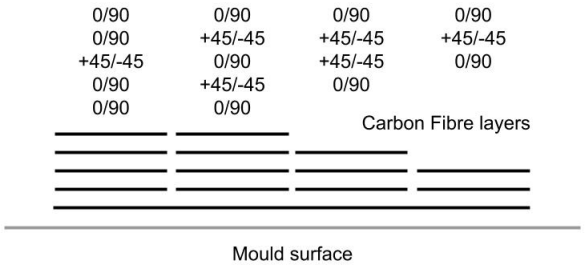

Figure 31: Order of various laminate layups created in the same resin infusion in side view.

Figure 32 shows how the fibre stacks were arranged on the mould. Problems were encountered during previous infusions as a result of the resin not quite reaching and wetting out the corners. This time extra peel ply was placed around the carbon fibre and the infusion mesh was cut to the size of the carbon plys. This ensured all the carbon was wetted out successfully and none was wasted.

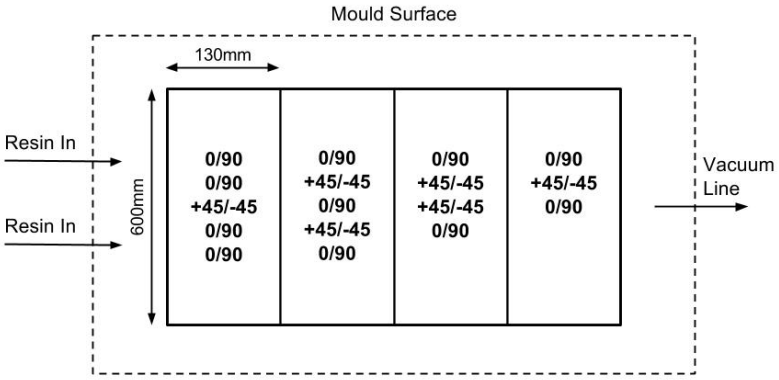

Figure 32: Order of various laminate layups created in the same resin infusion in top view. Note the location of the resin inlets at the end with the thicker laminates and tube to vacuum pump.

Figure 33 shows how each stack section of the laminate is to be used. An area of excess was included

in each stack to account for misalignment and allow for trimming to the correct size. The panels will then be split up into a top and bottom for two shear tests and three tensile test. This results in 12 tensile specimen split over 4 different stacks and 8 shear tests over 4 specimens.

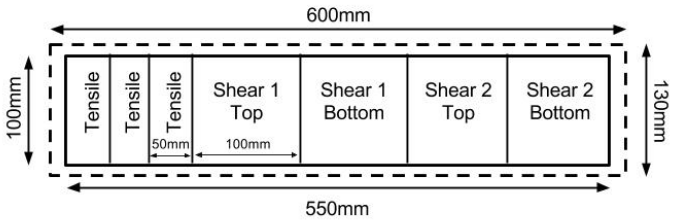

Figure 33: Variation of facesheets to be gained from each specific ply.

The infusion process was varied slightly to try and improve the laminate. One of these was to use two tubes to feed the resin. This was to give a more evenly distributed flow, and would allow the resin to reach the far corners easier, as shown in Figure 34. Another adaption was to place the tacky tape on the vacuum bag first, as opposed to placing it onto the plate. This was to avoid air escaping through small pockets created by overlapping parts of vacuum bag which had been encountered previously. This new method did seem to give a better seal, with no air found to escape from the bag.

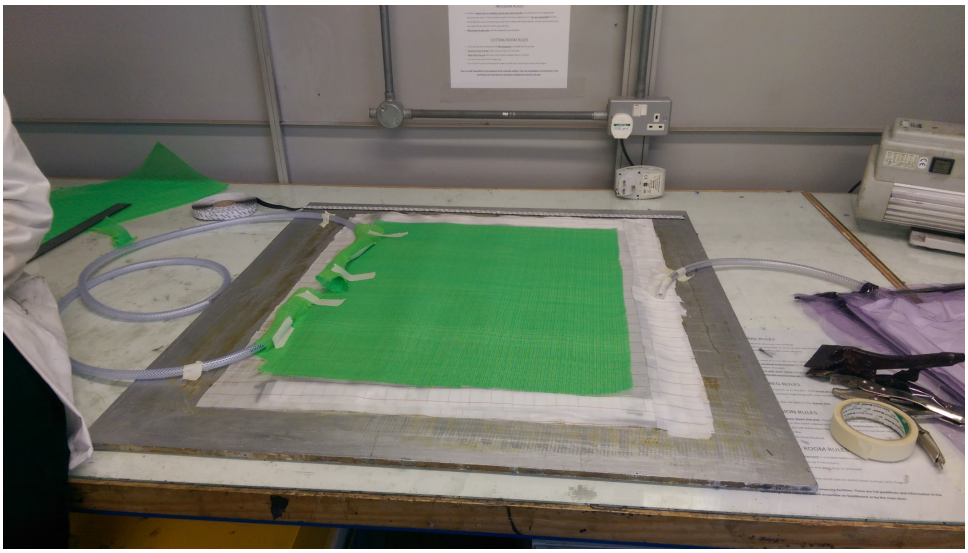

Figure 34: Infusion process. Note introduction of two feeding tubes instead of one.

4.2.2 Variations of carbon fibre laminate results

Three tests were undertaken for each layup variation, with no obvious outliers found. The three tests fpr each ply layup were then averaged to give the results in Table 8. The stiffnesses of the test samples were calculated in the same fashion as the glass fibre specimen, and where then compared to the stiffnesses calculated from the CLT code. To reduce the chance of the specimen slipping, the length placed within the grips was increased to 40mm, giving an unclamped length of 20mm.

A large discrepancy is shown between the theoretical Young's Modulus and that given from the test

	CF-X-3-T	CF-X-4-T	CF-X-5a-T	CF-X-5b-T
Tested average Young's modulus (GPa)	10.52	9.050	9.496	10.16
Calculated Young's modulus (GPa)	64.78	59.77	62.85	68.36
Average error (%)	515.8	560.8	561.9	573.0
Tested average maximum force (kN)	42.66	49.43	72.87	72.67
Tested average UTS (MPa)	632.0	599.1	694.0	660.7

Table 8: Data with average values over the three tests for each ply. Note the large percentage error between the CLT predicted and tested Young's modulus.

samples. Although some error was expected due to the vacuum bag not keep a perfect seel during manufacturing, the size of the error implied an issue also with the code.

One error could come from the assumed volume fibre fraction of 0.6. The necessary amount of resin was calculated but more was needed for many factors, including being absorbed by the peel ply and placing extra resin in the cups to avoid them running empty and feeding bubbles into the system. These factors will slightly alter the volume fibre fraction, leading to varying stiffness.

Another could be the short extension length between the grips. The section length placed in the grip was increased in an attempt to avoid slipping, at the expense of reducing the unclamped region. A longer initial speciman would have allowed a larger unclamped region, where the contrast in stress would have been reduced over a larger area. This may also explain the increased error compared to the earlier glass fibre tests, which had an unclamped length of 60mm compared to 20mm. Whilst this may have reduced the Young's modulus calculated after testing, the issue of slipping appeared to be resolved, with all test snapping at their peak loads, implying a brittle break. Increasing the length of the unclamped specimen would also allow the use of an extensometer, which would give a more accurate reading of the strain.

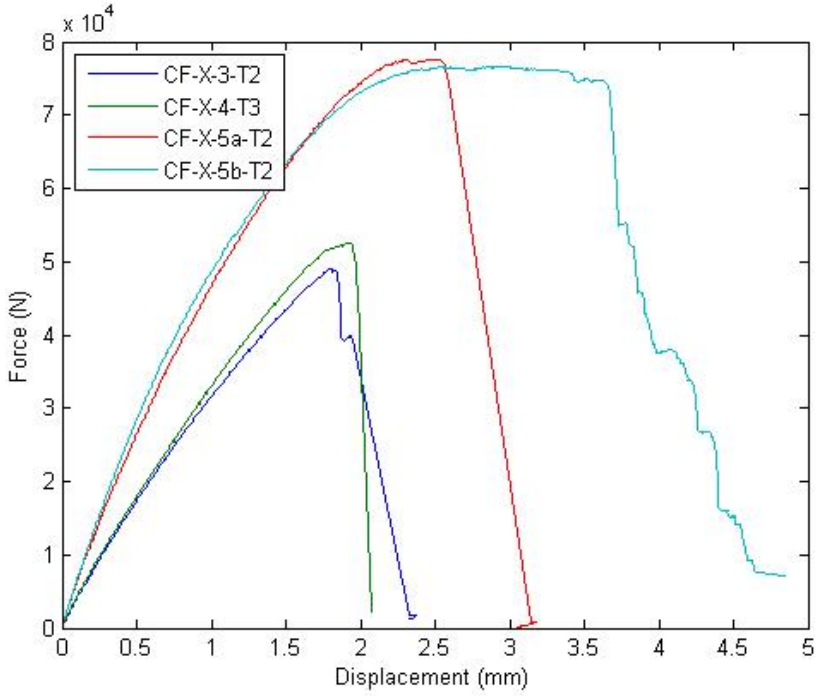

Figure 35: Load displacement graph comparing carbon fibre tensile test specimens.

A noticeable attribute of the load-displacement curves was the decreasing stiffness as the displacement

increased. This trend was especially clear in the five ply samples, which in some cases levelled out completely at a constant load before breaking. This could have been due to single lamina breaking at specific points before others, a typical trait in load-deformation plots where a series of small events spread over a range of the load lead to the curve gradually decreasing []. This trend is shown in Figure 36 [27].

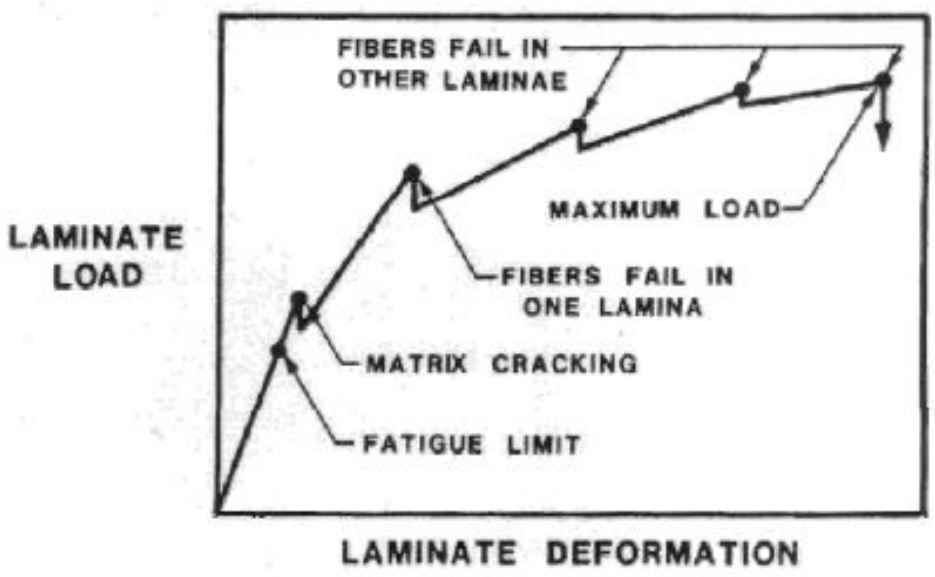

Figure 36: Reduction in stiffness of a laminate in tensile testing as individial fibres fail.

If this assumption is to be taken as true, this shows that whilst the ultimate load did increase, if the tensile load taken by the monocoque were to go above that which the first lamina failed at, then the stiffness would reduce. Therefore the design limit load which it is safe to take the sample to is far lower than the ultimate load, labelled the fatigue limit in Figure 36. If this load wasn't to be met however then using more lamina in the laminate would give the benefit of increased load for unit of displacement.

Noticable differences were noted between the thicker and thinner specimen. These include the greater twisting of the thinner laminates, where after testing the samples are more twisted than the 5 ply specimen. The CF-X-3-T and CF-X-4-T samples were also more susceptible to free-edge delaminations as shown in Figure 37, which are normally created by high interlaminar stresses [28]. Interlaminar stress is usually greatest at layer interfaces, of which there were less in the CF-X-3-T and CF-X-4-T specimen. Having less layers in the laminate therefore may lead to higher interlaminar stresses, causing premature failure.

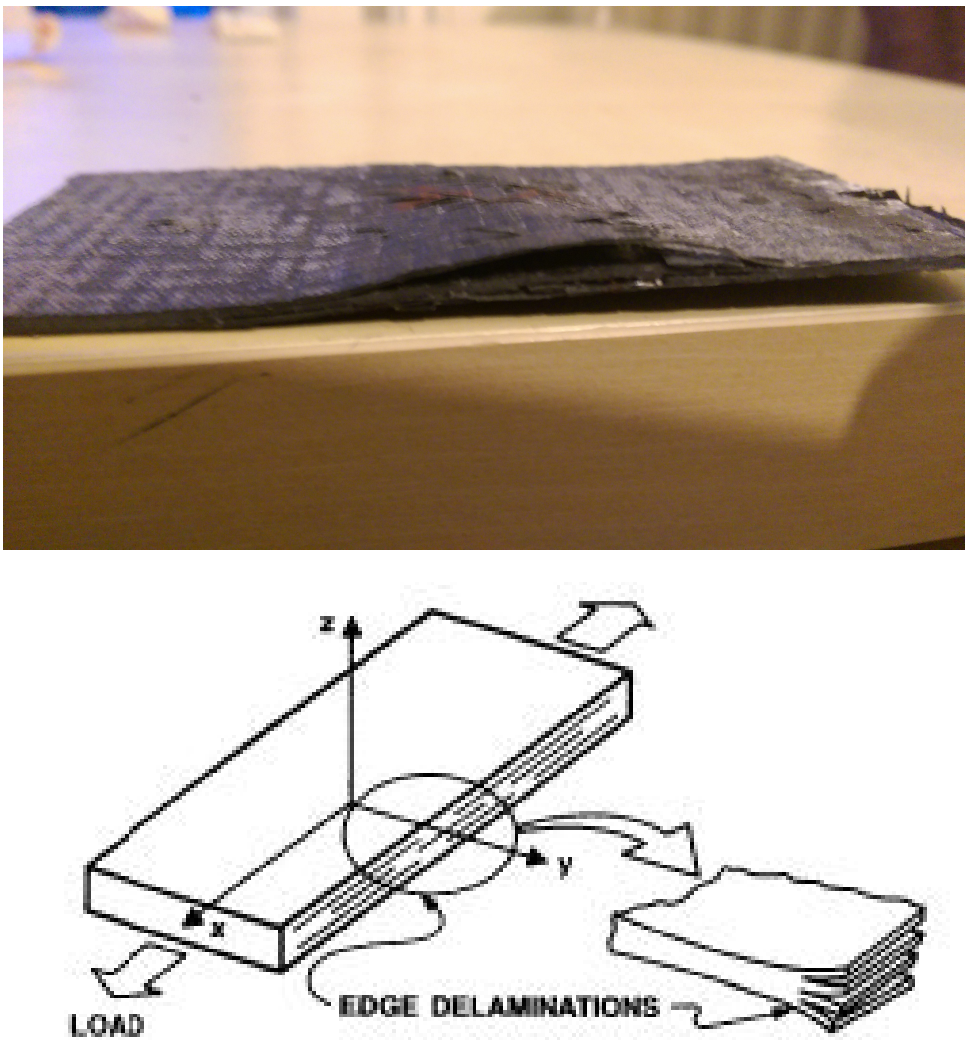

Figure 37: Free edge delamination in tensile testing (above) and example (below).

Interlaminar stresses are ignored in Classical Laminate Theory, and whilst these local high stresses will dominate the laminate strength, the stiffness of a laminate is controlled by the global stresses [28]. This means this is unlikely to be the main reason for the large difference between the code and test Young's modulus.

In addition, placing 45/-45 degree plies on the outside are more likely to create a compressive stress and reduce the chance of delamination [28]. The opposite would occur with 0 degree plies, meaning the tensile specimen may have failed prematurely from these free-edge delaminations. However, using 0 degree plies on the outside of the laminate is beneficial in bending, with fibres in the bending plane a greater distance from the centroid offering greater resistance to bending.

4.3 Equivalency tests

By Thomas Gough

With the steel bars of grade SAE/AISI 1010 gathered, a three point bending equivalency test could be carried out. As explained earlier this was to account for any compliance in the test rig and deduce an absorbed energy value for the baseline steel tubes.

Two tests were run to make sure no obvious experimental errors were made. As can be seen in Figure 38, the two curves show a very similar trend. The test was conducted until the maximum load was achieved, which was found to be 6062N for test 1 and 6070N for test 2.

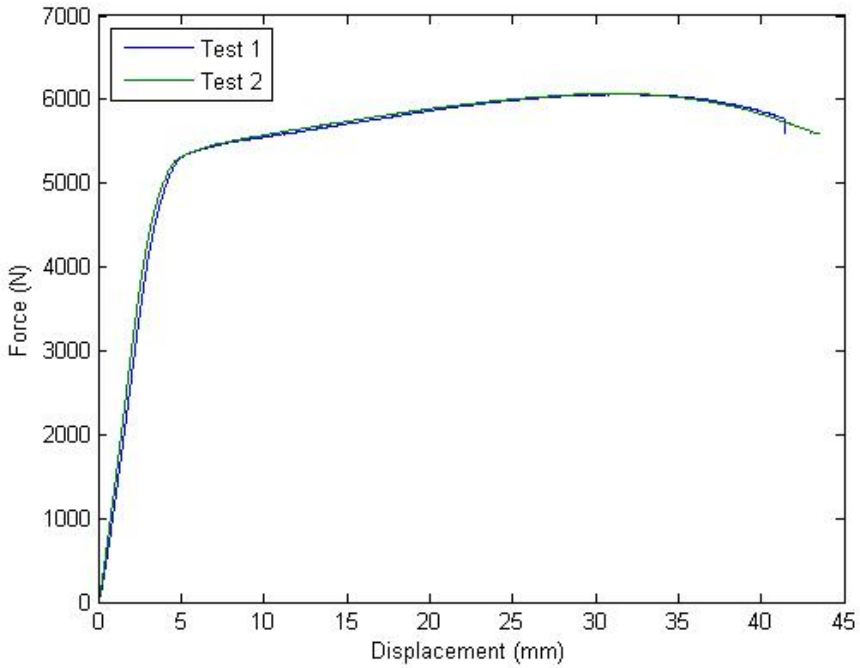

Figure 38: Load displacement graph of equivalency test with two SAE/AISI 1010 steel bars. Note similarity between the two tests.

For the purpose of calculations, the results of test 2 were used. Using section T3.31 of the Structural Equivalency Spreadsheet, the tested flexural rigidity was calculated as $1.68 \times 10^9 N/mm^2$. This compares to $3.45 \times 10^9 N/mm^2$ for the theoretical value, giving a rig compliance of 1231N/mm.

The absorbed energy was found by integrating the area underneath the force displacement curve up to a displacement of 12.7mm. The trapezium rule was used on the data in Microsoft Excel, and the absorbed energy was found to be 57.89J.

The gradient of the linear elastic region was calculated in the SES to be around 1360N/mm.

4.4 Glass fibre sandwich panel bonding

By Thomas Gough

For the sandwich panel bonding, a honeycomb bonding epoxy adhesive was used. Whilst this would increase the manufacturing costs the poorly performing epoxy resin previously used was inadequate. With this alteration it was hoped that the failure mode of the panel could be found. The epoxy adhesive was used for both the bending and shear panels.

To bond the facesheets and core together, the adhesive was applied through a nozzle onto the facesheets and spread to give an even layering. The panels were then placed onto the honeycomb core, and placed in a jig. This comprised of two plates placed on either side and four clamps used to compress the sandwich panel elements together. This was then left for 72 hours to allow complete

bonding, after which three point bend and shear testing could be undertaken. A major issue during the construction of this panel was no instruction as to how much adhesive to apply.

4.4.1 Second glass fibre three point bend test

As Figure 39 shows, although a greater force was achieved than the previous three point bend tests with glass fibre sandwich panels, the maximum force reached for GF-H-3-B2 was 367.8N which was still far too low. The necessary amount of adhesive to use was unknown, meaning more may have been required to create a stronger bond. The issue with this however was a whole 50ml tube was used for the bend and shear panels made concurrently, meaning using more would increase the price of a single panel further. This ignores that applying more adhesive may still not resolve the issue.

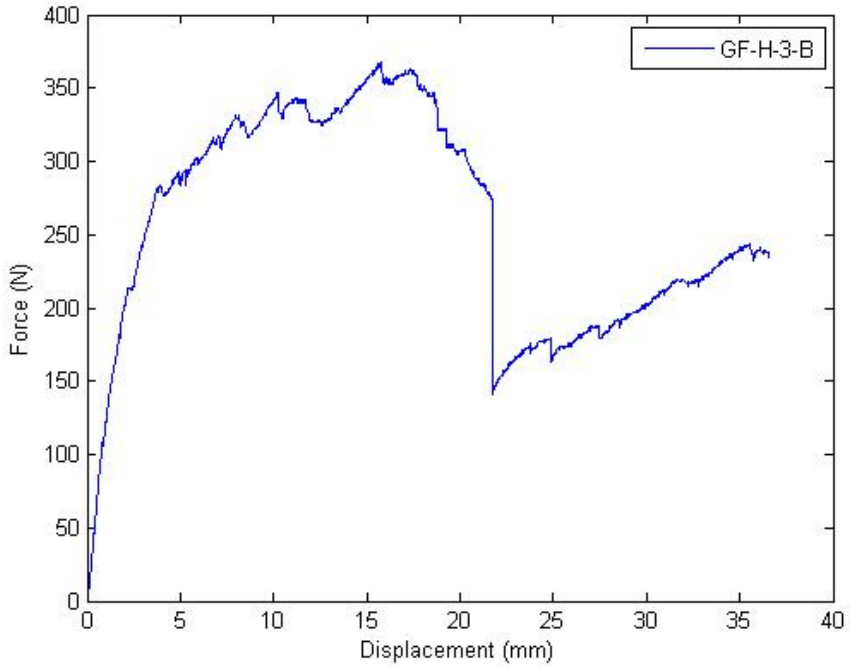

Figure 39: Load displacement graph of GF-H-3-B2 specimen in three point bending. Note the low failure load.

The jagged edges of the graph imply shearing, which can be assumed to be the adhesive breaking under the loading.

4.4.2 Glass fibre shear tests

100mm x 100mm glass fibre sandwich panels were also created to practise the perimeter shear tests required in section T3.31.5. The purpose of this test was to determine the skin shear strength, shown through an initial peak in the load-deflection curve, followed by the maximum force required to punch through the sandwich structure. This must meet the specified force of 4kN in section T3.33.3 for the monocoque front bulkhead support, and 7.5kN in section T3.34.4 for the monocoque side impact. With no calculations made to predict the performance, conducting the test on these three ply specimen would give a good indication of the loads met by a sandwich panel.

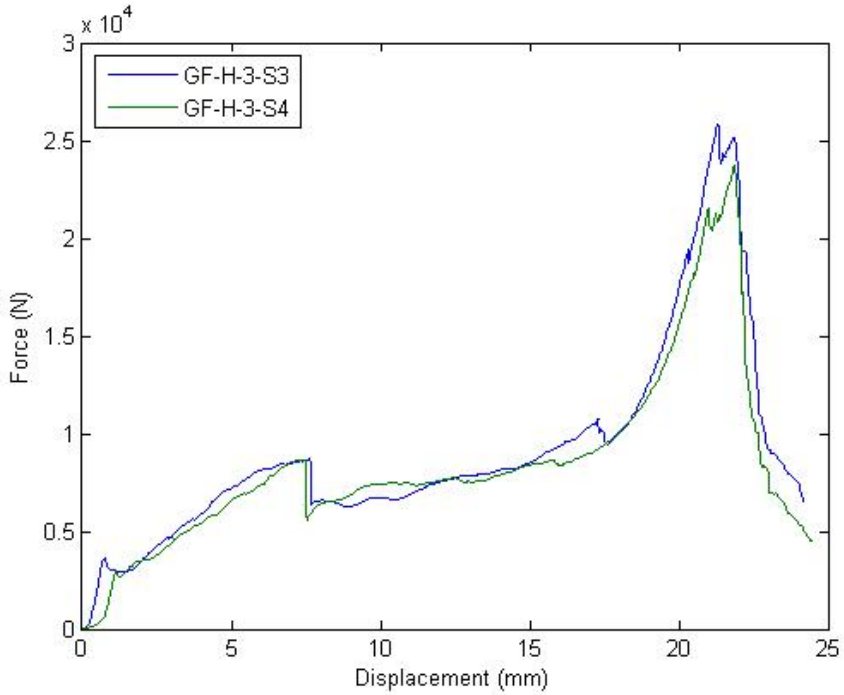

Figure 40: Load displacement graph of glass fibre shear perimeter tests with honeycomb core.

As shown in Figure 40 the two tests easily meet the required 4kN and 7.5kN required for the Monocoque Front Bulkhead Support and Monocoque Side Impact regions respectively. These loads are met by just the skin shear strength of 8.691kN and 8.651kN for GF-H-3-S3 and GF-H-3-S4 respectively, let alone the maximum forces of 25.81kN and 23.74kN. Whilst the load initially drops after the skin shear strength is met, a long period of slowly increasing load with displacement is given as the core is compressed. This compression is obvious in Figure 41 The load then rises rapidly once the core cannot be compressed further due to the second facesheet, which slowly fractures in a number of events, unlike the sharp drop in load from the first facesheet break.

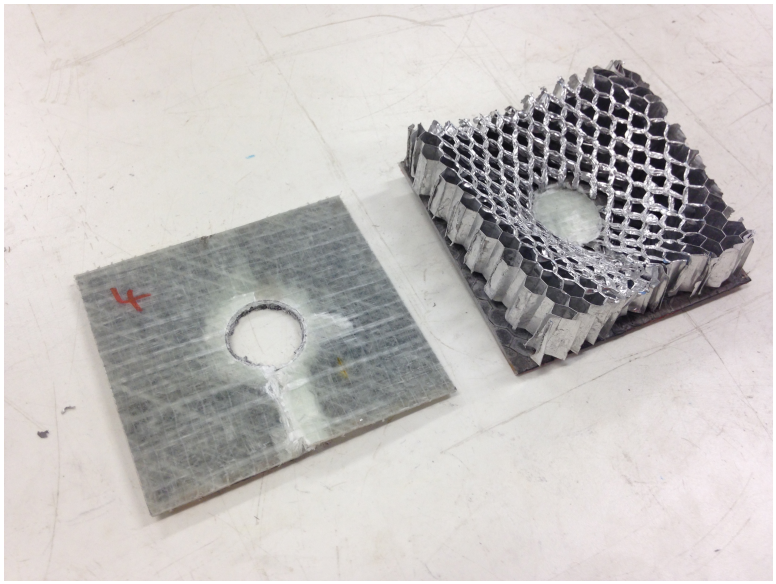

Figure 41: Damage caused by shear perimeter test on GF-H-3-S4.

The ease at which the tests were passed for these specimen meant that the likely limiting factor for

the Monocoque Side Impact region in terms of testing would be the three point bend test.

Although four tests were run, problems were encountered on GF-H-3-S1 and GF-H-3-S2, meaning their data was not included.

4.5 Carbon fibre shear perimeter repeatability tests

By Thomas Gough

With these tests completed the four different carbon fibre stacks were bonded to the honeycomb core and made into eight punch tests. The forces reached at both peaks are shown in 9. As can be seen all tests apart from the three ply facesheets meet the 7.5kN load with the skin shear strength alone.

		3 ply		**4 ply**		**5a ply**		**5b ply**	
		1	2	1	2	1	2	1	2
First Peak	Force (kN)	7.163	7.209	7.777	8.433	10.44	10.41	9.327	11.01
	Displacement (mm)	6	5.732	5.336	5.214	6.149	5.545	5.514	6.164
Second Peak	Force (kN)	41.93	36.90	61.69	57.74	84.21	71.82	89.36	85.91
	Displacement (mm)	23.53	22.81	24.56	24.31	24.24	23.25	24.84	24.89

Table 9: Carbon fibre punch tests with honeycomb core and varying skin laminates.

As expected increasing the number of layers in the facesheets resulted in both greater skin shear strength and ultimate strength. Using the CF-H-5b-S configuration also lead to a larger ultimate strength. A reason for this is that woven material is normally used in materials to resist punctures as the strands overlap each other. This leads to the strands behaving at full strength in a much shorter distance than the two layers of unidirectional fabric which make up a biaxial lamina, creating a material with a higher puncture strength [26].

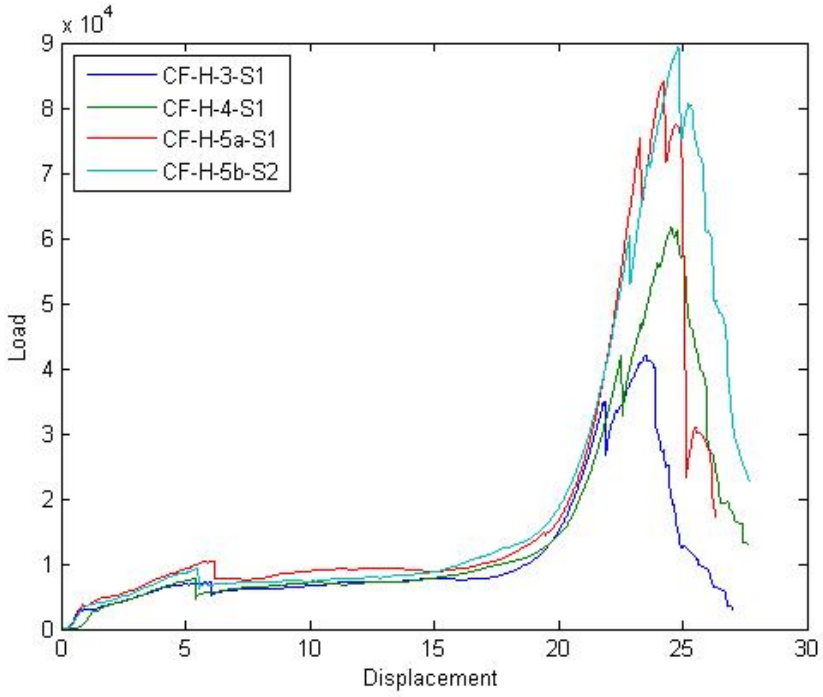

Figure 42: Comparison of carbon fibre punch tests with different skin layups and honeycomb core.

4.6 Introduction of foam core

By Thomas Gough

To try and eliminate the problems associated with bonding the core and facesheets the use of a foam core was investigated. This specific core was drilled to allow the resin drilled to allow resin to pass from the top to bottom surface, and grooved to distribute the resin to the laminate on the 'tool side' [29]. This arrangement allowed the whole sandwich panel to be infused in one process, reducing the production time and eliminating the need to use an adhesive.

To compare the foam cored panels to the honeycomb ones, a 250mm x 500mm sandwich panel was manufactured with glass fibre skins. This would allow a 500mm x 150mm three point bend panel to compare against the result in Section 4.4.1, as well as five 100mm x 100mm shear perimeter tests.

Whilst the same glass fibre laminate stack was used of 0/90, 45/-45, 0/90 sheets, the foam core could only be purchased in 10mm or 25mm thicknesses. The 25mm core was chosen as it was the only core available which was grooved and drilled, whilst this would also give improved flexural rigidity. Although this meant the foam core panel had an immediate advantage in terms of its improved area moment of inertia, the maximum load of the honeycomb panel was limited from the adhesive, meaning a comparison of the core materials could not be made for the three point bend test.

4.6.1 Foam cored three point bend test

As shown in Figure 43 the maximum load is hugely improved to a value of 7.650kN at a displacement of 16.49mm with the introduction of the foam core. This far exceeds the necessary 4.9kN required from the side impact section of the Structural Equivalency Spreadsheet despite only having a width

of 150mm. Whilst reaching the necessary load, the thinner panel did not meet the required flexural rigidity of 3455Nm^2 with a value of 2831Nm^2. In addition, due to the shallower linear gradient, the absorbed energy, calculated by determining the area underneath the curve up to 12.7mm is only 47.81J compared to the necessary 57.89J.

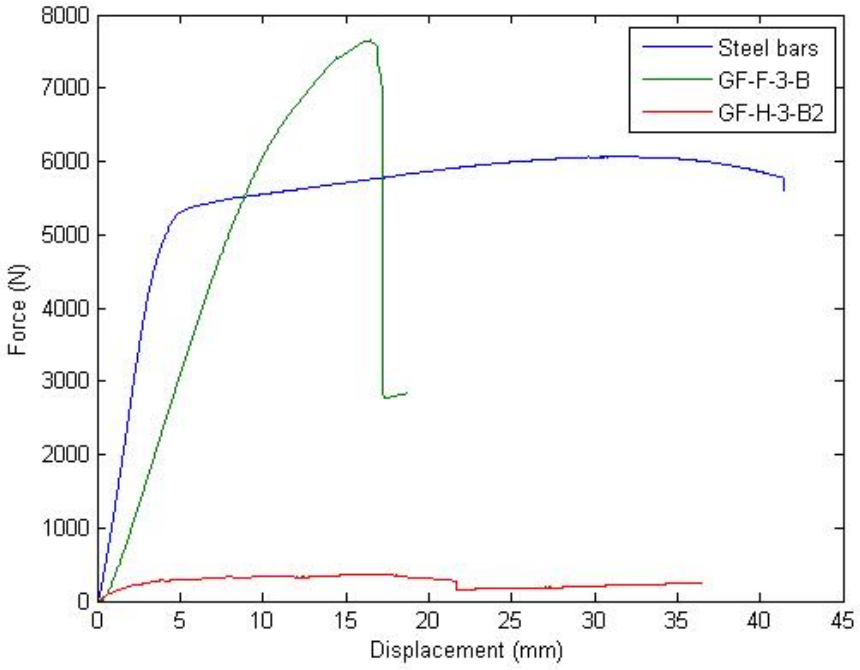

Figure 43: Load displacement graph comparing three point bend test with honeycomb and foam core, with glass fibre skins. A comparison is also made to the two steel bars equivalency test.

4.6.2 Foam cored shear perimeter test

Foam cored perimeter shear strength tests with glass fibre facesheets were also completed and compared to the two honeycomb tests. Although five were created, the results of only three were included because of issues in the testing proceedure. As Figure 44 highlights all the foam cored tests achieved greater skin shear and maximum loads. The greater depth of the foam core seems to give a greater compression area underneath the impacter, possibly explaining the larger region of slow load increase.

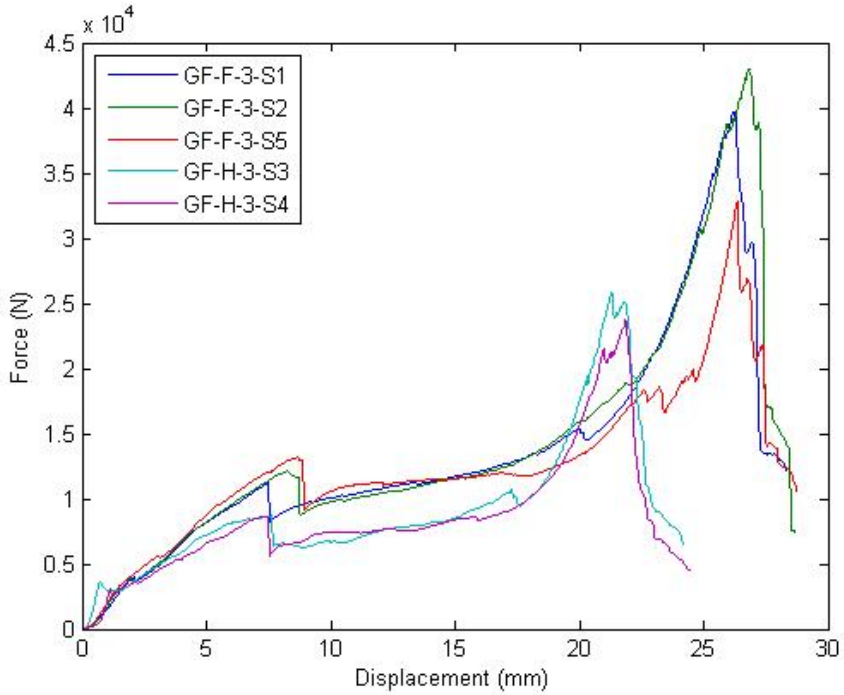

Figure 44: Comparison of honeycomb and foam core panels with glass fibre skins in shear testing.

Figure 45 shows similar cracking in the facesheet created from the load applicator on the top face. The impact region in the core foam shows little crushing in comparison to Figure 41 where a large portion of the core has been deformed. The crack on the edge of the specimen in Figure 46 has occured due to the compression on the core not being dispersed in the same fashion as the honeycomb crushing over a wider area, leading to a brittle snap.

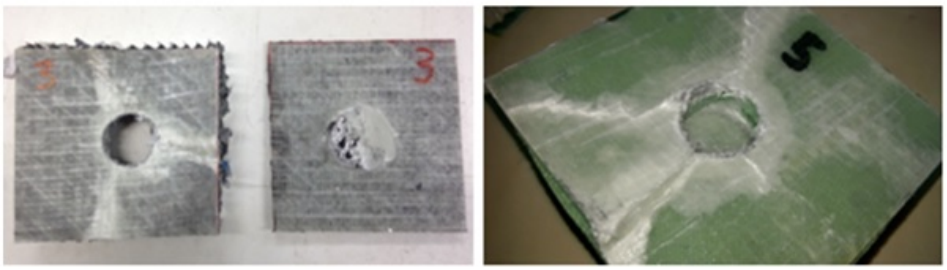

Figure 45: Comparison of damage created from perimeter shear test for honeycomb core (left) and foam core (right) specimen.

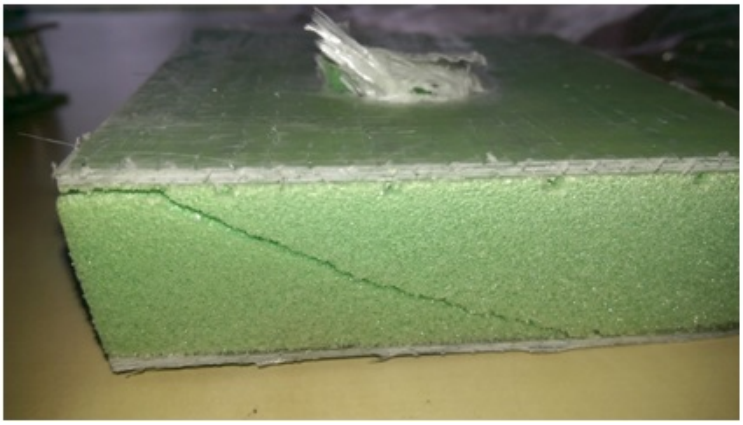

Figure 46: Core shear which occurred during foam perimeter shear testing.

4.6.3 Relative costs

The material costs behind manufacturing a single 500mm x 275mm three point bend panel are highlighted in Table 10. The costs were for quantities bought during the manufacturing process and ignored savings made from bulk ordering. It should be noted that initial costs for items such as adhesive applicators and nozzles were ignored, as well as the materials which were free to use in the TSRL.

	Honeycomb	**Foam**
Two Facesheets (GBP)	19.78	19.78
Core (GBP)	8.64	10.11
Adhesive (GBP)	12.20	0.00
Total (GBP)	40.62	29.89

Table 10: Comparison of cost required to construct a side impact zone three point bend sample based on resources from Easycomposites.com. GBP is pound sterling.

This shows that the cost of creating a foam cored panel is cheaper than an aluminium honeycomb based one, due to the additional cost of applying a bonding adhesive. Not only does this increase the price, it also means the panel has to be manufactured in two stages. This is due to the necessity to bond the panel together after the facesheets have been manufactured. As the foam cored panel could be infused at the same time this meant 72 hours which were needed to bond the honeycomb and skins were saved, reducing the manufacturing time of one panel from four days to one. The decision was therefore made to use the cheaper, easier to manufacture and more resilient foam core material.

4.7 Failure mode calculations

By Thomas Gough

With the carbon fibre tensile tests completed to deduce the Young's modulus E_f and ultimate stress σ_f, the failure mode equations shown in 3.3 can now be used to determine the weakest failure mode, and whether this was greater than the required maximum force. The required data for the foam core is shown below:

With the core diameter now known as 25mm, the flexural rigidity of the side impact panels based

Property	Units	Easycell 75
Compressive Strength	MPa	1.33
Tensile Modulus	MPa	75
Shear Strength	MPa	1.09
Shear Modulus	MPa	27.75

Table 11: Material properties of EASYcell 75 foam material.

on the tensile tests and the code are shown below:

	3 ply	4 ply	5a ply	5b ply
Code	8350	9630	13300	15300
Tensile Test	1356	1458	2014	2273

Table 12: Comparison of flexural rigidity in Nm^2 calculated based on CLT code and tensile tests based on EASYcell75 foam core.

The percentage error is the same as with the Young's modulus, meaning none of the panels based on the tensile tests would pass the required flexural rigidity. Although none of the laminate configurations met the necessary flexural rigidity, a three ply laminate was created for the first side impact laminate test with issues during the manufacturing of the facesheets assumed to reduce the stiffness. Based on the data in 11 and the calculated E_f of 10.52GPa and σ_f of 632.0MPa, the following failure forces for each force were calculated.

A note should be made as previously stated that the value of σ_f is an approximation due to the multi-axial stress state beneath the load applicator [18].

The maximum loads for the face yield, face wrinkling and core shear failure modes are shown below in Table 13. The indentation load can be calculated once the indentation depth is known during the test, which is assumed to be the depth the load applicator reached at maximum loading. In Table 13 an indentation depth of 10mm is assumed as a first approximation. The shear deflection is taken into account for the face yield, but not for the core shear due to the negligible effect adding shear deflection creates. This is mainly due to the facesheets being far smaller than the panel length, the ratio of which is cubed as shown in equation 14

	Face yield	Facesheet wrinkling	Core shear	Indentation
Failure Load (kN)	140.6	13.66	15.80	16.03

Table 13: Maximum loads for failure loads based on a CF-F-3-B configuration panel.

These calculations therefore predict the panel will easily pass the necessary 4.9kN load and will fail first through the wrinkling effect created from buckling in the axial direction. Whilst the face yield is much larger than the other failure modes it should again be noted the value of σ_f is expected to be much lower in the three point bend test.

4.8 Side Impact Laminate Test

By Thomas Gough

4.8.1 First side impact panel

With the decision made to use a foam core and three ply facesheets, a three point bending test was performed on the representative 500mm x 275mm panel.

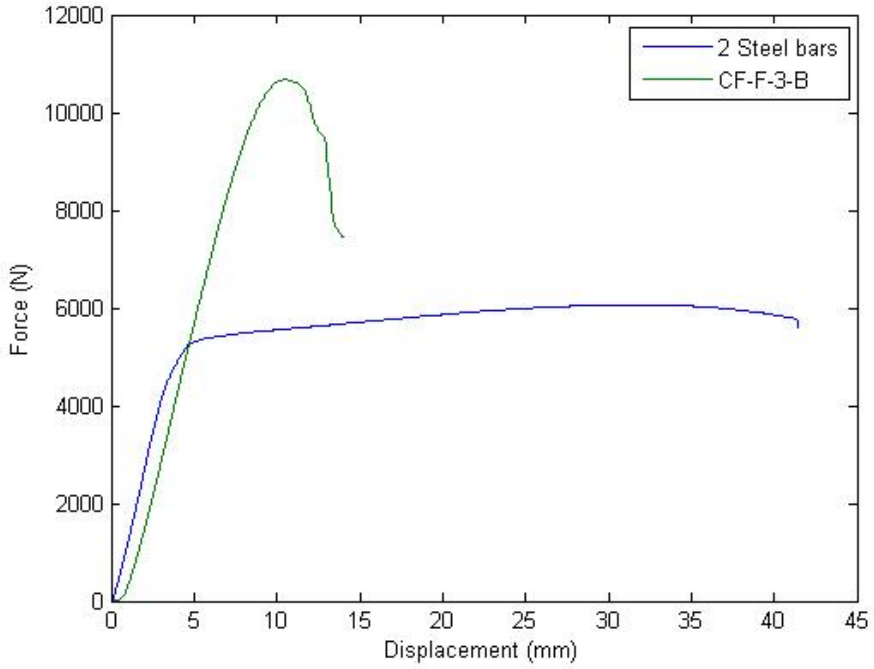

Figure 47: Load-displacement graph comparing CF-F-3-B configuration panel and two regulation steel bars.

Figure 47 clearly shows the maximum load achieved in the panel was greater than the steel bars, with a peak force of 10.69kN at a displacement of 10.47mm. Whilst still greater than required, it is less that than the 13.66kN predicted from facesheet wrinkling.

Despite the peak load occuring before 12.7mm, the absorbed energy at this point was still greater in the panel at 82.65J compared to 57.89J.

The Structural Equivalency Spreadsheet was used to determine whether the panel met the flexural rigidity. The skin modulus of elasticity was calculated using two values of displacement and load in the linear-elastic region, which was multiplied by the area moment of inertia. With a calculated value of 16.2GPa, the facesheets have a far higher effective stiffness than the 10.52GPa calculated from tensile testing. For this panel therefore the flexural rigidity was close to the value for two steel bars, however due to the vagueness in determining the start and end of the linear-elastic region it meant the value of effective stiffness also varied, making it difficult to grant a definite pass for this panel. A possible reason for this could have been the voids noted on the bottom surface as shown in Figure 48, implying a poor quality. If the quality of production in this panel was improved a greater stiffness may have been achieved.

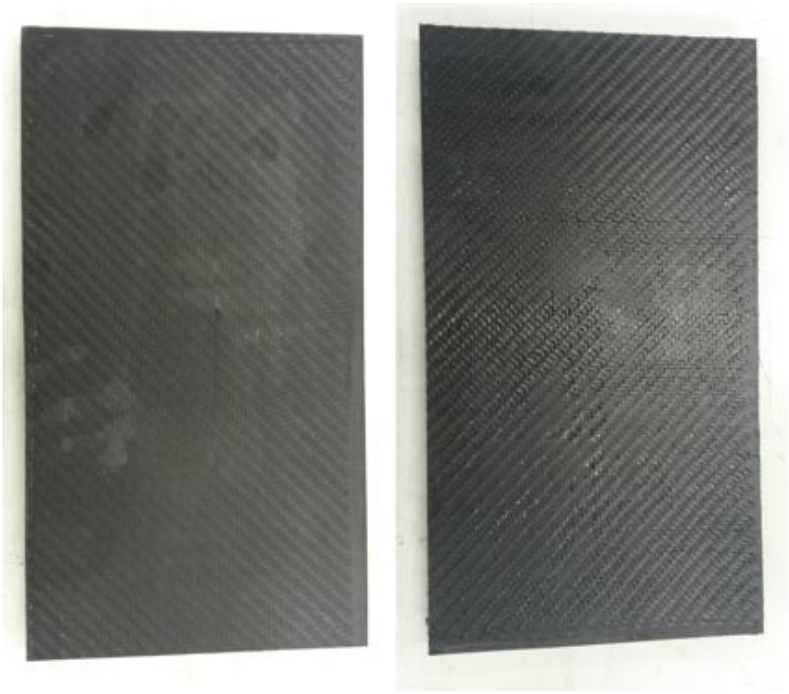

Figure 48: CF-F-3-B sandwich panel. Note voids on the surface (right).

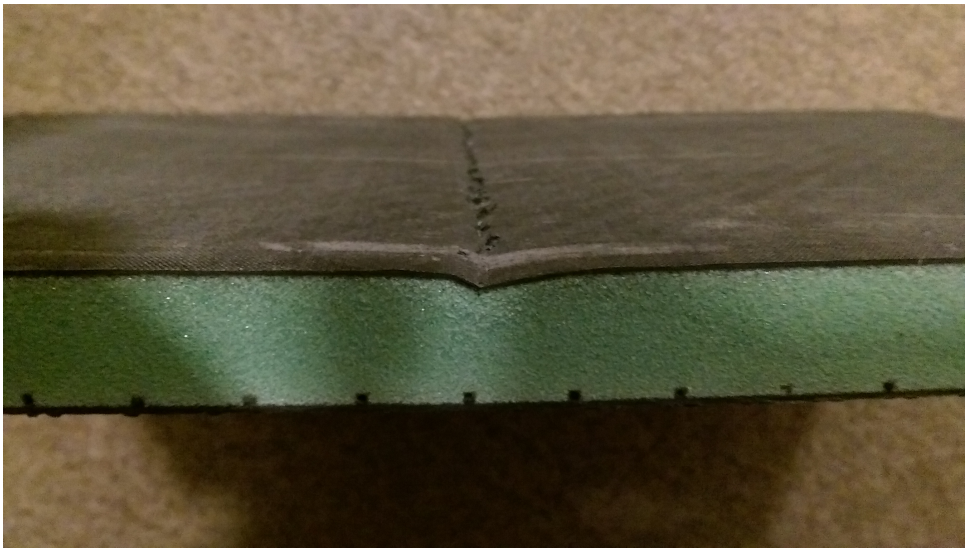

Figure 49: CF-F-3-B facesheet failure.

With the indentation depth now known to be 10.47mm, as well as the increase in effective stiffness, the recalculated indentation failure load was 21.52kN, whilst the facesheet wrinkling load became 20.03kN. This meant the theoretical failure mode core shear and the difference between theoretical and tested peak load had increased. As Figure 49 shows the facesheet had failed under compression loading, with a crack along the whole width of the panel under the load applicator. It was clear that a skin failure had still occurred, however the multi-axial stress state under the load applicator was assumed to be the trigger of this, leading to a microbuckling of the facesheet.

An additional issue was the ultimate stress of the facesheets calculated by the SES. Whilst the force at panel failure was greater than that of the steel bars the ultimate stress was far lower. Although stated as a necessity in the rules, the SES states that

	Flexural Rigidity (Nm^2)	Ultimate Force (kN)	Ultimate Stress (MPa)	Young's Modulus (GPa)	Dissipated Energy (J)
Steel	3450	6.062	365	200	57.89
Carbon Fibre Panel	3450	10.69	103	23.8	82.65

Table 14: Comparison of two SAE/AIAI1010 steel tubes and CF-F-3-B panel.

For 2015 the rules have changed to prove equivalence on absorbed energy rather than strength. This evaluation is based on the mandatory physical test data [30].

Because of this the decision was made to neglect the ultimate stress calculated in the SES.

4.8.2 Second side impact panel

With the flexural rigidity of the three ply panel very similar to the two steel bars, the decision was made to create a five ply panel, which in theory should pass the test with greater ease due to the thicker facesheets. The 5a ply configuration was used, with the additional 45/-45 layer offering a more quasi-isotropic sandwich panel which would be beneficial in the real chassis, but of less benefit for the test.

The theoretical failure loads were again calculated but this time with the data from the 5a ply tensile tests.

	Face yield	Facesheet wrinkling	Core shear	Indentation
Failure Load (kN)	239.4	21.12	16.25	21.76

Table 15: Maximum loads for failure loads based on CF-F-5a-B panel.

Again all the failure loads exceed the necessary 4.9kN, as would be expected. For this panel the theoretical failure mode was core shear due to the increase in skin thickness having a greater effect on the skin wrinkling failure load. Using the Young's modulus calculated from the SES the indentation and facesheet wrinkling loads increased to 25.14kN and 25.59kN respectively. As Figure 50 shows however a similar crack has appeared to CF-F-3-B, with little damage apparent in the core. Again the stress under the load applicator is assumed to have caused the premature failure.

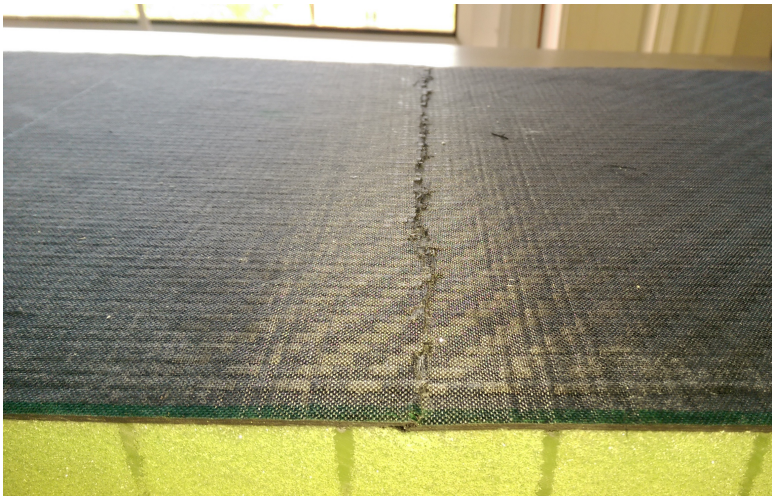

Figure 50: CF-F-5a-B facesheet failure. Note similarity to failure on CF-F-3-B panel.

Although both panels broke under skin failures, the lack of increase in the predicted core shear maximum load shows the foam core is a limiting factor. The loads required by the SES are passed, however if more strength was required in the future then a different core material may be necessary.

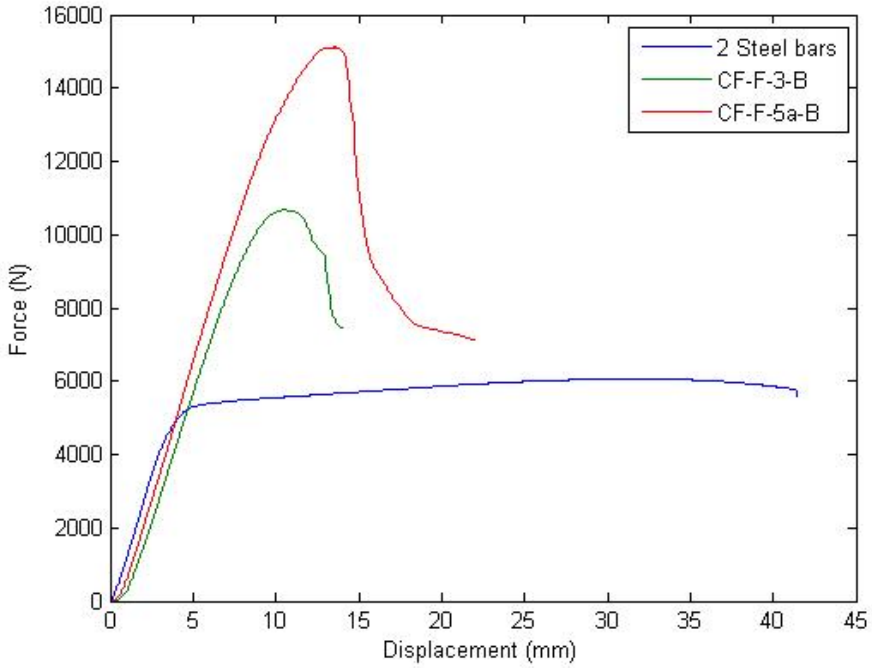

Figure 51: Load displacement comparison graph for CF-F-3-B and CF-F-5a-B panels in three point bend test with regulation two steel bars.

Using the thicker laminate gave the expected increase in area moment of inertia, leading to a flexural rigidity of around 3590, greater than the required 3455Nm^2.

	Flexural Rigidity (Nm^2)	**Ultimate Force (kN)**	**Ultimate Stress (MPa)**	**Young's Modulus (GPa)**	**Dissipated Energy (J)**
Steel	3450	6.062	365	200	57.89
Carbon Fibre Panel	3590	15.12	104	16.9	102.8

Table 16: Comparison of two SAE/AIAI1010 steel tubes and CF-F-5a-B, with values calculated using the SES.

The five ply panel can therefore be seen to pass the necessary flexural rigidity, maximum load and absorbed energy requirements.

4.9 Chassis design improvements

By Joe Edwards

4.9.1 Second iteration

The second iteration of the chassis aimed to increase the accuracy of the model and work towards a more realistic and manufacturable design. Whilst this would not be the final model, it should

highlight any potential difficulties in the monocoque design that could be addressed by the third and final design.

This second design achieved the shortcomings of the first by introducing the constant radius blends as well as planar panels. This was done with 3D modeling as opposed to just surfaces, as seen in iteration one. The three dimensional nature of the model allowed the exploration of; mounting holes for components and subsequently inserts, the joining of panels and therefore their modularity and joining method.

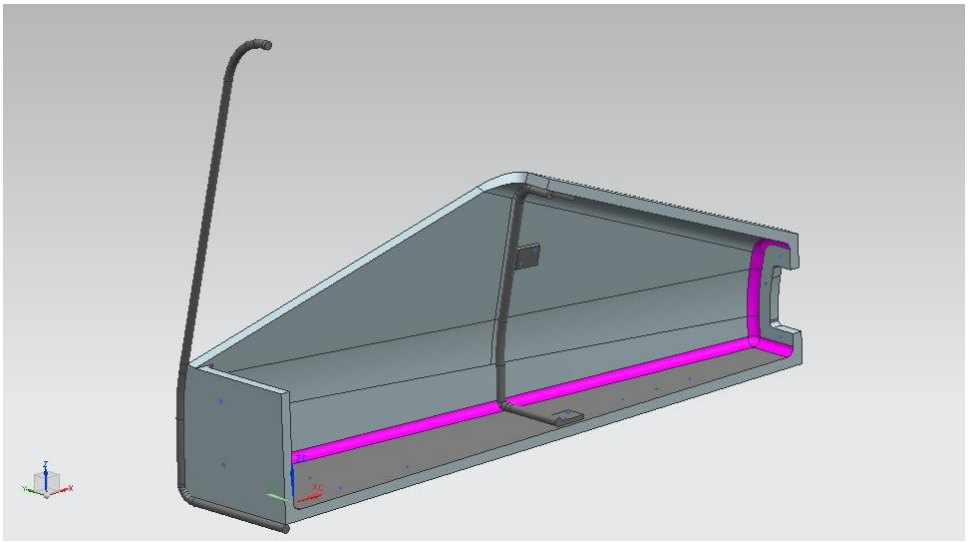

Figure 52: Second iteration of chassis design.

It was at this second design stage, whilst designing the optimal suspension that the decision for a semi-monocoque chassis was made. This decision was made to allow versatility of choice with respect to; rear suspension, engine and subsequent space frame geometry. The decision also avoided a vastly more complex rear chassis geometry to fit the rear suspension.

The joining of panels was also decided upon as a result of the discussions raised from the chassis model. A cut-and-fold method was chosen for the angled joints; such as the two spanning the length of the chassis. A Mortise and Tenon joint was decided upon for the perpendicular joints, such as those seen between the chassis and the floor, front bulkhead and firewall.

Specific types of inserts and their subsequent geometry was also decided upon, these were made from Tufnol with Aluminium_2024 sleeves.

Overall the new chassis was of a much simpler geometry, using the planar faces and constant radii blends aforementioned. The manufacturability would subsequently be improved, due to requiring only resin infusion for both types of joint and some routing for the Mortise and Tenon. The bending jigs required to achieve the cut and fold method would also be far simpler than any alternative.

4.9.2 Third iteration

4.9.3 Design

The third chassis model was used in order to refine the model for final manufacture. This was to incorporate all of the design decisions made within the project thus far such as inserts and joints, in addition to modeling details such as modularity and the integration of the rear space frame.

Inserts were integrated into the design by analyzing the various components in the 13/14 SUFST car and modeling appropriately sized inserts in the correct places. Inserts were placed in order to house the following components; Foam nose, Pedal Box, Steering Rack, Suspension Mounts, Gear Stick and Mechanism, Cockpit Space Frame, Driving Seat and the Rear Space Frame.

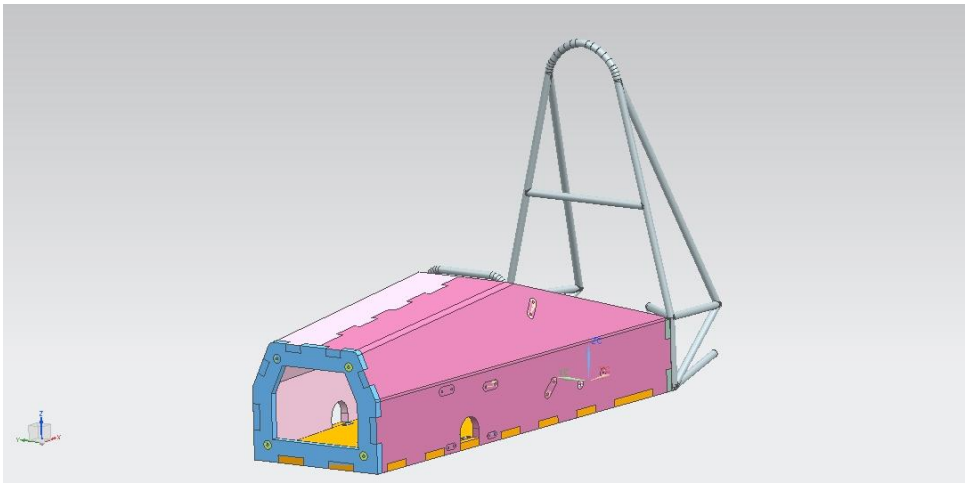

Figure 53: Third iteration of chassis design.

The joints were fully modeled, this includes the Mortise and Tenon joints between the; Chassis Right, Chassis Left, Nose Bulkhead and Firewall. In addition to a Twenty Five and Sixty-Five degree cut and fold joint running along the Chassis Right and Chassis Left - as seen above and below.

The integration with the space frame was in accordance with the 2015 Formula SAE Rules T3.35 and T3.40, using two M8 bolts for an attachment point at intermediate locations.

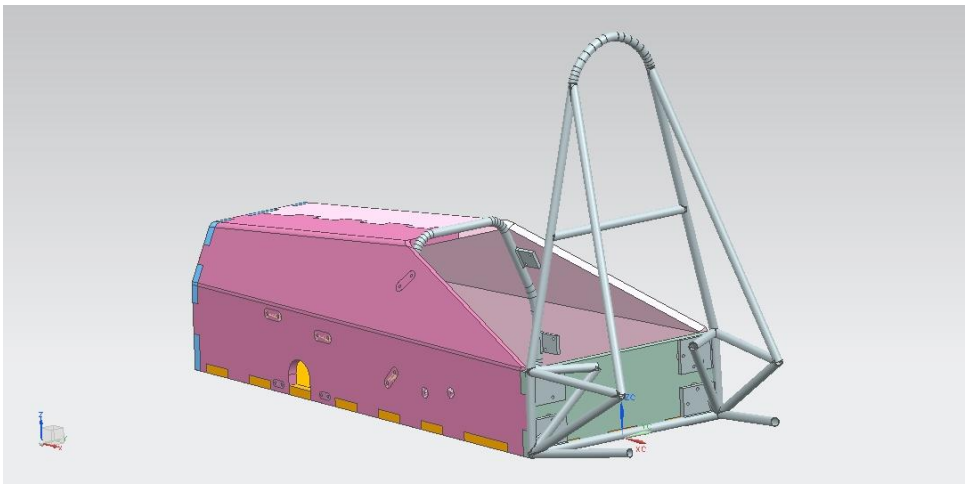

Figure 54: Second iteration of chassis design.

The modularity was determined by the method used to achieve the cut and fold joints. The panels are required to be bonded in position for up to twelve hours; they must therefore be assembled around a jig to keep them in position. This involves bonding the Chassis Left and Chassis Right into position, before lifting the panels off of the Jig and subsequently bonding the Floor, Front Bulkhead and Firewall into position, using Resin Infusion along the inner joint. The Rear Space Frame would be attached last before commencing the rest of the car build. This chassis jig is beyond the scope of the project, as no chassis will be manufactured.

4.9.4 Future Improvements

The chassis modeled will have to be modified for Formula Student purposes. The new chassis geometry should be optimised to fit the relevant Formula SAE Rules for that specific year with regards to chassis, cockpit and driver requirements, in addition to the optimal suspension geometry. Following this any modification will almost exclusively be with respect to the inserts and their positions in the chassis. All of the inserts and their positions are dictated by the various car components including, suspension, pedal box, driver seating and rear space frame these components should be designed and manufactured prior to beginning the chassis build. Once the additional components have been made, the bonding jig and subsequent panels can be manufactured.

4.10 FEA of simplified chassis (whole chassis)

By Antons Kasjanics

Before a full-scale chassis could be manufactured a finite element model has been constructed to verify whether the design as a whole is feasible, so that any changes could be applied before the chassis is assembled. The finite element model has been validated, therefore the results obtained from the full chassis analysis are assumed correct, unless proven otherwise by tests.

4.10.1 Finite element model

As previously stated in section 3.8.2, the composite skins were modelled as 2D shell elements and the sandwich panel core with any inserts was modelled using 3D solid elements. The approach is slightly different due to more complex geometry, where the sandwich panel core has been modelled using 3D TET elements. The skins could have been modelled using 2D QUAD elements, but MSC Nastran does not support 3D PENTA (pyramid with a square as the base) elements, therefore the skins have been modelled as 2D TRIA elements.

Triangular elements are known to be stiffer than quadrilateral in some cases and therefore may result in stress concentrations. This effect will be taken into account when analysing the results.

The FEA model was analysed without any roll hoops to show that the structure would pass all requirements without any metal stiffners. In reality, the deflections for some load cases should be even less if the metal tubing was not ignored.

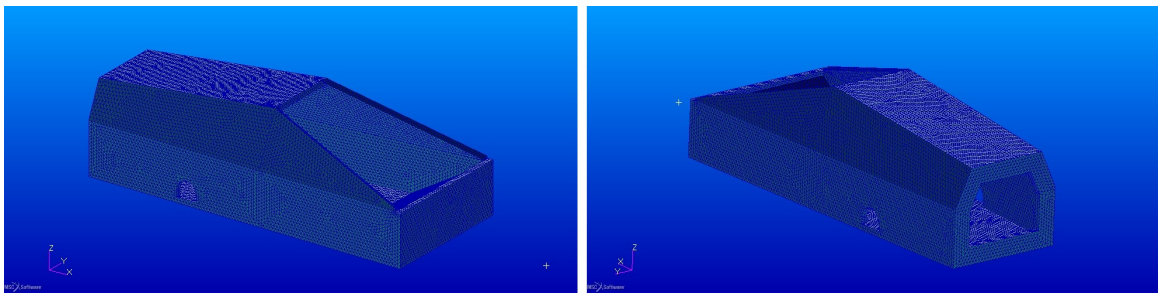

Figure 55: Final chassis mesh.

The core material is defined as isotropic and is assumed homogenous, hence specific coordinate systems need not be defined, as all material properties are the same at any point and in any direction.

The lamina material is defined as 2D orthotropic, three layers of which are then stacked up using the built in Laminate modeller at specific angles. For the material to act correctly, local coordinate systems have to be defined. The X and Y axes are defined to be in-plane, the Z axis is the out-of-plane direction.

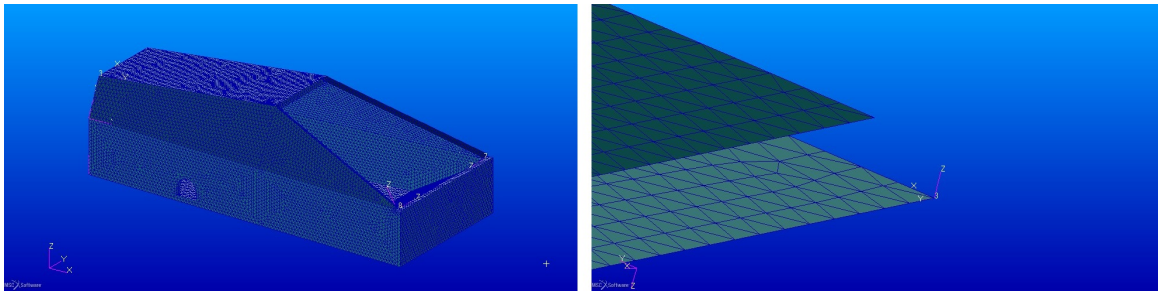

Figure 56: Final chassis local coordinate system.

4.10.2 Loads and boundary conditions

The boundary conditions for all of the load cases were the same the structure was not allowed any translations at four of the base corners, the base is meant as the floor of the chassis. The rotations however were allowed. A set of loads were applied to the structure to analyse its behaviour. Two of the loads have been defined in the FSAE rules, the rest have been selected by the team and are assumed to represent some of the race conditions, which the chassis might experience. The load cases are as follows:

1. Side impact force of 7kN (FSAE)
2. Force of 12kN applied at a certain angle on the front hoop (FSAE)
3. Front impact force of 7kN
4. Force of 3kN representing maximum loading from the suspension
5. Side impact and loading from suspension at the same time

Most of the loads are applied through the use of RBE3 rigid elements, which ensure that the loads are distributed evenly over a defined area. For the front hoop load case the force has been applied at a single node with the use of an RBE3 element the results obtained were not convincing. When applying a point force, the stress resulting in the neighbouring elements tends to infinity due to

the nodes having infinitesimal area, known as stress singularity. If this is a purely numerical issue, the stresses should not propagate further than 1-2 elements from the load application point. If the stresses are acceptable further away from the point of application, the structure is assumed to withstand the loads prescribed.

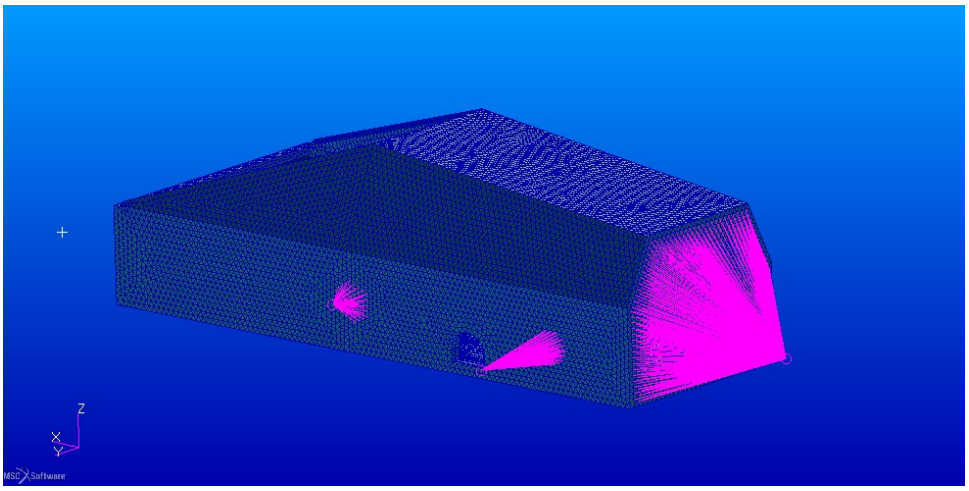

Figure 57: Final chassis RBE3 elements for load application.

4.10.3 Materials

The lamina material was defined as 2D orthotropic, E11 = E22 for a bi-axial fibre. Using the lamina properties, a three-ply composite material was defined, with each ply thickness calculated by

$$\text{ply}thickness = \frac{\text{total thickness}}{\text{number of plies}} \times \text{fibre fraction}$$

As for the three-point bend tests, the total skin thickness was assumed from other composite specimen manufacture. The core material has been defined as isotropic. The material strength and stiffness factors rely only on the core material properties any effect of the resin within the core structure is ignored due to being assumed negligible.

4.10.4 Results

Two restrictions were mentioned in the FSAE rules on any analysis the maximum deflection should not exceed 25mm and the material should not fail at any point. The tensile strength of the skin material for a composite layup was defined by the manufacturer as 1860 MPa, compressive strength as 1470 MPa and in-plane and inter laminar shear strengths as 98MPa. A Tsai-Wu composite failure criterion was used to evaluate the failure of the composite material. A correlation factor of 0.5 was also used.

The test requirements were all passed with a good margin. The expected stress concentration for a point load was within the allowable failure index, indicating that in reality the actual maximum failure index is even lower. The resulting contour fringes and a table of maximum values can be seen below:

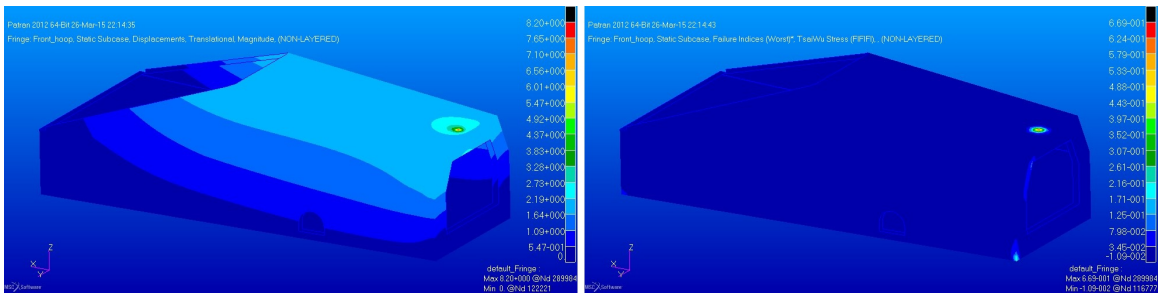

Figure 58: Front hoop applied load; Left- displacement fringe; Right - failure indices (Tsai-Wu).

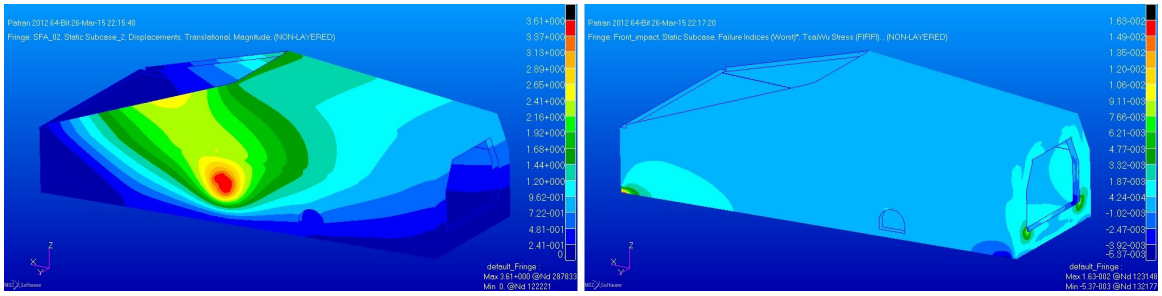

Figure 59: Side impact load; Left - displacement fringe; Right - failure indices (Tsai-Wu).

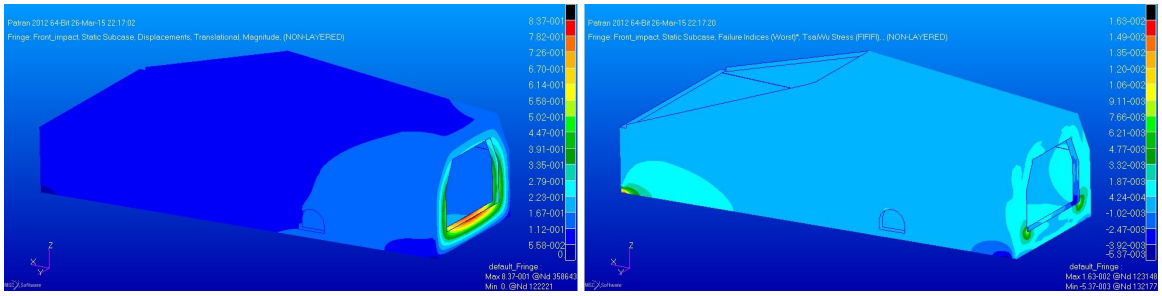

Figure 60: Front impact load; Left - displacement fringe; Right - failure indices (Tsai-Wu).

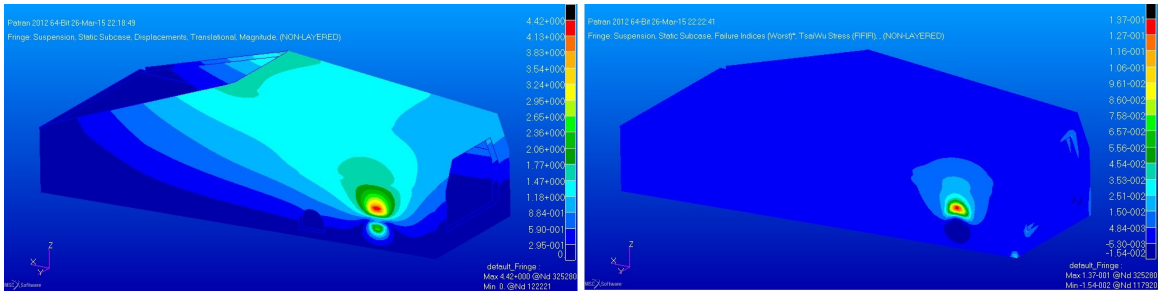

Figure 61: Front suspension load; Left - displacement fringe; Right - failure indices (Tsai-Wu).

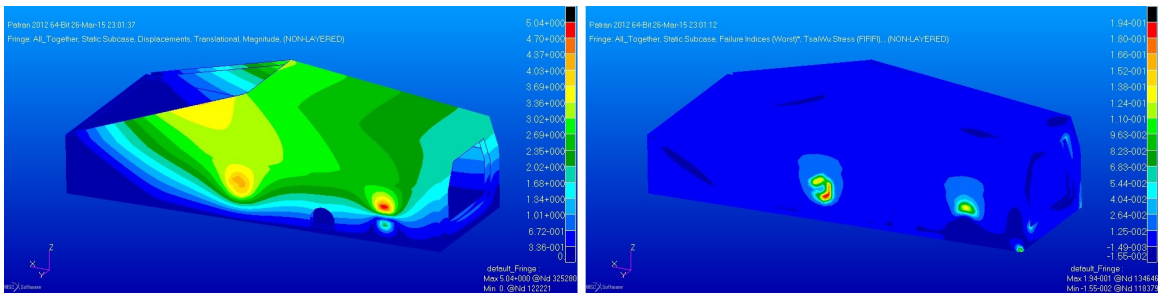

Figure 62: Side impact and suspension load; Left - displacement fringe; Right - failure indices (Tsai-Wu).

Table 17: FEA - full chassis loading results

Load Case	Max. Deflection (mm)	Max. Failure Index	Combined Margin of safety
Front hoop	8.2	0.669	0.331
Side impact	3.61	0.193	0.807
Front impact	0.837	0.0163	0.96652
Front suspension	4.42	0.137	0.8232
Side impact + Front suspension (applied at the same time)	5.04	0.194	0.7984

The combined Margin of Safety was defined as the minimum of the two safety margins one based on the allowable deflection and the other based on the material failure criteria. The margin of safety was calculated as:

$$M.o.S = 1 - \frac{\text{Result}}{\text{Allowable result}} \tag{26}$$

4.11 Inserts design

By Thomas Rickard

An insert is a piece of material placed inside the sandwich panel structure which is used as an attachment point for other components. The insert material replaces the core material which in this case is PVC foam. It must have sufficient strength to handle and transfer the loads generated by the attachment of other structural components. There are two main types of inserts, hot bonded and cold bonded. Hot bonded inserts are integrated (bonded) during the sandwich panel production. Cold bonded inserts are placed into an existing panel and potted with resin. Inserts can also either be the full or partial thickness of the panel [31].

4.11.1 Rules

Rules that apply to attachments points can be found in [9] under T.3.40 and T.3.41. One of the main rules is that attachment points between the monocoque and other primary structures must be able to carry 30KN in any direction. There are also additional rules that stipulate the load carrying ability of other attachments such as the drivers harness but these require less load. The design and testing therefore focuses on passing the requirements of 30KN assuming that the inserts can be refined for

lower loads in the future. Some important specifications mentioned in the rules are:

- Primary attachment points require 2mm steel backing plates and a minimum of 2 M8 bolts.
- The laminate, mounting plates, backing plates and inserts must have sufficient shear area, weld area and strength to carry the specified 30kN load

4.11.2 Insert types and shapes

Attachment inserts can be through-the-thickness, fully potted or partially potted [32]. Figure 63 shows the difference between these methods. An advantage of potting inserts is that they can be positioned later on in the processes rather than during the panel manufacturing which may help prevent misalignment. Potted inserts usually have ridges or steps along their vertical sides to aid in bonding.

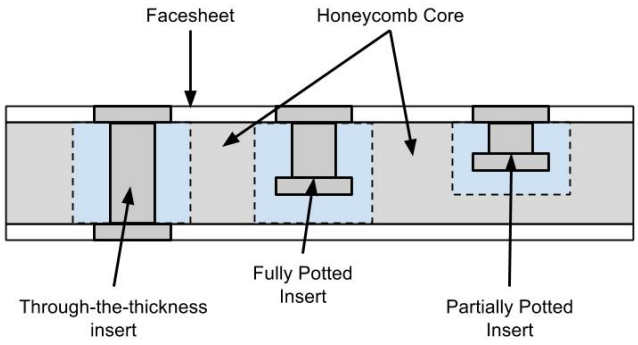

Figure 63: Difference between through-the-thickness, fully potted and partially potted inserts.

Instead of fixing an insert by potting, the core can be replaced and this is achieved by 'hot bonding' the alternative core during the manufacture of the flat panel. This also allows multiple inserts to be groups together. The simplest core replacements have flat vertical sides which are connected by a butt joint the core material. [33] suggests that shaping insert boundaries so that they are inclined to the panel faces smooths out material discontinuities reducing local stress concentrations at the edge of the insert. Figure 64 shows an illustration of this. A benefit of using a core insert over a potted one is that the core insert can be shaped accurately (by CNC milling for example) to provide the best load transfer. This also means it can be optimised by the removal of material unlike a potted area.

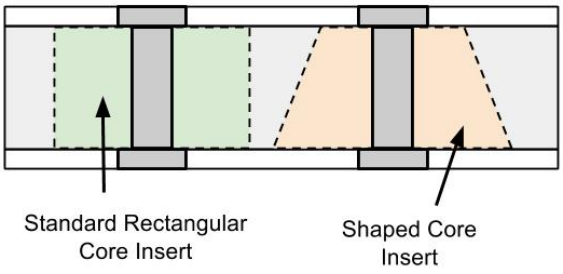

Figure 64: Different core insert shape, with rectangular (left) and shaped (right).

Although benefits can be achieved using this methods they require more complex machining and preparation of the materials making them unfavourable for this project. Using aluminium as a core insert is also an option. An aluminium core insert can be easily tapped allowing attachments to be bolted directly into the structure without needing a nut.

As the rules stipulate that 2mm steel backing plates or an equivalent must been used for attachments to primary structures it follows that a through-the-thickness insert must be used. The next choice is whether to pot the insert or replace the honeycomb with a hot bonded core insert. Using the cut-and-fold method has some influence here as it is harder to accurate position hot bonded core inserts so that they are in the correct position after the panels have be folded, it is far easier to do this when using a fully moulded technique.

A method that lends itself to easy manufacturing is to use a hot bonded core replacement material combined with a push fit aluminium tube and backing plates. The aluminium tubing prevents compressive loads when tightening bolts and is easy to source and machine to the correct tolerances. The sleeve can also be fitted after complete construction for improved tolerances. The core replacement provides the load transfer into the surrounding area and the backing plate provides the necessary shear perimeter. Figure 65 shows the different options available.

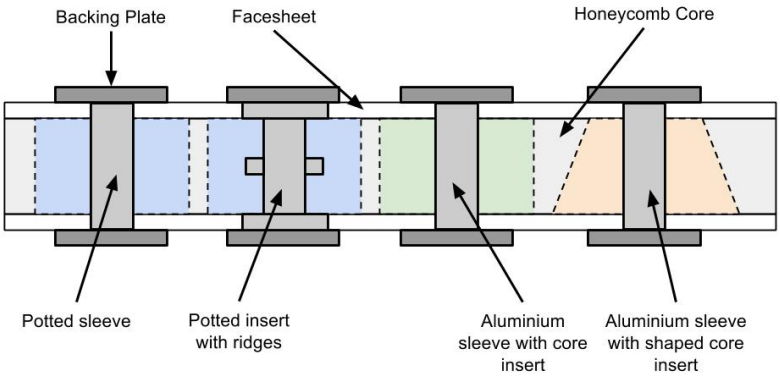

Figure 65: Different insert options.

The rules state that attachments to primary structures must be able to withstand 30KN. Primary structures in this context include the main and front roll hoops, bulkheads and members that transfer load from the driver restraints. Different inserts may be used for other areas which take reduced

loads (less than 30KN). Here partially potted inserts may be useful due to their reduced weight. The correct insert must be able to transfer the following types of load:

- Tensile, normal to the surface
- Compressive, normal to the surface
- Shear, in the direction of the facesheet
- Bending
- Torsion

4.11.3 Material selection

Inserts can be made of various materials including aluminium, wood, high density foam and engineering plastics. Table 18 shows some generic properties of these insert material.

Material	**Tufnol**	**PVC**	**Al 2024-0**	**Hardwood**
Tensile Strength (yield) (MPa)	68	55	81	80
Compressive Strength (MPa)	310	?	81	40
Shear Strength (MPa)	90	?	125	?
Young's Modulus (GPa)	6.3	3.1	73	12
Density (Relative)	1.36	1.74	2.77	0.7

Table 18: Properties of different insert materials. Note some data could not be found for PVC and Hardwood.

Tufnol was chosen because of its high strength and low density in comparison to the other materials. Although roughly the same cost as aluminium tufnol also benefits from better machinability and no corrosion issues when placed in contact with carbon fibre.

4.11.4 Tensile strength (transverse load)

Failure modes affecting the tensile strength for a transverse load are:

- Pure shear rupture of the core
- Shear and tensile rupture of the core
- Tensile rupture of the potting compound

In this case the rules state that a 2mm backing plate must be used on both sides of the insert at so the transverse load capability is determined by the shear strength of the core and facesheet. The adequate shear area can be calculated from the perimeter shear test results. The SES (structural equivalency spreadsheet) provides a section for calculating this which is shown in figure 66. The value of the skin thickness is actually set to 1.35mm but the spreadsheet has formatted the visual output to a 1 in the figure. It should be noted that the perimeter shear strength was taken from the carbon-honeycomb panels and that carbon-foam panel are predicted to perform better as shown by he fibreglass tests. The calculations for tensile loads are also valid for compression loads for through-the-thickness inserts.

	Attachment 1		Attachment 2		Attachment 3		Attachment 4	
Attachment Status	PASS		PASS		N/A		N/A	
Fastener dia., mm	8	PASS	8	PASS	0	FAIL	0	FAIL
No. of fasteners	2	PASS	2	PASS	0	FAIL	0	FAIL
Bracket to hoop weld length, mm	80	PASS	80	PASS	0	FAIL	0	FAIL
Bracket thickness, mm	2	PASS	2	PASS	0	FAIL	0	FAIL
Bracket perimeter, mm	194		194		0		0	
Skin thickness, mm	1		2		0		0	
Insert Perimeter, mm	194		194		0		0	
Skin thickness, mm	1		2		0		0	
Backing plate thickness, mm	2	PASS	2	PASS	0	FAIL	0	FAIL
Backing plate perimeter, mm	194		194		0		0	
Skin shear strength, MPa	68		68		68		68	
Perimeter shear strength, kN	35	PASS	52	PASS	0	FAIL	0	FAIL
Perimeter shear strength, kN	35	PASS	52	PASS	0	FAIL	0	FAIL

Figure 66: Insert specifications in the structural equivalency spreadsheet (SES) for the main roll hoop.

The SES implements the following formula where the shear strength is calculated by the peak load attained in the perimeter shear tests. The perimeter shear area is calculated from the insert, backing plate and skin thickness as show below.

$$\text{Load capability} = \text{shear area} \times \text{perimeter shear strength}$$

It was found that an insert with a perimeter of >190mm gave a pass.

4.11.5 Shear Strength

For a sandwich panel four different failure modes are possible when using carbon fibre facesheets. These modes are tension, shear-out, dimpling and bearing [32]. [32] suggests the equations below to calculate these failure modes for CFRP facesheets. Equation 28 is used to calculate the maximum in-plane load against failure in tension:

$$Q_t \leq \frac{1}{K_e^{'}}(w - b_i)t_s\sigma_{t,ult} \tag{27}$$

$$\rightarrow Q_t = \frac{1}{2}(100 \times 10^{-3} - 10 \times 10^{-3})(1.35 \times 10^{-3})(632 \times 10^{6}) = 38.894 \times 10^{3} N \tag{28}$$

Where:

w = Panel width

b_i = Insert diameter

t_s = Facesheet thickness

$\sigma_{t,ult}$ = ultimate tensile strength of facesheet

e = Edge distance

$K_e^{'}$ = stress concetration factor depending on $\frac{b_i}{w}$ and $\frac{e}{w}$

Equation 30 is used to calculate the maximum in-plane shear-out load [32]. The original formula from [32] failed to take into account the shear strength provided by the bond between the grouped insert and the facesheet. This bond is normally weak in comparison with the facesheet strength but in this case provides a substantial force due to it's hot bonded characteristics.

$$Q_s \leq 2t_s(e - \frac{b_i}{e})\frac{1}{cos\alpha}\tau_s + (\tau_{Epoxy} \times \pi(r_p - r_i)^2) \tag{29}$$

$$\rightarrow Q_s = 2(1.35\times10^{-3})(50\times10^{-3} - \frac{10\times10^{-3}}{50\times10^{-3}})\frac{1}{cos0}\tau_s + ((50\times10^{6})\times\pi(15^{-3} - 5\times10^{-3})^2) = 23.052KN \tag{30}$$

Where:

α = Angle of failure direction

τ_s = In-plane shear strength of facesheet

e = Distance from insert centre to edge in shear-out direction

r_p = Potting radius

r_i = Insert radius

Values for the max tension and shear out load are multiplied by two to take into account the required two inserts (with M8 bolts) per attachment point, this results in a maximum tension load of 76.788KN and a maximum shear load of 46.103KN. Due to the use of foam as the core material dimpling is not a valid failure method and so was ignored. The compression strength of the facesheet was unknown and therefore a bearing load capability could not be calculated. The results suggest the inserts will failure by shear out under in-plane tension loads.

4.11.6 Edge influence

Edge influences for out-of-plane loading dependent mainly on the core and are only present where there is a free edge on a panel. The reduced load carrying capacity can be expressed as shown in equation 31.

$$P^*_{SS} = P_{SS}\eta_{EN} \tag{31}$$

Where:

P^*_{SS} = Reduced load carrying capacity

P_{SS} = Initial load carrying capacity before before edge effect

η_{EN} = Edge coefficient for normally loaded inserts

The edge coefficient can be calculated using equation 32 for $e \leq 5b_p$ where e is the distance between the insert centre and panel edge and b_p is the insert potting radius. It should be noted that the edge coefficient is equal to 1 if the panel has edge close-outs.

$$\eta_{EN} = 0.55\sqrt{\frac{e}{b_p}} - 0.05\frac{e}{b_p} \tag{32}$$

[32] states that due to the complex nature of composite facesheets tests are required to gather usable data for edge coefficients in shear loading (in-plane loading). Due to the limited number of tests no edge coefficient data will be able to be collected. It will be assumed that the tests will be carried out under the worst possible edge conditions compared to those that would be found on the car. The results should they pass the regulations will guarantee the worst possible loading case making use of the inserts on the car chassis valid. No edge closeout mechanism will therefore be used on the test panels. Figure 67 shows the final dimensions of the proposed inserts.

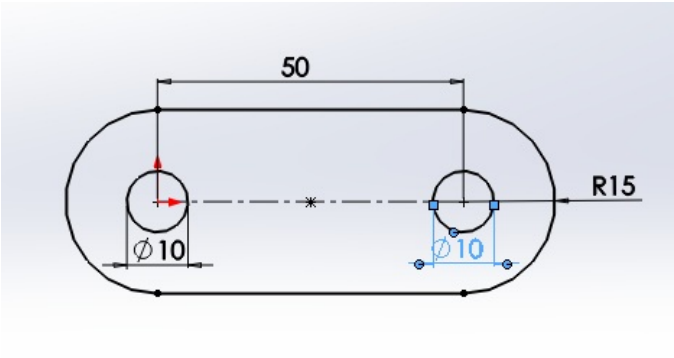

Figure 67: Final design dimension of the inserts to be used for primary structure connections

4.12 Joints design

By Joe Edwards

4.12.1 Overview

Due to the geometry of the chassis, and its semi monocoque nature, designing and manufacturing the design required a variety of joining methods. Whilst researching these joining methods two key aspects were imperative, which were, ease of manufacture and weight. Structural failure modes were analysed in addition to these design requirements in order to choose the most appropriate method. Whilst ideally tests of all alternative joints with our specific face sheet and core would be desirable to make the decision, monetary and time restrictions meant this wasnt feasible. As a result publications on similar methods were sought, and aided to an informed decision.

The first design challenge was to put a radius between two planar panels; this has up to four different solutions, e - h, as seen in figure 68, taken from [34]. The solution we opted for was the cut and fold method. This allowed the outer skin to remain continuous, whilst the inner skin had a strip removed to ensure to the skin didnt crush whilst bending. The other solutions, primarily used metallic materials manufactured to the required radius, which the sandwich panels would then fit into. This method whilst preferable for ease of manufacture would have been far heavier, not only due to the metallic materials themselves, but also the inserts that would have been required to fit them.

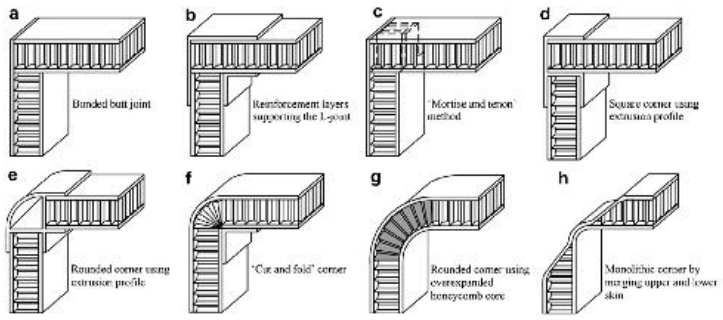

Figure 68: Different types of joints.

The second design challenge was to fit two panels together perpendicularly. Initially the first method would be preferable, however upon testing the panels significantly large angles (above 70 degrees) would cause a tensile failure in the outer face sheet. This could be resolved by increasing the face sheet thickness or strength **??**, however this would again add weight. A Mortise and Tenon joint was decided upon. This method is low in weight and very simple to manufacture, requiring only the routing of the core and skin. Other options such as the bonded Butt joint wouldnt be as strong due to having less surface area bonding and no physically interlocking parts. Any monolithic joints were negated due to the complexity of manufacture whilst machining the core to 45 degrees.

4.12.2 The cut-and-fold joints

The nature of the chassis geometry dictated the angle to which the panels were to be bent. Although there are two separate joints, with their own individual angles (25 and 65 degrees), the joint with the most severe angle will be tested. Testing this panel alone is primarily due to monetary restrictions, but it will also be the weaker of the two panels. The panel itself will have higher tensile stress concentrations in the outer face sheet, have more of its core removed to enable the bending and have less area available for bonding the inner joint. As a result of the higher tensile loads in the outer face sheet, the panel will be more susceptible to tensile failure in said face sheet from compression of the joint. The subsequent facing thickness or facing strength could be increased to reduce this effect, should it become an issue. Less core material, such as that required around the joint in the cut and fold method, will increase its susceptibility to transverse shear failure. This cannot be improved by adding additional panel thickness, as any additional thickness would then have to be removed to enable bending. Finally having less area on the inner face sheet for bonding will reduce the strength of the joint; increasing the likelihood of void-based failure due to difficulty of manufacture.

4.12.3 The Mortise and Tenon joint

The chassis design requires a perpendicular panel joint between the floor, chassis, front bulkhead and firewall. The joint will be exposed to three different experimental tests; the first of which would be a shear test, applying a load in the plane of one panel, with the perpendicular panel being fixed. Such a test would result in the loads at which core shear failure, de bonding and subsequent crack development would occur. Visual representations of the failure and the associated expected Load-Displacement graph is seen in figure 69, taken from [34]. Please note the values are arbitrary, its merely the effect of various stages of failure on Load-Displacement that are of value from the figure. The tensile and compressive tests would give the loads required for failure in the joint, these would

likely occur due to core shear failure, tensile and compressive failure in the inner and outer face sheets respectively for an tension test and vice versa for a compressive test. The shear failure could be remedied by increasing the panel thickness, however due to the whole chassis being of uniform thickness this would increase the weight considerably, it would therefore be preferable to increase the core strength or panel thickness.

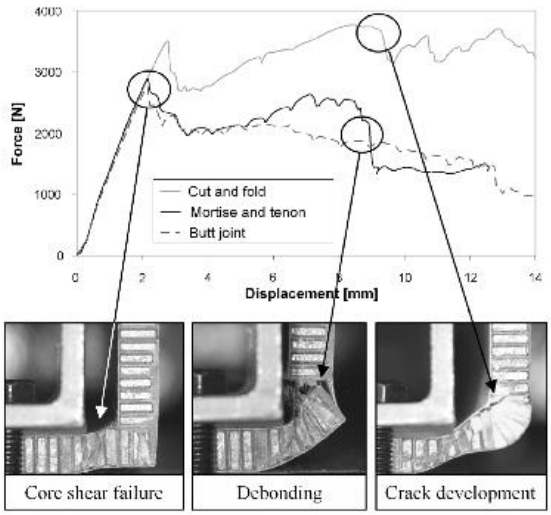

Figure 69: Joint failures.

Ultimately these failures were predicted to occur at lower loads due to the reduced surface area for bonding, in addition to having no mechanically interlocking parts in alternative joints such as the Butt joint. Metallic components were negated for joining the panels, due to their weight, similarly to the cut and fold joint. These lower loads sustained by a Butt joint were seen in tests using similar sandwich panels [34]. Note the lower force at which the joint fails.

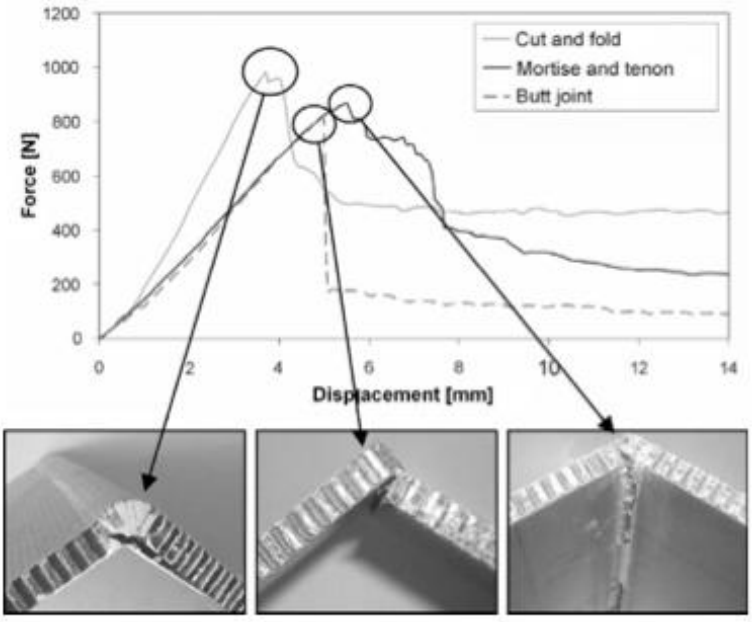

Figure 70: Joint failures for different types of joints.

A Mortise and Tenon joint was also used connecting the two sides of the chassis in a planar joint. This was again chosen due to its ease of manufacture and predicted superior performance over a

Butt joint for a planar panel this would just involve the face sheet overlapping the other panels core, alternatively on the inner and outer face. The joint will again be exposed to a compressive, tensile and shear test. The tensile test will result in a tensile bonding failure between the two cores and a bonding shear failure between the face sheet and core. This could be subsequently improved by perfecting the resin infusion process. The compressive test could lead to general buckling of the panels, subsequent shear crimpling and potential face wrinkling as a result of adhesive bond or core compression failure [31]. The shear test could lead to a shear failure of the core itself, or any of the compression failures specifically at the interlocking parts of the panel. This could be solved by increasing the panel thickness or core strength, both of which are ill favored options due to the subsequent increase in weight.

4.13 Manufacturing insert and joint rigs

By Joe Edwards

4.13.1 Cut-and-fold and insert testing rig

The nature of the chassis geometry lead to bent panels with a specified angle between them. The testing of the panel with the largest angle; in tension and compression required a more complex testing rig due to the actuation only being able to occur on one fixed axis. The test itself was upon the strength of the joint only, as a result the rig had to ensure that the forces from the machine were applied to said joint. These results will be compared to our Finite Element model of the whole chassis. This comparison will show if the expected chassis loads as specified in the 2015 Formula SAE Rules, Article 4 supersede the strength of the panels practically tested [4]. In addition to the joint test, the rig also had to be utilized for an in plane shear test for the inserts as per 2015 Formula SAE Rule T3.40.1 [9]. This required the rig to be used in pure tension. For the joint test, the resulting rig needed to be able to pivot such that the loads werent applied to the clamped parts potentially resulting in core shear failure. The pivot also ensured pure tension was adhered to for the insert in plane shear test. Due to budget constraints any form of bearing arrangement wasnt feasible and the pivot was subsequently provided by a H9/D9 tolerance for the hole and shaft respectively. To ensure a uniformly applied load, sleeves we made for each bolt to sit in the inserts. Further to this, a shimming solution was used to ensure the mounting plates sat flush on the face sheets, again ensuring no asymmetric loading across the plates and subsequently the bolt, sleeve, inserts and finally joint.

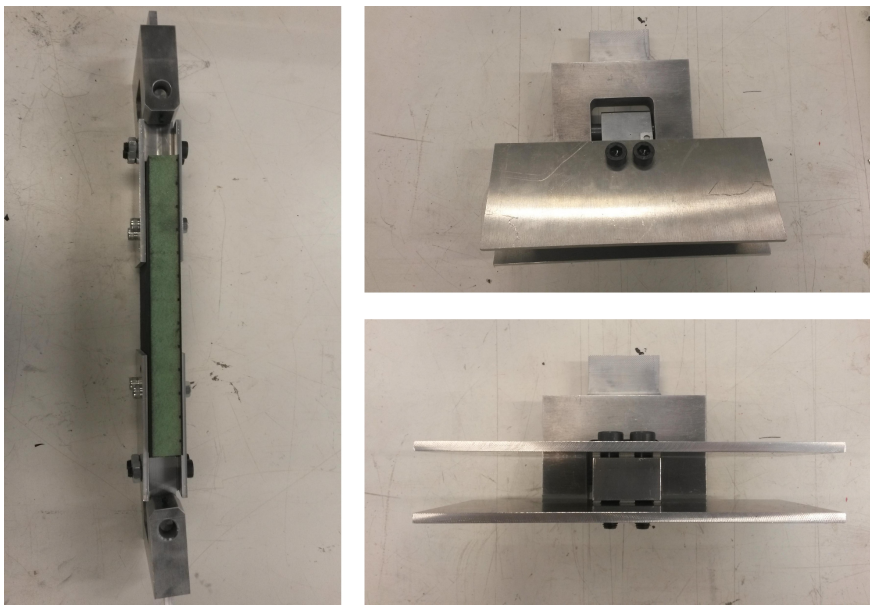

Figure 71: Insert and joint testing rig. Note the metal faces were rotated and shortened to allow them to be placed on the joint specimen.

Another analysis of the stress concentrations and subsequent displacement of the components with the maximum stress applied was carried out. This gave the following results. Again this yields a total deflection of 0.27mm, which is 0.10% of the total axial length, again negligible.

Table 19: Joint and insert testing rig FEA result

Component	**Deflection (mm)**	**Maximum Stress concentration (MSC)/MPa**	**Safety Factor (TYS/MSC)**
Y - Bracket	1.8×10^{-1}	151	2.74
Pivot Pin	1.12×10^{-1}	399	1.03
Pivot Bracket	5.32×10^{-2}	1.49	2.78
Whole Assembly	0.2732	N/A	0.8232

Table 20: Insert and joint testing rig deflection and stress results from an FEA simulation.

4.13.2 Cut-and-fold manufacturing jig

In order to achieve the cut a fold joint a standard panel must go through the routine resin infusion process. Following this an appropriate slat must be removed from the inner face sheet to allow for bending. Achieving the final bent panel is done in two parts, the first of which is bending the panel to the required angle, and the second is holding it in that position for a prolonged period whilst the epoxy sets.

The rig used must be structurally strong enough to overcome the force from the bent core and outer face sheet during the bending process. In addition the resulting jig assembly must be sufficiently accurate to ensure the panel is bent to the correct angle uniformly along is width.

Figure 72: Cut-and-fold bending jig in closed configuration, used for creating joint panels with a 65 degree bend.

The resulting design, as seen in figure 72 accomplishes the structural requirements by using four sets of 12mm thick MDF for cradling the panel, supported by two 18mm steel rods and 12mm thick MDF base for support. The whole structure is bonded using ample amounts of Gorilla Glue. An appropriate chamfer was applied the jig, where it meets the inner joints to prevent the two from bonding. The joint is held accurately in place using laser cut panels, which are clamped together using the ratchet strap arrangement shown above.

4.14 Manufacturing of joint and insert specimens

By Thomas Rickard

This section outlines the joints and inserts manufacturing process. A far more in detail account can be found in the logs supplied on the CD as extra material. Samples were manufactured by cutting out sections of foam and replacing them with tufnol inserts.The panel was then infused with carbon inner and outer skins in one go as done previously. Switching from Aluminium honeycomb to foam greatly improved the ease and efficiency of embedding insert into the core material.

Figure 73 shows the tufnol inserts being placed into a joint panel. The locating holes were milled slightly large than the insert to allow room for the resin to flow into and fill securing the insert.

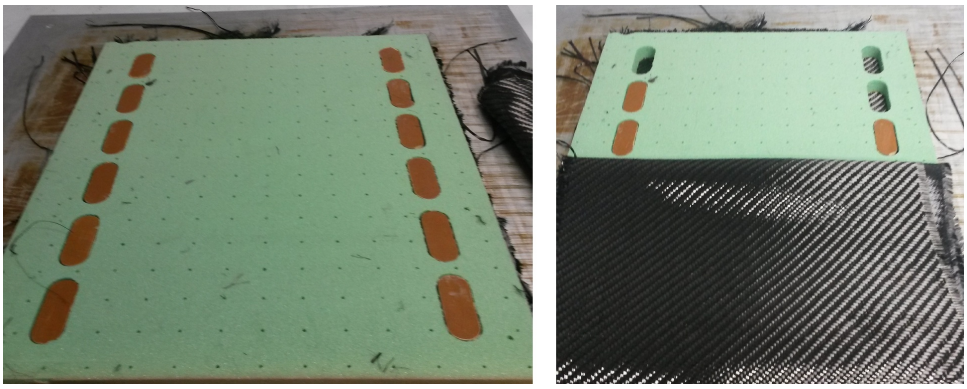

Figure 73: Tufnol inserts placed into pre-cut holes in the foam core before resin infusion.

Figure 74 shows the cured panel with trimmed edge and a groove cut down the centerline. The tufnol inserts can be faintly seen along the top and bottom of the panel. The groove down the centreline was cut to allow the panel to be bent. Although a joint panel is shown figure 74 the insert panels were manufactured in an identical way. Instead of having a groove cut the insert panels were half the size of the joint panels and featured two extra rows of inserts. The panels measure 250mm long compared to 500mm for the joints panels.

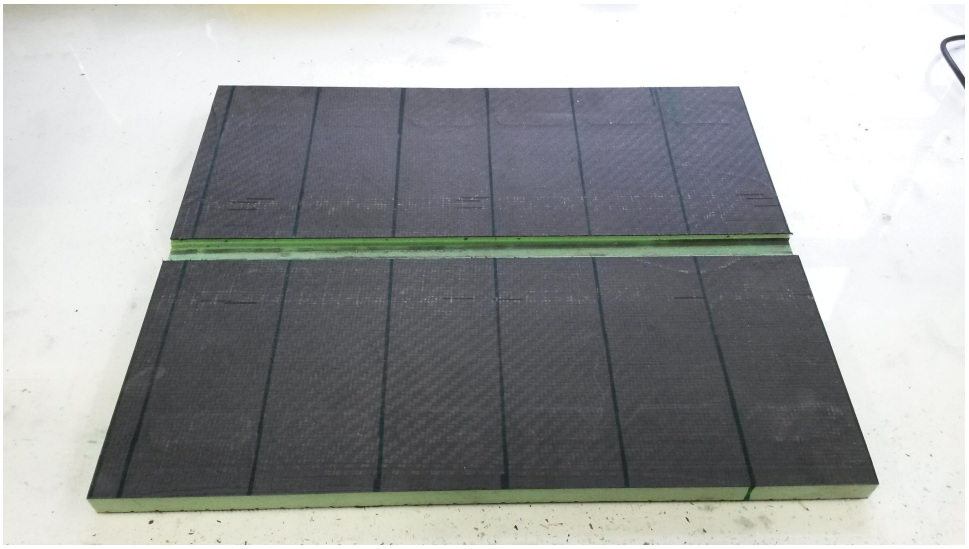

Figure 74: Panel trimmed to size with a groove cut down the centerline ready to be folded.

After being cut into individual strips the joint panels were place in the folding jig. Here an epoxy paste with glass microspheres was applied to the groove areas and the panels were clamped and forced into shape using ratchet straps as shown in figure 75. During the bending process some cracks were heard and although it was unclear as to whether it was the facesheet, foam or solid epoxy but it would suggest that a 65 degree bend may be slightly too large. It may have also been caused by the epoxy cured in the grooves and resin flow holes in the foam. there was a groove fairly close to the bend which raised one side of the bend and it is believe that this may have been the actual source of the cracking noise rather that the facesheet or foam.

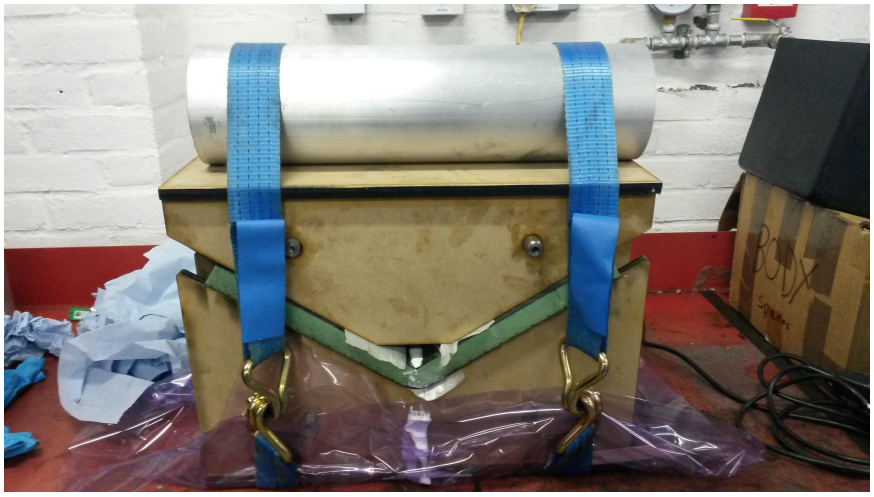

Figure 75: Panel being folded in the joint jig.

Next the inner reinforcing joint was laid up as shown in figure 76. Originally this joint was meant

to be resin infused for layup consistency and performance. However, limitations in jig size and panel cutting required the panels to be pre-cut to the 100mm width and resin infusion of such a small area was not possible or worth the effort. instead standard wet layup was used to create the inner joint as shown in the figures below.

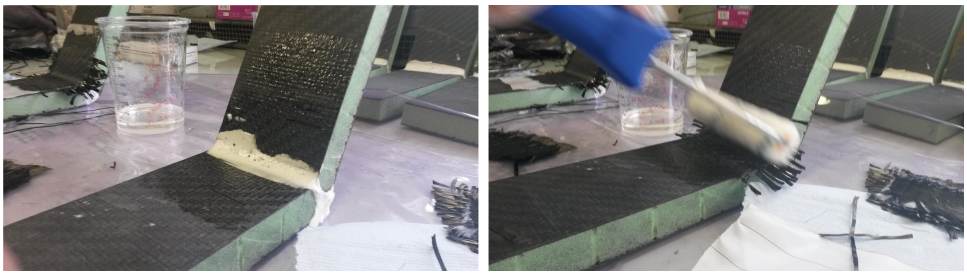

Figure 76: The inner joint carbon fibre reinforcement made using wet layup of four carbon fibre plies.

After all the inner joints had been laid up the locating holes in the inserts had to be drilled ready for the metal sleeves. The holes were drilled in the EDMC workshop on a standard milling machine as shown in figure 77. At the same time as drilling the panels metal sleeves were cut and drilled on the lathe to the correct size. That size was a 8mm inner diameter to take an M8 bolt and a 10mm outer diameter to create a tight fit when pressed into the drilled holes.

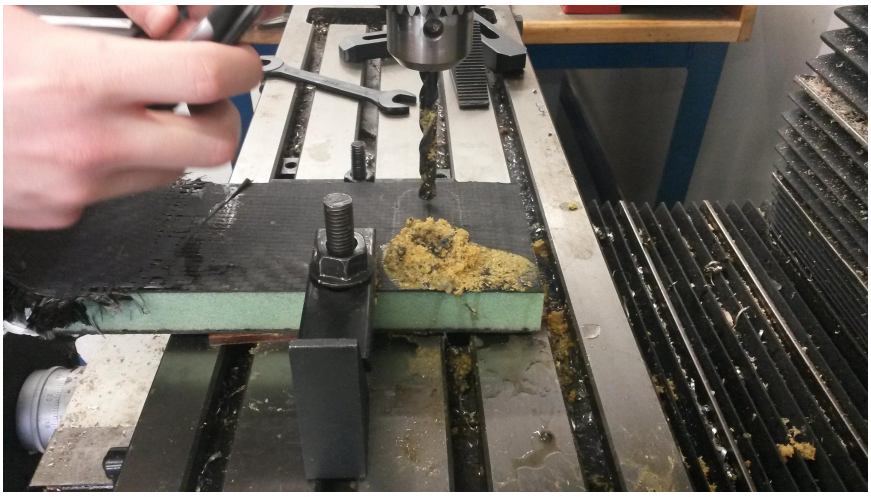

Figure 77: Holes being drilled into a joint panel to accommodate the metal sleeves.

The sleeves were pressed into the drilled holes and the rig fastened firmly ready for testing of the panels.

5 Design: Stage 3

In this section results from the insert and joints tests are shown and discussed and the procedure for manufacturing a full size panel or scaled model is outlined.

5.1 In plane pull out insert tests

By Thomas Gough

Two tests were created to deduce whether the attachment points could sustain the 30kN load required from section T3.40.1. The specimen were loaded into the test rig as explained in the insert testing log.

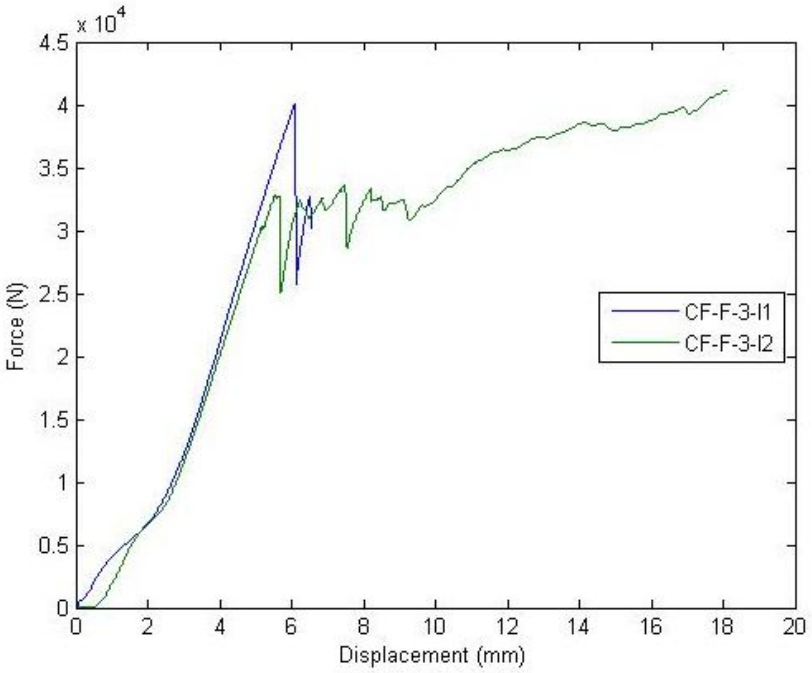

Figure 78: Load displacement graph of insert tests to determine strength of attachment points.

Figure 78 shows that the maximum tensile load carried by both specimens exceeded the required 30kN. The load taken before the first substantial drop was 40.08kN at a displacement of 6.091mm for CF-F-3-I1 and 32.87kN at 5.632mm in CF-F-3-I2. Although both tests exceeded the load, the first cracking noises were detected at around 30kN, implying part of the structure was beginning to fail. As specifically stated in Article T3.40.6

no crushing of the core is permitted.

This meant CF-F-3-I1 was stopped after this first drop in load, whilst the second test was continued to deduce the damage caused after this point. Numerous defects can be seen when comparing CF-F-3-I1 and CF-F-3-I2. The first of these is the dragging of the sleeves through the facesheet on CF-F-3-I2 as shown in Figure 79 due to the greater displacement it was tested to. The slowly increasing load after this peak could be due to foam core becoming crushed and denser, requiring a greater load to crush it further as the displacement increased. To begin this crushing however the strength of the facesheets had to be overcome, indicated by the first peak.

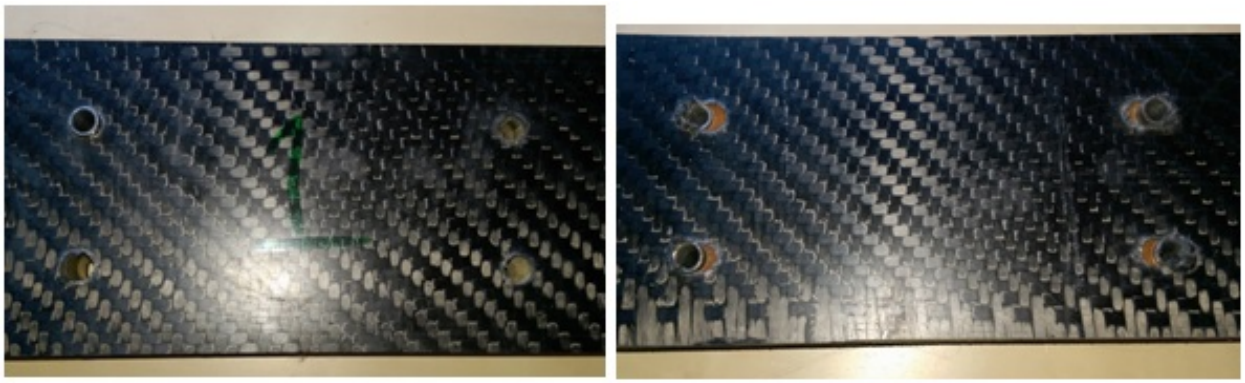

Figure 79: Movement of the inserts caused by continued tension of insert test, with CF-F-3-I1 (left) stopped after the first drop in load and CF-F-3-I2 (right) continued.

There appeared to be no deformation of the tufnol insert, implying the whole tufnol insert was being pulled through the foam core as opposed to just the bolt and sleeve. This would explain the damage shown in Figure 80. CF-F-3-I2 shows the facesheet separating from the core. This could be caused by the tufnol insert being taller than the foam core, thus when the insert is pulled through the core it forces the facesheet apart. This in turn creates a shear on the core, creating the cracks also shown.

Figure 80: Damage caused by continuation of insert test, with CF-F-3-I1 (left) stopped after the first drop in load and CF-F-3-I2 (right) continued.

With the lack of damage created in CF-F-3-I1 in comparison to CF-F-3-I2, it can be assumed that no crushing of the core occurred before the first load peak, which in both tests exceeded 30kN.

5.2 Joint tension tests

By Thomas Gough

Three tests were conducted on joint panels to determine the tensile force required to break the panel. Although no required load had to be met, they were tested to deduce the effectiveness of the joint bending and compared to an FEA simulation with unbroken facesheets. The setup is shown in Figure 81 below.

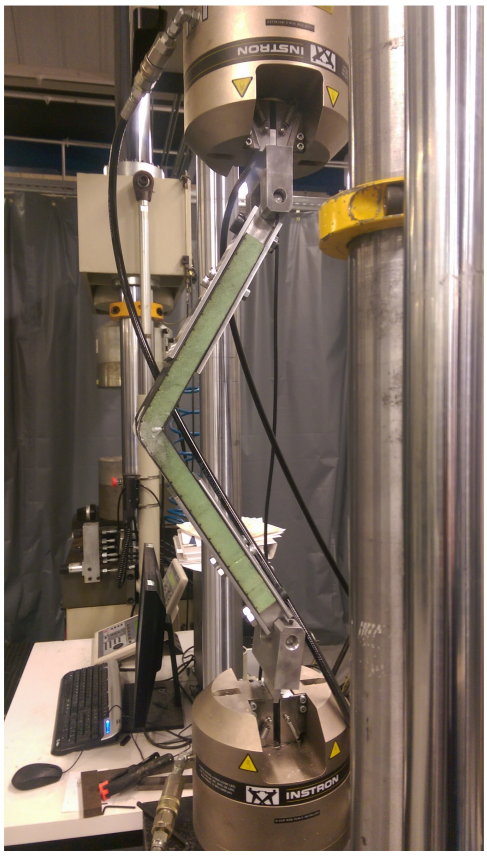

Figure 81: Joing tension and compression test setup.

In all cases the crack first propagated within the core at the bend as expected. In CF-F-3-JT1 and CF-F-3-JT2 the crack continued in the loaded direction before meeting the outer facesheet. Due to an error setting up the first test the machine was left in load mode by accident, leading to the displacement rate increasing near the breaking, leading to a larger displacement and larger crack. The crack made in CF-F-3-JT3 was far shorter than the other two, as shown in 83. Whilst the core was also coming away from the outer facesheet these two cracks did not propagate into one. This smaller crack may explain the fluctuating loads near the peak as opposed to a fast drop in load, with the foam remaining intact and stopping the load reduction.

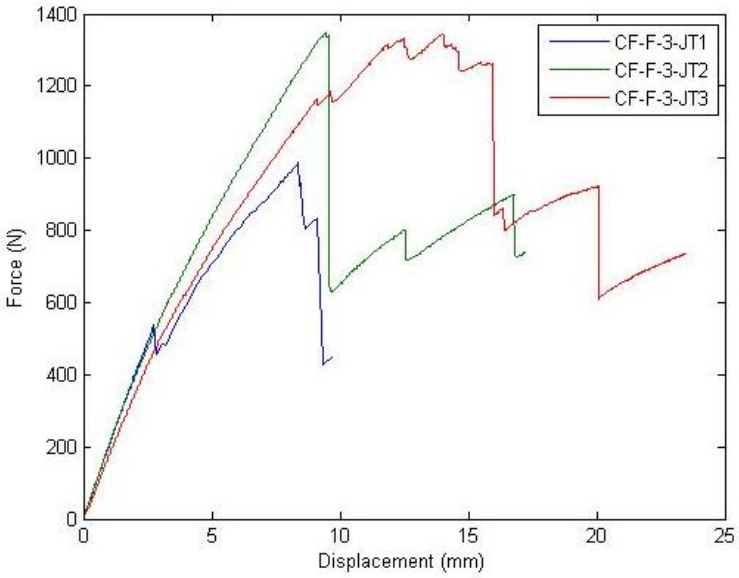

Figure 82: Load displacement graph of tension test to determine strength of 65 degree joint.

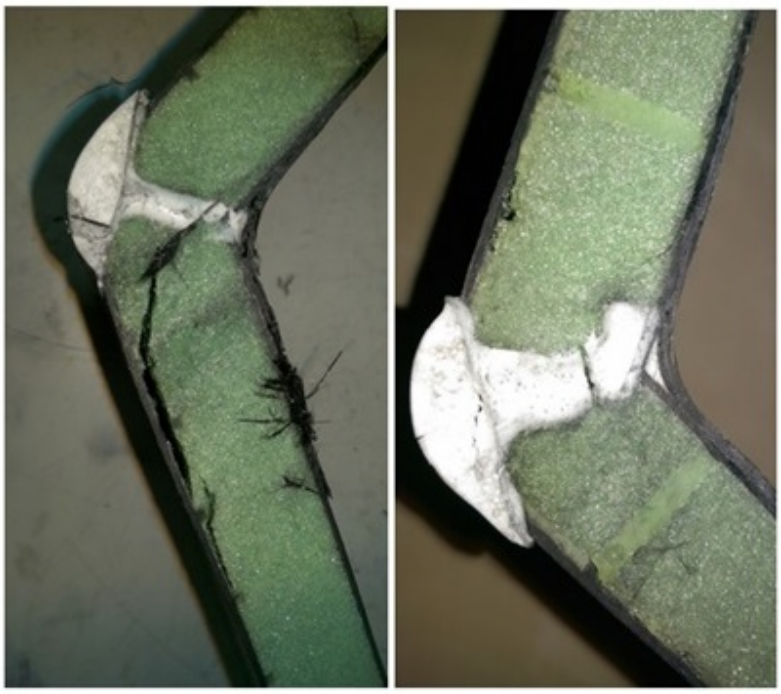

Figure 83: Comparison of core damage sustained in CF-F-3-JT2 (left) and CF-F-3-JT3 (right).

The location of the first major break ranges between 8mm and 16mm of displacement as seen in Figure 82. This variation could be caused by the amount of epoxy used in the bend as some would be squeezed out of the crevice during the bending. Despite the variation in displacement the peak loads reached by CF-F-3-JT2 and CF-F-3-JT3 were very similar, shown in Table 21. The ultimate load reached in CF-F-3-JT1 was considered an anomoly due to the error in setup.

No damage was noted in the facesheets, especially in the wet layup region on the inside of the bend where the epoxy held the plies intact.

Test	Maximum Force (kN)	Displacement (mm)
CF-F-3-JT1	0.9889	8.375
CF-F-3-JT2	1.349	9.469
CF-F-3-JT3	1.345	14.01

Table 21: Maximum loads reached for tension tests on 65 degree joint panels.

5.3 Joint compression tests

By Thomas Gough

Compression tests were also completed on three joint panels. As Figure 84 shows the ultimate compression load was very similar to the ultimate tensile load, despite the very different loading characteristics and failure. The displacement to peak load was far greater, occurring around 20-25mm with a short elastic region and large inelastic region. This large displacement meant the panels could be bend to around 90 degrees without excessive damage caused.

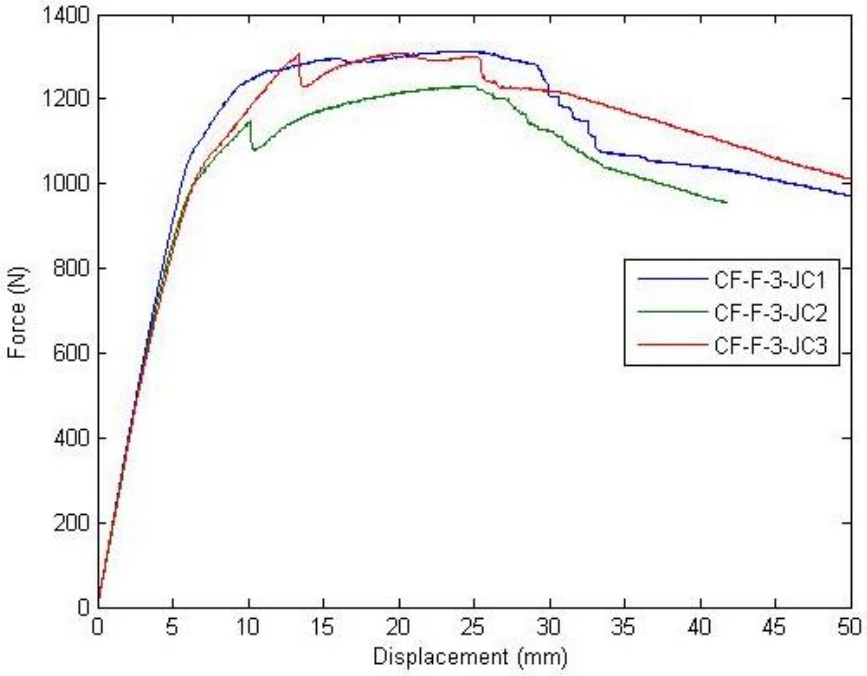

Figure 84: Compression test to determine strength of 65 degree joint.

All three panels shows very similar stiffnesses in the elastic region, although the displacement at which the first drop in load varies. CF-F-3-JC1 showed no decline in load until the maximum load was achieved. Instead there is a greater region of level load before a number of small failures. This led to a quicker reduction in force from the ultimate load. The similar maximum forces achieved are shown in Table 22.

Test	Maximum Force (kN)	Displacement (mm)
CF-F-3-JC1	1.314	23.65
CF-F-3-JC2	1.230	24.68
CF-F-3-JC3	1.311	20.35

Table 22: Maximum loads reached in compression tests for 65 degree joint panels.

Figure 85 shows a crack developed in a compression test. These cracks could be seen in CF-F-3-

JC2 and CF-F-3-JC3 but not test CF-F-3-JC1, implying the crack developed from the drop in load occuring around 10mm. As Table 22 highlights the panel with no crack achieved the greatest load.

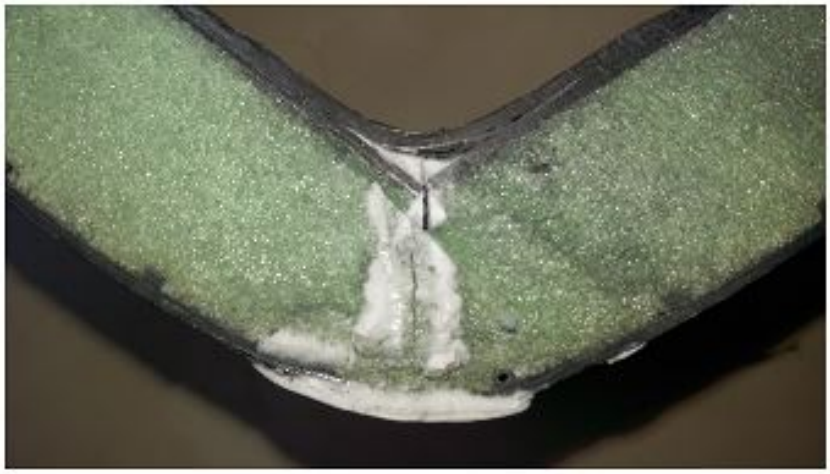

Figure 85: Crack in CF-F-3-JC3 compression joint test.

Again no damage could be seen in the facesheets on either the outside or inside. It can be deduced therefore that the carbon fibre facesheets are able to cope with stresses applied during the joint manufacturing proceedure and under tension and compression loads.

5.4 Joint panel FEA

By Anton Kasjanics

For the radius tests a very simplified finite element model was used. The model did not have any fillets, which should reduce stress concentrations in the corners, but the fibres were assumed to be continuous, as well as the core material. It was expected that the finite element model should be stiffer than the actual test specimen, but the stress concentrations at the bend could be higher.

The following mesh was used: the skins were assumed very thin and discretised using 2D QUAD4 shell elements. The core material was defined using 3D HEX8 elements. With a mesh refinement study conducted it was deduced that a target element size of 5mm is fine enough.

The model was fixed at one end (rotations were allowed) with a distributed load applied along the face on the opposite side. The load was applied along a specific direction to comply with the experimental setup. This setup is shown in Figure 86.

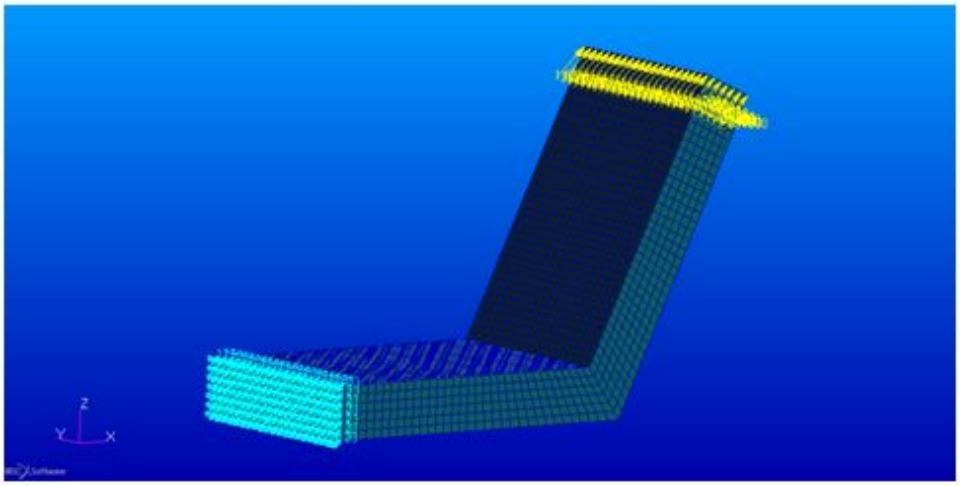

Figure 86: Applied load and fixings.

Several loads were applied to obtain a load-displacement curve, which could be compared with the test results. As expected, the FEA predicted a stiffer structure as shown in Figure 86, but the difference in results is not too large, indicating that the manufacturing approach was good enough to keep the structure strong.

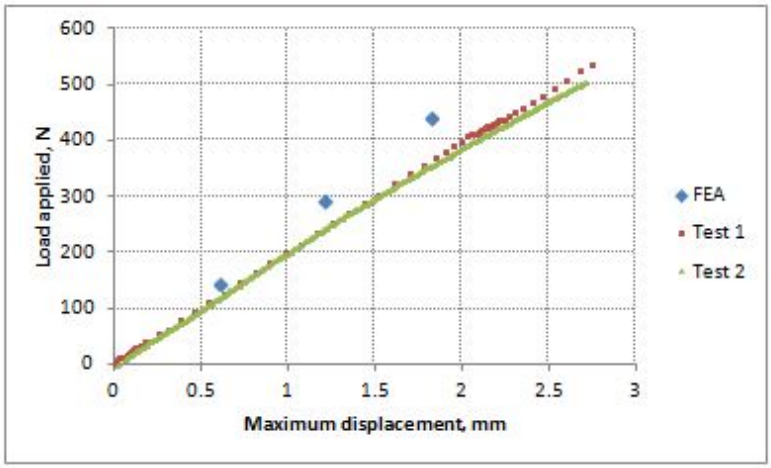

Figure 87: Load displacement comparing tension tests to FEA simulation.

Figure 88 gives the expected stress concentration, with high stress in the inside of the joint. As previously stated the real sample had a fillet in the form of the wet lay up laminate which would reduce the stress concentration.

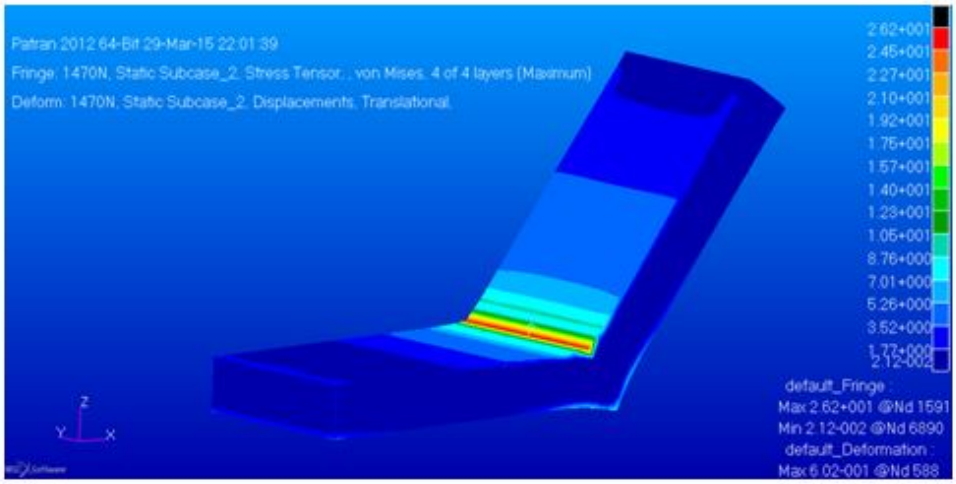

Figure 88: Stress contours created in joint tension test.

5.5 Full panel manufacturing cycle

By Thomas Rickard

Due to time constraints a scale model could not be produced however techniques for constructing the various elements such as joints and inserts have been proven so far by the project. The following section outline the manufacturing process required to construct either a scaled model or a full size car. The car should be designed such that it is constructed of three panels as seen in the project chassis design. These three panels can then be manufactured in the following way

Stage 1: Purchase a sheet of PVC core foam of the correct thickness and density.

Stage 2 - part 1: CNC mill out the panel shape and all the insert locations (A side panel is shown in the figure, two of these and a floor panel will have to be made). Then mill out the inserts out of the specified insert material (engineering plastics/aluminium). Alignment holes should also be milled so that at later stages the panel can be replaced on the table for extra work.

Stage 2 - part 2: CNC mill out rabbet/lap joints which will be used to join panel later on. The inserts should be placed in their respective holes ready for lamination.

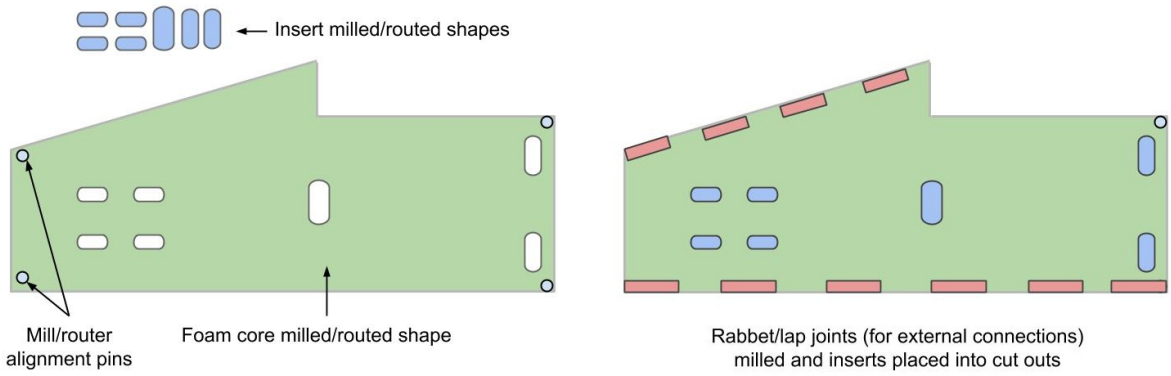

Figure 89: Full panel manufacturing - Part 1: Full panel manufacturing; Left - stage 2 part 1; Right - stage 2 part 2

Stage 3: Resin infuse both carbon facesheets in one go. This also fixes the inserts into place. A possible extra feature - The layup of fabric and foam can be assisted by the used of a projector with software that maps the image to the size of the panel.

Stage 4: The panel is placed back on the CNC router/milling machine where strips of the inside facesheet are cut out to facilitate the cut-and-fold joints. A final trim of the outer perimeter is also done to get rid of any unwanted fibreglass

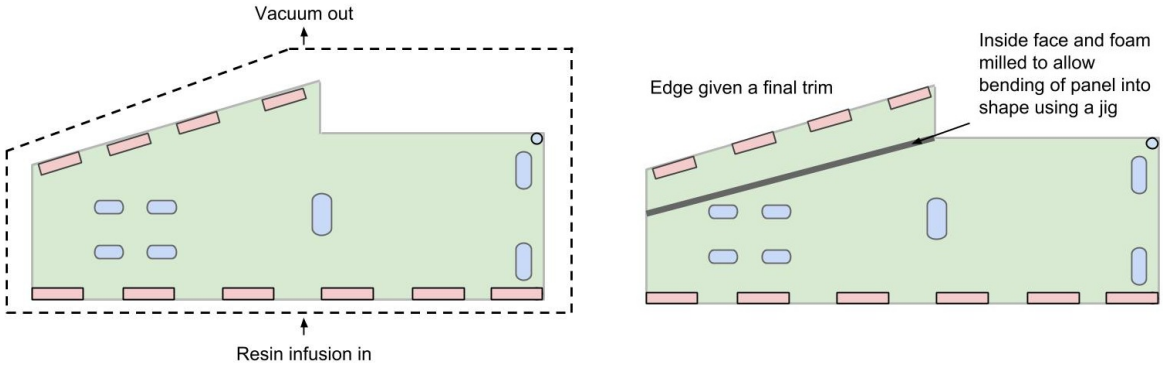

Figure 90: Full panel manufacturing - Part 1: Full panel manufacturing; Left - stage 3; Right - stage 4

Stage 5: The two side panels and floor panel are placed in wooden/aluminium jigs, folded and glued to the correct shape. The joints are then reinforced with extra carbon fibre using resin infusion.

Stage 6: All three panels are brought together, bonded and reinforced with extra carbon fibre.

6 Critical Comparison

By Thomas Rickard

6.1 Weight

To compare the potential mass of a carbon-foam chassis and a space frame chassis A weight estimate was applied to the chassis geometry. Mass for the inserts are known and the joint masses are predictable. The chassis was considered to have CF-F-5a-B side impact zones measuring 500mm by 275mm and CF-F-3-B zones everywhere else. Using this configuration the mass prediction should be very conservative as no true optimisation has been carried out on the panels, inserts and joints. Table 23 shows the the calculated panel masses while table 24 shows the calculated joint and insert masses.

Table 23: Mass of finished 3ply and 5 ply Panels with a conservative 50% resin content

Laminate - 3 ply	**Mass g/mˆ2**	**Laminate - 5 ply**	**Mass g/mˆ2**
Single Facesheet	1200	Single Facesheet	1950
Single Resin (50%)	1200	Single Resin (50%)	1950
Foam Core	1800	Foam core	1800
Total Panel	6600	Total Panel	9600

Table 24: Mass of joints and inserts

Joints		**Inserts**	
Joint mass - fibre (g/m)	200	Insert mass (g)	70
Joint mass - resin (g/m)	200	Number of inserts	24
Joint length - cut and fold (m)	4.66	Total insert mass (g)	1680
Joint length - mortise/tenon (m)	5.175		
Mortise/tenon mass (g)	4140		
Cut-and-fold mass (g)	1864		

When applying these masses to the full chassis with a surface area of $2.4m^2$ a total combined mass of 33.46kg is calculated as shown in figure 25. This includes the mass of the tubular space frame and an extra 10% leeway granted for manufacturing tolerances. Last years Formula student space frame chassis (2013/14) had a mass of 37kg and so the carbon-foam chassis would potentially offer a mass saving of 3.5 kg over a similar design. Although this design is still lacking a suitable bridge structure across the rear it highlights that weight can be saved using this approach. Should it be refined a much greater weight saving may be possible, in the region of >5 kg.

Table 25: Mass of tubular sub frame and combined total chassis

Sub Frame Tubes		**Combined masses**	
Sub frame length (m)	6.371	Total mass with joints and inserts (g)	24349
Steel density (g/cm^3)	7.87	Sub assembly mass (g)	6068
Steel density (g/m^3)	7.87E+06	Total car mass (g)	30417
Cross section (m^2)	0.0001210	Total car mass + 10% (g)	33459
Tube volume (m^3)	0.0007711		
Total tube mass (g)	6068		

6.2 Finish and fit

The composite panels can be made with a predetermined finish such as a gelcoat . Laying up the panels flat it is easy to get a good finish with absolutely minimal fibre distortion. Folding of the panels at large angles does create distortion to the outer which can been seen a small cracks. Joins at the base and vertical center-line of the chassis require extra laminating work and this causes and uneven and noticeably different finish in these areas. It is recommended than these areas be filled with epoxy and microspheres and faired to create a smooth seamless surface. It may be a good idea to put decals or racing stripes along these areas where as the rest of the car can be kept as bare carbon which is aesthetically pleasing and lightweight (compared to a painted surface). Apart form the external panel joints minimal work would be needed to prepare the surface for paint should it be required. The small aluminium plates used for moulds specimens during this project were generally very scratched and in bad condition causing a poor surface. For a full car a new mould surface would be needed. The best choice for this would be glass. Glass can be highly polished and will enable a mirror like finish on the external surface of the panel.

6.3 Aerodynamic devices

The cut-and-fold technique used in this project can be effective at creating mould-less simplified structures but cannot replicate any double curvature often required by aerodynamic devices. While the chassis acts as a bluff body and can therefore be made using the cut-and-fold method, sidepods and nose cones must be made using traditional moulded methods. The traditional method requires a female mould and/or a plug to be constructed in order to carry out the lamination.

6.4 Recommendations (Future improvements)

The facesheets could be subject to more tests to help predict the performance of the inserts. It would be good to test bearing and shear failure modes more thoroughly. Tests could also be carried out on individual plies to determine there exact properties as instead of the facesheet as a whole. The tensile test specimen could be improved. The specimen should be increased in length, which would also allow the use of an extensometer to gain more accurate strain readings.

The final design in this report proposes a semi-monocoque with a flat floor. Although this is a simple design it might not be the preferred choice depending of the configurations of other systems and further confidence gained by additional testing. A profiled floor is common amongst Formula Student cars and could be adopted to this design fairly easily. The floor would need to have several cut-and-fold joint as well as dedicated jig just like the two sides of the vehicle. The profile of the sides would have to be adjusted to accommodate this. A future team may also wish to extend to a full monocoque. This requires extra long side panel with additional inwards folds which can be achieved. It would require an elongated jig and some form of heat testing of the panel in order to be safe. Folding the structure in this area also limits the rear suspension geometry fair significantly but a satisfactory geometry may be found by angling to panel so it tapers more and the floor than the top.

Further investigation could be made into the structural degrading of the joint area caused by the cut-and-fold technique. Imaging may help provide an insight into the damage caused in the outer

skin especially for large fold angles.

The insert testing was limited due to time constraints and there are many options that could be explored in this area. Firstly several different insert materials could be substituted. Some suggestions include aluminium and different grades of Tufnol. The shape of the inserts may be manipulated to create a larger bonding/potting perimeter i.e. have a wavy perimeter. They could have cut outs to save weight, however due to the use of resin infusion there would have to be a thin skin placed on top of the cut out to prevent resin from flowing into the cavity. Scarf joints could be used instead of butt joins between the foam core and the insert material. Partially potted insert should also be tested thoroughly while varying parameters such as potting diameter and insert height. This is import as partially potted insert can be added at the end of manufacturing giving the designers so leeway.

Laminate optimisation could be carried out so difference areas of the car are designed with differing fibre stacks and orientations based on the local forces in that area. So far this has not been done as the main focus was satisfying the rules based on the side impact region and proving the feasibility of such a chassis. Extras test panel would need to be made and tested for each different layup order/orientation change.

7 Conclusion

By Thomas Rickard

Structural Considerations and Formula Student rules

This project has proved that a carbon monocoque chassis is structurally achievable within the given weight of a steel space frame. It has also proven that this is possible using the cut-and-fold technique as opposed to the more common method of using prepreg and an autoclave. Both FEA and physical tests have been used help achieve this result.

Weight

The predicted combined mass of the semi-monocoque and steel sub frame is 33.5kg, a reduction of 1.5kg over the previous years SUFST steel space frame. This is a conservative estimate of a somewhat unrefined process. In the future optimisation of the layup stacks and inserts should reduce the mass further. At it's current mass it could be argued that it is not worth pursuing over an optimised space frame. However, with further development the monocoque's mass could be reduced much more than an equivalent space frame and potentially ofter a more streamlined manufacturing option.

Ease of manufacture

The method of manufacturing test panels and future full size panels has improved throughout the project. Initially panels were made by resin infusing individual facesheets and then secondary bonding was used to join the facesheets to the honeycomb core. Later on in the project this was changed to an all in one infusion using a specially drilled foam core that allowed resin to flow from one side to the other. This cut the manufacturing time to roughly a third of the original time. The change to foam also allowed an accurate method of insert placement to be achieved by the use of CNC milling. This drastically reduces the labour required by automating the process and subsequently decreases the chance of manufacturing mistakes.

Reliability of manufacture

The resin infusion method proved fairly tricky to initially get right but after making several mistakes and gaining experience it was shown to be a reliable way of producing the carbon fibre panels. Secondary bonding caused issues early on and the bond between the aluminium honeycomb and composite facesheets could not be made structurally acceptable and consistent. Switching to a PVC foam dramatically increased the performance and reliability of sandwich panels as they could be manufactured in a single infusion. The reinforcement layered over the cut-and-fold joints was shown to be withstand a consistent loading across several specimens proving reliability of the method even though an inferior wet layup method was used.

Testing results

Despite initial difficulties meeting the requirements in three point bending whilst using an aluminium core, switching to a foam core dramatically improved results as well as reducing manufacturing time. This meant the flexural rigidity, maximum load and absorbed energy were all passed in line with SES calculations.

The shear tests conducted were easily passed. Although the final side impact configurations were not

tested, glass fibre skin with foam core panels did, whilst carbon fibre honeycomb samples proved to be stronger than their glass fibre counterparts. This meant it was assumed the final configuration would also meet the requirements. In plane pull out insert tests for attachments also met the necessary 30kN load.

Did we meet our objectives and aims

All of the specified Formula tests have been passed. These include 3 point bending, shear and insert tests. Extra tests of the joints were successfully carried out to valid the cut-and-fold design. Test repeatability was not analysed as extensively as would have been preferred due to the limited number of specimens produced. This was a combined result of monetary and time constraints.

Unfortunately the scale model could not be made in time to meet the projects deadlines and so the final dimensional stability and accuracy of such as chassis could not be analysed. It is thought that the dimensional stability and accuracy would be acceptable as the method used for embedding inserts can be used to give some leeway in the final location of the attachment points allowing for small inaccuracies.

Overall

Overall the project has proved that it is feasible to design and manufacture a Formula Student chassis using a carbon-foam sandwich structure shaped with the cut-and-fold technique. It has also highlighted that extra testing should be carried out to further ensure and enhance the possible performance of such a structure.

8 References

References

[1] *SUFST Website*, Available at: www.sufst.com, Last accessed: 02/12/2014

[2] *How cars work*, Available at: http://www.howcarswork.co.uk/modules/articles/ article.php?id=16, Last accessed: 02/12/2014

[3] Wright, P. (2001) *Formula 1 Technology*, SAE international, Society of automotive engineers, inc. Warrendale, pa. Warrendale

[4] *Composite Materials Technology in Formula 1*, Available at: http://www.formula1-dictionary.net/Big/Composite% 20Materials%20Technology%20in%20Formula%201%20Motor%20 Racing.pdf, Last accessed: 02/12/2014

[5] *Scarbs chassis construction*, Available at: http://scarbsf1.com/chassisconstruction.html, Last accessed: 02/12/2014

[6] *FSAE Forum cut-and-fold technique*, Available at: http://www.fsae.com/forums/archive/index.php/t-5126.html?s=5ce42bd67e1ff12ad0ef134603742939, Last accessed: 02/12/2014

[7] *Vacuum bagging tutorial*, Available at: http://www.instructables.com/id/Vacuum-bagging-basics./, Last accessed: 02/12/2014

[8] *Tut Formula Carbon Monocoque*, Available at: http://tut-f.com/making.html, Last accessed: 02/12/2014

[9] *FSAE Rules 2015*, Available at: http://www.fsaeonline.com/content/2015-16%20FSAE%20Rules%20revision%2091714%20kz.pdf, Last accessed: 02/12/2014

[10] Milliken, F. (2009) *Race Car Vehicle Dynamics*, 1994, Warrendale

[11] *SUFST Shear Plate Report*, Available on CD in references folder

[12] *Formula Student Pat's Corner*, Available at: https://www.formulastudent.de/academy/pats-corner/advice-details/article/overview-for-new-teams/, Last accessed: 02/12/2014

[13] Smith, C. (2009) *Tune to win*, 2004

[14] Deshpande, Cambridge University, *sandwich-panel-design* Available at: http://www3.eng.cam.ac.uk/DesignOffice/cmiCD03_student/lecturenotes/2002/1b/paper8/mmm/notesC/ 1B2001P8MMML08F.pdf , Last accessed: 18/03/2015

[15] T700S Data Sheet, TORAYCA, *toray-t700s*, Available at: http://www.toraycfa.com/pdfs/T700S DataSheet.pdf, Last accessed: 04/02/2015

[16] Dr S. Walker, *Spacecraft Structural design, Chapter three*

[17] A. Petras, M.P.F. Sutcliffe, Cambridge University, *Failure-honeycomb-sandwich-panels* Available at: http://www2.eng.cam.ac.uk/ mpfs/papers/PS1999a.pdf, Last accessed: 27/03/2015

[18] Craig A. Steeves, Normal A. Fleck, Cambridge University, *Collapse-mechanisms-sandwich-beams* Available at: http://www-mech.eng.cam.ac.uk/profiles/fleck/papers/157.pdf, Last accessed: 27/03/2015

[19] *Classical Lamination Theory*, Available at: www.composite-tutorial.com, Last accessed: 02/12/2014

[20] *Design of Composite Sandwich Panels for a Formula SAE Monocoque Chassis - Oregon*, Available at: http://ir.library.oregonstate.edu/xmlui/handle/1957/46918?show=full, Last accessed: 02/12/2014

[21] Professor Ole Thybo Thomsen, *Composites Engineering Design and Mechanics, Composite Laminate Plates I*

[22] Classical Lamination Theory, eFunda *efunda* Available at: http://www.efunda.com/formulae/solid_mechanics/composites/comp_laminate.cfm, Last accessed: 18/02/2015

[23] Professor Ole Thybo Thomsen, *Composites Engineering Design and Mechanics, Composite Laminate Plates II*

[24] *Aerospace metal specification* Available at: http://asm.matweb.com/search/SpecificMaterial.asp?bassnum=MA2014T6, Last accessed: 23/03/2014

[25] David Richardson, *The Fundamental Principles of Composite Material Stiffness Predictions* Available at: http://www.swcompositesgateway.co.uk/Property-Prediction.pdf, Last accessed: 23/03/2014

[26] ZIPP *zipp-woven* Available at: http://www.zipp.com/technologies/composite/woven.php, Last accessed: 19/02/2015

[27] Professor Ole Thybo Thomsen, *Composites Engineering Design and Mechanics, Failure in Composites I*

[28] Jones, Robret M. (1999) *Mechanics of Composite Materials*, 1994, CRC Press

[29] EASYcell75, Easy Composites *EASYcell-75* Available at: http://www.easycomposites.co.uk/downloads/TDS/EC-TDS-EASYCell-40-75.pdf, Last accessed: 25/03/2015

[30] 2015 Structural Equivalency Spreadsheet (SES) /textit2015-SES

[31] Dr S. Walker, *Spacecraft Structural design, Chapter three, page 11*

[32] European Cooperation For Space Standardisation (ECSS), *Space engineering - Insert design handbook* , ECSS-E-HB-32-22A

[33] Elena Bozhevolnaya, *Structurally graded core inserts in sandwich panels* , Composite Structures, Volume 68, Issue 1, April 2005

[34] Sebastian Heimbs and Marc Pein, *Failure behavior of honeycomb sandwich corner joints and inserts*

A Appendix - Theory

A.1 Classical Lamination Theory code

Listing 1: Uses classical lamination theory to calculate global properties of the specified laminate

```
# Classic laminate theory

import math as m
import numpy as np

#------------------------------------------------------------------------#
# Properties of generic ply with 60% fibre volume
#------------------------------------------------------------------------#

'''
These can be uncommented as used as a general standard modulus carbon
fibre instead of the more detailed laminate properties defined and
calculated next.
'''
# E11 = 134e9
# E22 = 7e9
# G12 = 4.2e9
# v12 = 0.25
# v21=v12*E22/E11

# Rupture stresses
# S_1t = 1270e6   #Stress - longitudinal - tensile
# S_2t = 42e6     #Stress - transverse - tensile
# S_1c = 1130e6   #Stress - longitudinal - compression
# S_2c = 141e6    #Stress - transverse - sompression
# T_12 = 63e6     #Stress - rupturelongitudinal - shear

#------------------------------------------------------------------------#

#------------------------------------------------------------------------#
# Properties of the laminate
#------------------------------------------------------------------------#
'''
Here the laminate properties can be defined. The same properties are
used for all plys, however, the ply thicknesses can be individually
set. The ply angles and thicknesses are stored as a list of tuples
where each tuple is defined as (ply-angle, ply-thickness)

If using the generic properties above the 'Raw properties',
'Rupture stress' and 'Macromechanical properties' should be commented
out
'''
# Raw properties
Ef = 230e9                  # Elastic Modulus of Fiber 275.6e9
Em = 2.76e9                 # Elastic Modulus of Matrix 2.76e9
Gf = 114.8e9                # Shear Modulus of Fiber
Gm = 1.036e9                # Elastic Modulus of Matrix
Sc = 1.47e9                 # Compressive Strength
vf = 0.2                    # Poisons Ratio of Fiber
vm = 0.33                   # Poisons Ratio of Matrix
V = 0.6                     # Volume Fiber Fraction
Df = 1800                   # Density of Fiber
Dm = 1600                   # Density Ratio of Matrix
```

```
# Rupture Stresses
S_1t = 1270e6    #Stress - longitudinal - tensile
S_2t = 42e6      #Stress - transverse - tensile
S_1c = 1130e6    #Stress - longitudinal - compression
S_2c = 141e6     #Stress - transverse - sompression
T_12 = 63e6      #Stress - rupturelongitudinal - shear

# Macromechanical properties calculations
E11=Ef*V+Em*(1-V)
E22=(Ef*Em)/(Em*V+Ef*(1-V))
v12=vf*V+vm*(1-V)
v21=v12*E22/E11
v23=vf*V+vm*(1-V)*(1+vm-v12*Em/E11)/(1-vm**2+vm*v12*Em/E11)
G12=(Gf*Gm)/(Gm*V+Gf*(1-V))
G23=E22/(2*(1+v23))
Den=Df*V+Dm*(1-V)

# Lamination stack
plys_degrees = [(0, 0.3e-3),
                                (90, 0.3e-3),
                                (45, 0.2e-3),
                                (-45, 0.2e-3),
                                (90, 0.3e-3),
                                (0, 0.3e-3)]

# Convert angles to radians and calculate total thickness
plys_radians = [(ply[0]*m.pi/180, ply[1]) for ply in plys_degrees]
total_thickness = 0
for ply in plys_degrees:
        total_thickness += ply[1]
#-----------------------------------------------------------------------#

#-----------------------------------------------------------------------#
# Stiffness coefficient and A matrix calculations
#-----------------------------------------------------------------------#
Q11 = E11/(1-v12*v21)
print Q11
Q22 = E22/(1-v12*v21)
Q12 = v21*Q11
Q21 = v12*Q22
Q33 = G12

Q11p, Q12p, Q13p, Q22p, Q23p, Q33p = [], [], [], [], [], []
a = 0

# Stiffness coefficients for each ply p at its respective angle
for ply in plys_radians:
        if ply[0]==0:           # If fibre orientation is 0
                Qp=np.array([[Q11, Q12, 0],
                                        [Q12, Q22, 0],
                                        [0, 0, Q33]])

        else:                   # If fibre orientation is not 0
                Q11p.append(Q11*(m.cos(ply[0])**4)+(Q22*(m.sin(ply[0])
                    **4))+(2*(Q12+2*Q33)*(m.sin(ply[0])**2)*(m.cos(ply
                    [0])**2)))
                Q22p.append(Q11*(m.sin(ply[0])**4)+(Q22*(m.cos(ply[0])
                    **4))+(2*(Q12+2*Q33)*(m.sin(ply[0])**2)*(m.cos(ply
                    [0])**2)))
                Q33p.append((Q11+Q22-2*(Q12))*(m.sin(ply[0])**2)*(m.cos(
                    ply[0])**2)+Q33*((m.cos(ply[0])**4)-(m.sin(ply[0])
```

```
                    **4)))
                Q12p.append(((Q11+Q22-4*Q33)*(m.sin(ply[0])**2)*(m.cos(
                    ply[0])**2))+(Q12*((m.cos(ply[0])**4)+(m.sin(ply[0]))
                    **4)))
                Q13p.append(-m.cos(ply[0])*m.sin(ply[0])*( (m.cos(ply
                    [0])**2)*Q11 - (m.sin(ply[0])**2)*Q22 - ((m.cos(ply
                    [0])**2)-(m.sin(ply[0])**2))*(Q12 + 2*Q33) ) )
                Q23p.append(-m.cos(ply[0])*m.sin(ply[0])*( (m.sin(ply
                    [0])**2)*Q11 - (m.cos(ply[0])**2)*Q22 - ((m.cos(ply
                    [0])**2)-(m.sin(ply[0])**2))*(Q12 + 2*Q33) ) )

                Qp=np.array([[Q11p[-1], Q12p[-1], Q13p[-1]],
                                        [Q13p[-1], Q22p[-1], Q23p
                                            [-1]],
                                        [Q13p[-1], Q23p[-1], Q33p
                                            [-1]]])

        aPly=Qp*(ply[1]/total_thickness)

        a = a + aPly
#-----------------------------------------------------------------------#


print 1/total_thickness * a
print '-----------------------------------------------------------',

a_inverse = np.linalg.inv(a)
print a_inverse
print 'Youngs Modulus: ' + str(1/a_inverse[0,0]/1000000000) + 'GPa'

e_x = (1/a_inverse[0,0])
v_xy = a_inverse[0,1]/a_inverse[0,0]
G_xy = a_inverse[2,2]/(total_thickness)

#-----------------------------------------------------------------------#
# Sandwich panel calculations
#-----------------------------------------------------------------------#

c = 25e-3       # Core thickness
w = 0.275       # Base of the beam
l = 0.4         # Length of the Beam



panelStiffness = (24*e_x*w*total_thickness*c**2)/l**3
```

B Appendix - Results

B.1 Test results and specimen lookup table

Each specimen has a code consisting of 4 sections i.e.

FG-H-3a-B1

Where the first section stands for the facesheet material used, the second section refers to the core material used, the thrid section refers to the test and number of the specimen, finally the fouth section refers to the laminate type.

Section 1 - Facesheet Material	**Description**
FG	Fibre Glass
CF	Carbon Fibre
Section 2 - Core Material	
H64 - H	Honeycomb - 6.4 mm Hex Size (From Easycomposites)
PVC75 - F	PVC Foam Core - 75Kg/mˆ3 (From Easycomposites)
Section 3 - Stacking Order	
FG-X-3-X	1x3 layers: Biaxial 0/90 900gsm
CF-X-3-X	1st layer: Easycomposites Twill 2/2 0/90 450gsm 2nd layer: Easycomposite Biaxial +/-45 300gsm 3rd layer: Easycomposites Twill 2/2 0/90 450gsm
CF-X-4-X	1st layer: Easycomposites Twill 2/2 0/90 450gsm 2nd layer: Easycomposites Biaxial +/-45 300gsm 3rd layer: Easycomposites Biaxial +/-45 300gsm 4th layer: Easycomposites Twill 2/2 0/90 450gsm
CF-X-5a-X	1st layer: Easycomposites Twill 2/2 0/90 450gsm 2nd layer: Easycomposites Biaxial +/-45 300gsm 3rd layer: Easycomposites Twill 2/2 0/90 450gsm 4th layer: Easycomposites Biaxial +/-45 300gsm 5th layer: Easycomposites Twill 2/2 0/90 450gsm
CF-X-5b-X	1st layer: Easycomposites Twill 2/2 0/90 450gsm 2nd layer: Easycomposites Twill 2/2 0/90 450gsm 3rd layer: Easycomposites Biaxial +/-45 300gsm 4th layer: Easycomposites Twill 2/2 0/90 450gsm 5th layer: Easycomposites Twill 2/2 0/90 450gsm
Section 4 - Specimen Test	
B	3 Point Bending Test
S	Perimeter Shear Test
T	Tensile Test
J	Joint Test
I	Insert Test

C Expenditure

The table overleaf shows the expenditure of the project.

Group made orders						
Company	**Product**	**ID**	**Details**	**Price (inc VAT**	**Quantity**	**Total cost**
EDMC	Shear Test Rig			53.45	1	53.45
EDMC	Radius Test Rig			78.9	1	78.9
J.E	Load Applicator			41.4	1	41.4
Easycomposites	6.4mm (1/4) Aluminium Honeycomb 10mm 1250mm x 625m	AHC-064-Q-20	20mm x 1250mm x 625m	49.08	1	49.08
Easycomposites	Carbon Fibre 2/2 Twill 12k 450g 1m wide	CF-22-450-100	1m wide	24	2	48
Easycomposites	Carbon Fibre +/- 45deg BiAxial 300g 1m wide	CF-BI-300-100	1m wide	23.94	1	23.94
Easycomposites	50ml Twin Tube cartridge gun dispenser	CG-50ML	50ml	17.94	1	17.94
Easycomposites	ET538 Honey Comb Bonding Epoxy adhensive 50ml twin tub	ET538A	50ml	12.2	1	12.2
Easycomposites	Static Mixer Nozzles for 50ml Twin Tube	SMN-50ML	50ml	0.78	5	3.9
Easycomposites	EasyCell75G Infusion Grooved Closed Cell PVC Foam 25m	PVC75G-1-25	550mm x 545	67.69	1	67.69
Easycomposites	ET538 Honey Comb Bonding Epoxy adhensive 50ml twin tub	ET538A	50ml	12.2	4	48.8
Metal supermarket	AISI 1010 steel tubing		1m	10	3	30
					Total	475.3
SUFST Sponsored Order	**Date: 27/02/2015**					
Company	**Product**	**ID**	**Details**	**Price (inc VAT**	**Quantity**	**Total cost**
Easycomposites	Carbon Fibre 2/2 Twill 12k 450g	CF-22-450-100	1m wide	24	4	96
Easycomposites	Carbon Fibre +/- 45 Biaxial 300g	CF-BI-300-100	1m wide	23.94	2	47.88
Easycomposites	EL2 Epoxy Laminating Resin 1kg FAST	EP-L2-F-1	1 kg	20.1	1	20.1
Easycomposites	Glass Bubbles (Microspheres) 5L	FP-GB-5	5L (475g)	17.94	1	17.94
Easycomposites	EasyCell75G Infusion Grooved Closed Cell PVC Foam 25m	PVC75G-1-25	1020mm x 1090mm	67.69	1	67.69
Easycomposites	EasyCell75G Infusion Grooved Closed Cell PVC Foam 10m	PVC75G-1-10	1020mm x 1090mm	35.9	1	35.9
Easycomposites	Pultruded Carbon Fibre Tube 10mm (8mm) - 1m Length	CFPTUBE-10-8-1		11.34	1	11.34
Direct plastics	Tufnol Whale Sheet 300 x 300 x 25mm		25mm Thick	77.98	1	77.98
Direct plastics	PVC Grey Sheet 500 x 250 x 10mm		10mm Thick	7.98	1	7.98
					Total	382.81